THESIS APPROVAL

GRADUATE SCHOOL, KASETSART UNIVERSITY

Master of Engineering (Chemical Engineering)

DEGREE

Chemical Engineering	Chemical Engineering
FIELD	**DEPARTMENT**

TITLE: Modeling and Simulation of a Gas-Liquid Reactor in Co-current and Counter current Flows

NAME: Mr. Teeranun Nakyai

THIS THESIS HAS BEEN ACCEPTED BY

.....
THESIS ADVISOR

(Associate Professor Sunun Limtrakul, D.Sc.)

.....
THESIS CO-ADVISOR

(Associate Professor Terdthai Vatanatham, Ph.D.)

.....
DEPARTMENT HEAD

(Associate Professor Phungpai Phanawadee, D.Sc.)

APPROVED BY THE GRADUATE SCHOOL ON .....

.....
DEAN

(Associate Professor Gunjana Theeragool, D.Agr.)

THESIS

THESIS

MODELING AND SIMULATION OF A GAS-LIQUID REACTOR IN CO-CURRENT AND COUNTER CURRENT FLOWS

TEERANUN NAKYAI

A Thesis Submitted in Partial Fulfillment of
the Requirements for the Degree of
Master of Engineering (Chemical Engineering)
Graduate School, Kasetsart University
2010

Teeranun Nakyai 2010: Modeling and Simulation of a Gas-Liquid Reactor in Co-current and Counter current Flows. Master of Engineering (Chemical Engineering), Major Field: Chemical Engineering, Department of Chemical Engineering. Thesis Advisor: Associate Professor Sunun Limtrakul, D.Sc. 158 pages.

Mathematical models are developed for predicting gas-liquid reaction regime and reactor performance in co-current and counter current modes based on film model coupling with mixing cell model. The models were solved by boundary element method (BEM). These models were applied for three case studies including the gas liquid reactions of CO_2-NaOH, H_2S-Fe^{3+}(EDTA) and CO_2-Na_2CO_3. The simulation results showed that the reaction of CO_2-NaOH takes place only in the liquid film. Thus it is a fast reaction. The reaction of H_2S-Fe^{3+} (EDTA) is an intermediate reaction and takes place in both liquid film and liquid bulk. Thus, the reaction of CO_2-Na_2CO_3 is a slow reaction. The reactions take place only in the liquid film. The conversions for all case studies depend on the degree of flow mixing. Variation of mixing cell number, N from 1 to ∞ shows that the flow behavior as well as the reactor performance approach to those in a complete mixed flow at N=1 and a plug flow at $N=\infty$. Furthermore, a counter current mode for all case studies gives higher conversion than that in a co-current mode due to higher mass transfer in the counter current. The enhancement factor (*Ea*) for a plug flow system (at very high N) is the smallest and that for a CSTR is the greatest. Finally, predictions of the performances of the riser for H_2S removal and the downcomer for Fe^{3+}(EDTA) regeneration in the Lo-Cat air-lift reactor are in good agreements with the experimental results.

_____ _____ _____/_____/_____

Student's signature Thesis Advisor's signature

ACKNOWLEDGEMENTS

First, I would like to express my sincere gratitude and deep appreciation to my advisor and co-advisor, Assoc. Prof. Dr. Sunun Limtrakul and Assoc. Prof. Dr. Therdthai Vatanatham. They both made the experience of being a graduate student very fulfilling by being enthusiastic in my work. In addition, they give the guidance, supervision, comments, discussions and invaluable suggestions throughout this project. I would like to thank Prof. Palghat A. Ramachandran for helping all the MatLab program, valuable coments and guidance.

I am extremely grateful to Asst.Prof. Dr. Suchaya Nitivattananon and Asst. Prof. Dr.Nanthiya Hansupalak for their helpful suggestions and corrections of this work.

I deeply thank to the Kasetsart University Research and Development Institute (KURDI), Department of Chemical Engineering, Kasetsart University, National Research Council of Thailand (NRCT) and Center of Excellence for Petroleum, Petrochemicals, and Advanced Materials for financial support.

Additional thanks extend to all colleagues in both Assoc. Prof. Dr. Sunun's research group, Assoc. Prof. Dr. Therdthai's research group, and 13th Dormtory member for their warm friendship, suggestion and all supports. They always make me enjoy my life duringstudy in this program. I would like to thank Mr.Komson Thongtam for keeping me sane and helping me balance school with a little fun.

Finally, this thesis also belongs to my parents for supporting my decision to stay at Kasetsart University for three years and for keeping me relaxed.

Teeranun Nakyai

June 2010

TABLE OF CONTENTS

Page

LIST OF TABLES

LIST OF TABLES (Continued)

LIST OF FIGURES

LIST OF FIGURES (Continued)

LIST OF FIGURES (Continued)

LIST OF FIGURES (Continued)

LIST OF FIGURES (Continued)

LIST OF ABBREVIATIONS

a	=	Interfacial area per volume of reactor [m^2/m^3]
A_r	=	Cross section area of reactor [m^2]
B_m	=	Heat of reaction parameter for reaction j [-]
Bi_{mi}	=	Biot number for gas phase mass transfer [-]
Bi_H	=	Biot number for heat transfer [-]
c	=	Dimensionless components concentration [-]
c_i^g	=	Dimensionless gas phase concentration [-]
c_i^L	=	Dimensionless liquid phase concentration [-]
C	=	Dimensional components concentration [$gmol/m^3$]
$C_{i,ref}$	=	Reference liquid phase reactant concentration (Liquid feed condition) [$gmol/m^3$]
$C_{i,ref}^g$	=	Reference gas phase reactant concentration of component i (Gas feed condition) [$gmol/m^3$]
$\overline{C}_p$	=	Average mass heat capacity [$J/gmol\ s^{-1}\ K^{-1}$]
D_i	=	Diffusivity coefficients in the liquid phase [m^2/s]
f^g	=	Dimensionless gas flow rate [-]
f_i	=	Rate function for the variable i [-]
G	=	Weighting function used in BEM [-]
G_1	=	First weighting function, $\xi - a$ [-]
G_2	=	Second weighting function, $b - \xi$ [-]
h	=	Temperature dependency of solubility or volatility [-]
h_g	=	Gas phase convective heat transfer coefficient [$J/m^2s^{-1}K^{-1}$]
H	=	Solubility or vaporability [$Pa.m^3/gmol$]
Ha_j	=	Hatta number for reaction j [-]
$H_{i,ref}$	=	Reference Henry's law constant [$Pa.m^3/gmol$]

LIST OF ABBREVIATIONS (Continued)

K_{0i}	=	Constant term in the Taylor expansion of f_i [-]
K_{1ik}	=	Partial derivative of f_i with respect to c_k [-]
$(-\Delta H_r)$	=	Heat of reaction [J/gmol]
$(-\Delta H_s)$	=	Heat of solution [J/gmol]
$(-\Delta H_V)$	=	Heat of vaporization [J/gmol]
k	=	Reaction rate constant [gmol/m^{2}s]
$k_{g,i}$	=	Gas side mass transfer coefficient based on concentration driving force [m/s]
k_l	=	Liquid side mass transfer coefficient based on concentration driving force [m/s]
L_w	=	Square of the film thickness ratio [-]
Le	=	Lewis number [-]
m^g	=	Mass flow rate of gas phase [kg/s]
m^L	=	Mass flow rate of liquid phase [kg/s]
M_j	=	The kinetic reaction rate parameter for reaction j [-]
n^g	=	Molar flow rate of component in gas bulk [mol/s]
n^L	=	Molar flow rate of component in liquid bulk [mol/s]
N	=	Number of mixing cells [-]
N_i	=	Molar flux of component i [gmol/s m^2]
N_g	=	Number of mixing cells in gas phase [-]
N_l	=	Number of mixing cells in liquid phase [-]
NR	=	The number of reaction [-]
NS	=	The number of species [-]
p	=	Partial pressure [Pa]
p_{ai}	=	Concentration gradient of species i at ξ = a [-]

LIST OF ABBREVIATIONS (Continued)

p_{bi}	=	Concentration gradient of species i at ξ = b [-]
$p_{i,Z=0}$	=	Interfacial partial pressure of species i [Pa]
$p_{g,i}$	=	Gas phase partial pressure of species i [Pa]
Pe	=	PecletbNumber [-]
q	=	Heat flux [J/s m^2]
Q	=	Volumetric flow rate [m^3/s]
r	=	Dimensionless reaction rate of component [-]
R	=	Reaction rate [gmol/m^2]
s_i	=	Diffusivity ratio of component I [-]
s^g	=	Heat transfer dimensionless term for gas phase [-]
s^L	=	Heat transfer dimensionless term for liquid phase [-]
T	=	Temperature [K]
T^L	=	Bulk liquid temperature [K]
T^f	=	Temperature in the film [K]
T^g	=	Gas phase temperature [K]
U	=	Superficial velocity [m/s]
$u^g_{i,ref}$	=	Reference superficial velocity of gas phase being gas feed superficial velocity [m/s]
u^L_{ref}	=	Reference superficial velocity of liquid phase being liquid feed superficial velocity [m/s]
V_{cell}	=	Volume of reactor or cell [m^3]
Z	=	Direction of film thickness [m]
α_{gL}	=	Damkohler number for mass transfer [-]
β	=	Parameter of heat of reaction [-]
β_s	=	Parameter of heat of solution at interface [-]
β_V	=	Parameter of heat of vaporization at interface [-]

LIST OF ABBREVIATIONS (Continued)

γ	=	Arrhenius number for reaction [-]
γ_{Fi}	=	The effective gas to liquid flow rate ratio [-]
δ_h	=	Heat transfer film thickness [m]
δ_m	=	Mass transfer film thickness [m]
ε_g	=	Gas phase holdup [-]
ε_L	=	Liquid phase holdup [-]
ξ	=	Dimensionless mass transfer film thickness [-]
θ	=	Dimensionless temperature [-]
κ	=	liquid thermal conductivity [$J/m^2s^{-1}K^{-1}$]
ϕ_i	=	Osculating polynomials ($i = 1$ to 4) defined in Table 4 [-]
ρ_L	=	Density of the liquid phase [kg/m3]
θ^L	=	Dimensionless bulk liquid temperature [-]
θ^f	=	Dimensionless temperature in the film, T^f / T_{ref} [-]
θ^g	=	Dimensionless bulk gas temperature [-]
$\theta^f_{\xi=0}$	=	Dimensionless interfacial temperature [-]
$\theta^f_{\xi=1}$	=	Dimensionless temperature at the end of mass transfer film
τ	=	Stoichiometric parameter [-]
ν_{ji}	=	Stoichiometric coefficient of species i in any reaction j [-]
i	=	Component species [-]
j	=	Reaction [-]
f	=	Liquid film [-]
g	=	Gas phase [-]
L	=	Liquid phase [-]

MODELING AND SIMULATION OF A GAS-LIQUID REACTOR IN CO-CURRENT AND COUNTER CURRENT FLOWS

INTRODUCTION

Gas-liquid reactions are widely encountered industrial practice. The processes of importance are found in manufacturing processes for chemicals (e.g.hydroformylation, oxidation etc) and in gas purification/treatment systems. Examples in chemical industry can be found in large scale processes such as chlorination of benzene, cyclohexane oxidation, hydrochlorination of olefins, and p-xylene oxidation (Mills *et al.,* 1992). In addition, (Doraiswamy and Sharma, (1984)) listed more than fifthy industrial example of gas-liquid reaction including the type of gas-liquid reactor usually used. The common types of gas-liquid reactor are packed column, mechanically agitated contractors, spray column and buble column. The selection of a reactor type depends on reaction kinetic, mass and heat transfer.

A bubble column is one type of gas-liquid reactors and most frequently in the industries because of its excellent mass and heat transfer and low maintenance and operating costs. In a bubble column, a gas was dispersed in a liquid phase at the bottom through a suitable distributor. Since liquid holdup is large and liquid residence time can be varied over a wide range. Bubble columns may be used as reactors, absorbers, or strippers (Potter, 2003). A gas-lift reactor is the one type of a bubble column. The chemical processes industries increasingly are turng to gas-lift reactors for gas-liquid contacting operation such as the low weste conversion of ethylene and chlorine to dichloroethane (Smith, 1992), Hydrogen sulfide removal by the Lo-Cat process. The gas-lift reactor consisted of concentric pipes. The inside pipe serves as the riser, while the annualar space serves as the downcomer. Liquid circulation is induced by the density difference between riser and downcomer usually by injecting gas at the bottom of the riser. The induced liquid circulation is a major design characteristic of gir-lift reactor. It determines the residence time of the liquid in various zones of the reactor and controls importance reactor performance parameter

such as gas-liquid mass transfer. In the most common mode of gir-lifts and the bubble column, they may be operated in a semibatch, co-current, or counter-current manner.

Basically, there are three classic theories describing the mass transfer at gas-liquid interface, namely the film theory by Whitman (1923), the penetration theory by Higbie (1935) and the surface renewal theory by Danckwerts (1951). The film theory assumes that a stagnant liquid film will be established when the gas meets the liquid surface and instantaneous equilibrium will be established. The penetration theory has a physical explanation for the absorption process, which a liquid element comes from the bulk liquid phase to the gas interface and stays for a certain time then it leaves and gets replaced by another fresh element. The time that the element spends at the interface is called the "contact time" and the rate absorption is averaged with respect to this time. The surface renewal theory, on the other hand, assumes more realistically that different liquid elements stay for different contact times and the rate of absorption for each element is weighted with respect to a certain time distribution function. The film theory is a steady state model while the penetration and surface renewal theories are time dependent models.

The film and penetration theories were applied widely in the literature to describe the coupled mass and heat transfer phenomena in reactive and unreative absorption problems. However, very little attention, by comparison, was paid to the surface renewal theory due to its mathematical complexity. Among the three theories, the film theory is easier in visualizing the process of gas dissolution, diffusion, film reaction, and then the process of material transfer to the bulk liquid phase and subsequent reaction in the liquid phase. Also, the mathematical representation of the combined mass and heat transfer processes is relatively easier for film theory. Therefore, the film theory is still used in most numerical studies concerning gas-liquid reaction. For co-current and counter modes, the heat and mass balance in the film and bulk phase can be coupled to the reactor model by modified boundary conditions. The film model and reactor models are non linear second order differential equations which can be solved by Boundary element method.

The Boundary elements method has been applied to 1D boundary value problems in a number of contexts. The details are available in book by Ramachandran (1991). Additional references as applied to 1D problem are available (Ramachandran, 1994; Ngoasuwan *et al.,* 2001; Wei-Gao and Jing Wang, 2008; Zadravec *et al.,* 2008). Furthermore, this method has been applied to the cases of gas absorption with reaction which are chlorination of butanoic acid and oxidation of cyclohexane (Abhijart *et al.,* 2005). The BEM is suitable for analysis due to a number of its advantages, such as reduction of dimensionality for linear differential equations, ease of coding, smaller memories requirement, high accuracy and computational efficiency.

The mixing cell model is used to evaluate the performance of a gas-liquid reactor, which has mixing characteristics, intermediate to the ideal solution of plug flow and back mixing flow. The number of mixing cells indicates the flow behavior within the reactor. If the number of mixing cells approaches to one, the flow in the reactor is complete mixed (i.e., a CSTR) which has high degree of mixing. If the number of mixing cells approaches to infinity, it has low degree of mixing in contrast to CSTR (i.e., a plug reactor). The flow behavior in each cell is considered as well mixed.

A bubble column can be operated in either co-current or counter-current modes. The reactor performance of gas-liquid systems depends on the regime at which gas absorption is taking place and also on whether the reactions are taking place mainly in the film or in the bulk liquid. The behavior of co-current and counter-current mode may be in different regimes. This variation affects the mass transfer and mixing characteristics of the system. In additional, the effect of operating mode on the reactor performance does not appear to have well established in the literature.

Hence, the objective is to develop the models for studying the effect of operating condition on the reactor performance in co-current and counter-current modes using the mixing cell approach. In addition, the effects of cell number (N) of gas phase and operating conditions on reactor performance are studied. The models

are applied for three cases's gas liquid reactions of CO_2 and NaOH, H_2S and Fe^{3+} (EDTA), and CO_2 and Na_2CO_3 which are an industrially important systems. Furthermore, the mixing cell models were used to study the performance of the Lo-Cat gas-lift reactor on the H_2S removal under various operating conditions.

OBJECTIVES

1. To develop the mathematical models for reaction between gas and liquid phases coupling with gas-liquid reactor.

2. To study mass transfer in gas-liquid reaction by using the film theory.

3. To study mass transfer in a gas-liquid reactor using mixing cell model under the co-current and counter-current modes.

4. To apply the models to case studies i.e the reactions of CO_2 and NaOH, H_2S and Fe^{3+} (EDTA), and CO_2 and Na_2CO_3 in a gas-liquid reactor.

5. To study the performance of the Lo-Cat gas-lift reactor on H_2S removal and regeneration Fe^{3+} (EDTA).

Scopes

1. The mass transfer of gas-liquid reaction is studied using film theory

2. The performances of gas-liquid reactor in co-current and counter modes is studied using mixing cell approach.

3. The case studies are the reactions of NaOH and CO_2, H_2S and Fe^{3+} (EDTA), and CO_2 and Na_2CO_3 in a gas-liquid reactor.

4. The performances of Lo-Cat gas-lift reactor and its operation conditions on the H_2S removal efficiency were studied.

Benefits

1. The mathematical models of the gas-liquid reaction and reactor are useful for reactor design and operation.

2. Better mathematical models of the gas-liquid reaction and reactor should be available.

LITERATURE REVIEW

1. Gas-Liquid Reactors

Gas-liquid reactors are commonly used in chemical industrial. This is due to their advantages of mixing and heat transfer characteristic. The criteria by which a reactor is chosen for a specific case depends on the reaction rate, the concentration and the solubility of the reacting components.

The types of reactors used for gas-liquid reactions perhaps divided into two main types which are tower or column reactors, and tank reactors. The tank reactors are usually chosen when the reaction rate is slow or when a high liquid hold up is required. The tank reactor is also good choice when large temperature effects are present due to reaction solution or dilution. Difference types of column reactors are frequently used for gas-liquid reactions, where the reaction is irreversible or when higher gas hold up is required. The flow characteristic achieved in bubble column are closest to those of tank reactor, whereas packed column and trickle bed are used when the gas hold up is comparable to the liquid hold up. Table1 shows the common type of gas- liquid reactor. The general features of the reactors shows in Figure 1.

Table 1 Types of gas-liquid reactors

Types of reactors	Characteristics of reactor
Packed tower	Good all rounder, but must have gas to liquid molar flow rate =10
Spray tower	Good for very soluble gases high k
Staged bubble column	Needs mechanical mixer or pulsing device. Good for slightly soluble gases
Agitated tank	Cheap to build but needs a mechanical agitator

Source: Levenspiel (1999)

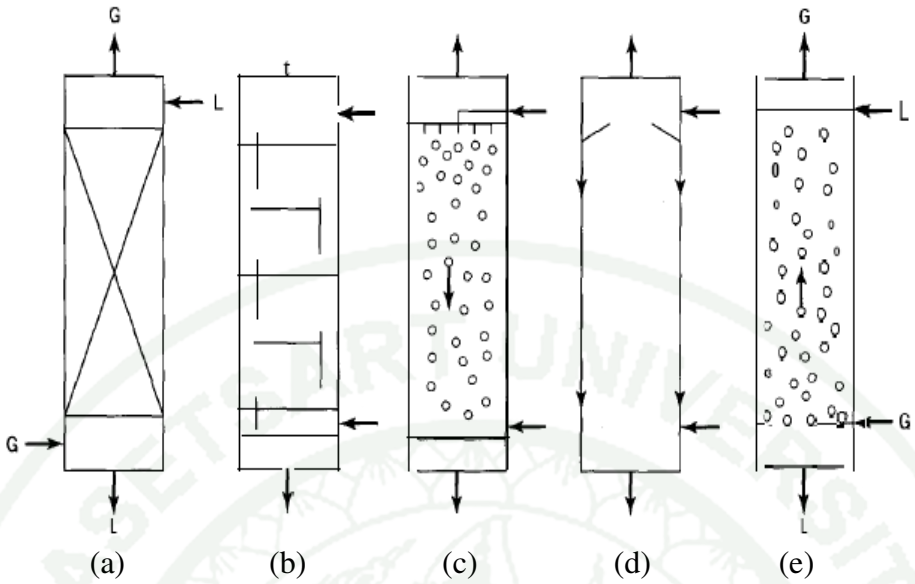

Figure 1 Types of tower or column reactors for gas-liquid reactions: (a) packed tower, (b) plate tower, (c) spray tower, (d) falling-film tower, and (e) bubble column.

Source: Ronald *et al.* (1998)

2. Bubble Column Reactor

A bubble column reactor is a vertical cylindrical vessel with a height to diameter ratio that is usually at least 1.5, and may be as large as 20. Gas is introduced near the bottom of the column through a set of nozzles, or a sparger. The holes are sized to give exit velocity of 100–300 ft/s, and the gas enters the liquid as jets, which break up into bubbles after a short distance. As the bubbles rise, they tend to coalesce and then break up again. The average bubble size depends mainly on the gas flow rate and physical properties of the liquid rather than on the orifice size.

In the simplest type of bubble column, gas is dispersed at the bottom. The bubbles are present throughout the reactor. One of the main design variables for bubble columns is the superficial velocity of the gas, which affects the gas hold up,

the interfacial area, and the mass transfer coefficient. The superficial velocity changes as gas passes up the column because of the decrease in hydrostatic head and changes in the total molar flow. When this changes is small, an average of the inlet and exit velocities can be used to predict the performance, though in some studies the velocity reported corresponds to the gas feed rate at the exit pressure. An important factor that is sometimes overlooked is the vapor pressure of the solution. The gas bubbles quickly become saturated with solvent vapor, which decreases the partial pressure of the reaction gas and increases the volumetric flow rate of gas in the reactor (Potter, 2003).

2.1 Fluid dynamic and regime analysis

The fluid dynamic in bubble column has a significant on the operation, and performance of bubble column reactors. The flow regime depends on column geometry, operating condition, and physical properties of the phase. The flow regimes in the bubble columns can be classified to four types which are homogenous (bubbly flow), heterogeneous (churn –turbulent), slug flow, and annular flow regime which can be described the detail as follow as and the appearance of these flow regime is illustrated in Figure 2 (Taitel, 1980; Hyndman *et al.,* 1997).

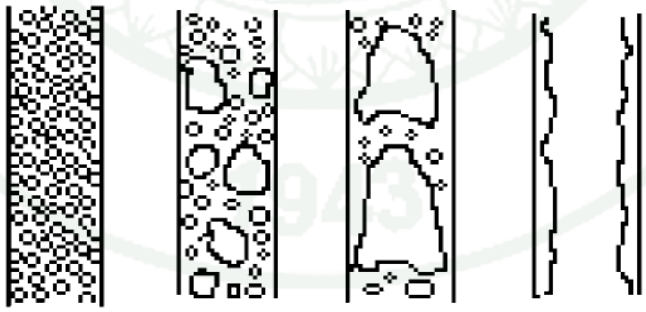

Figure 2 Flow pattern of vertical column: (a) homogeneous bubbly flow, (b) heterogeneous, (c) slug flow, and (d) annular flow.

Source: Hyndman *et al.* (1997)

The homogenous regime, also called the bubbly regime which can be obtained at low superficial gas velocity that is approximately less than 5 cm/s in semibath columns. This flow regime gives a small size bubble and rise velocity (Schumpe and Grund, 1986). The heterogonous regime, also called Churn-turbulent regime is obtained at high superficial gas velocity that means the bubble size is large as compare to the homogenous regime. In chemical, petroleum, and biochemical industries, the bubble column reactors normally operate in the bubble or churn-turbulent regimes.

The slug flow regime has been only observed in small diameter laboratory column at high gas flow rates (Schumpe and Grund, 1986). This regime obtained in the column diameter up to 15 cm. Figure 3 shows the flow regime map which describes quantitatively the dependence of flow regime on column diameter and superficial velocity (Deckwer *et al.,* 1980).

The annular flow regime in which the lighter fluid flows in the center of the pipe, and the heavier fluid is contained in a thin film on the pipe wall. The lighter fluid may be a mist or an emulsion. Annular flow occurs at high velocities of the lighter fluid, and is observed in both vertical and horizontal wells. As the velocity increases, the film may disappear, leading to mist or emulsion flow. When the interface between the fluids is irregular, the term wavy annular flow may be used.

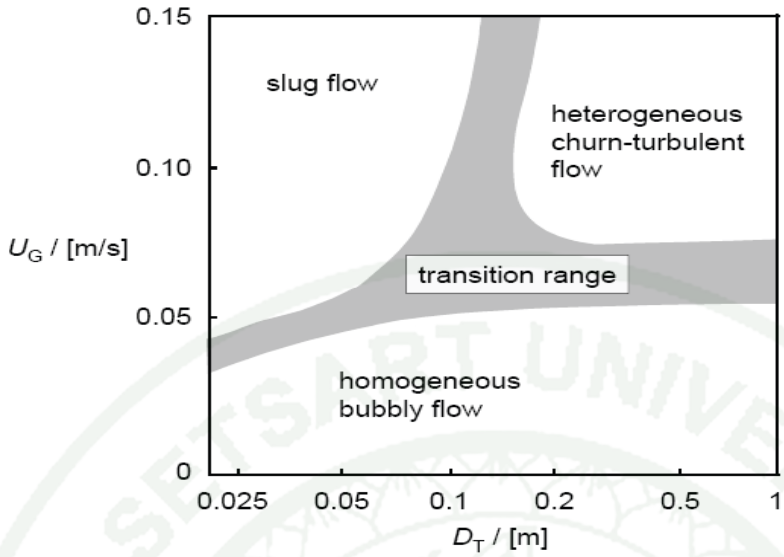

Figure 3 Schematic of flow regime map for a bubble column

Source: Shah *et al.* (1982)

2.2 Gas hold up

Gas hold up is a dimensionless key parameter for design the process that characterizes transport phenomena of a bubble column system (Luo *et al.,* 1999). It is basically defined as the volume fraction of gas phase occupied by the gas bubble. The magnitude of gas hold up radial gradient depends on gas velocity, column diameter, physical properties of the system, and operating conditions (Wu Y *et al.,* 2001). The exits various correlations in literature in order to predict the gas hold up in both two phase bubble columns. The following, several frequently used gas hold up correlations for bubble columns are summarized.

The gas hold up can be calculated from the correlation below (Akita and Yoshida, 1973).

$$\frac{\varepsilon_g}{(1-\varepsilon_g)^4} = 0.2\left(\frac{D_C^2\rho_l g}{\sigma}\right)^{\frac{1}{8}}\left(\frac{D_C^3\rho_l g}{\mu_l^2}\right)^{\frac{1}{12}}\left(\frac{v_g}{\sqrt{gD_C}}\right) \qquad (1)$$

where D_C is a column diameter, ρ_l the density of liquid, g a gravitational acceleration, μ_l the viscosity of liquid, v_g the superficial gas velocity, σ the interfacial tension, and ε_g a gas hold up.

Additional, the gas hold up equation can be calculated as follow (Kumar *et al*., 1976).

$$\varepsilon_g = 0.728U - 0.485U^2 + 0.097U^{36} \quad (2)$$

where

$$U = v_g \left(\frac{\rho_l^2}{\sigma(\rho_l - \rho_g)} \right)^{\frac{1}{4}} \quad (3)$$

for a noneletrolyte liquid phase, gas hold up can be calculated from the correlation below (Hikita *et al.,* 1980)

$$\varepsilon_g = 0.672 \left(\frac{u_{sg}\mu_l}{\sigma} \right)^{0.578} \left(\frac{\mu_l^4 g}{\rho_l \sigma^3} \right)^{-0.131} \left(\frac{\rho_g}{\rho_l} \right)^{0.062} \left(\frac{\mu_g}{\mu_l} \right)^{0.107} \quad (4)$$

where u_{sg} is a superficial gas velocity.

Krishna and Van Baten (2003) was presented the relationship between experimental data on gas holdup and superficial gas velocity which note a change in the slope in the ε–U curve. They found that the transition point that the gas holdup has increased with increasing gas flow rate. The appearance of this curve is shown in Figure 4.

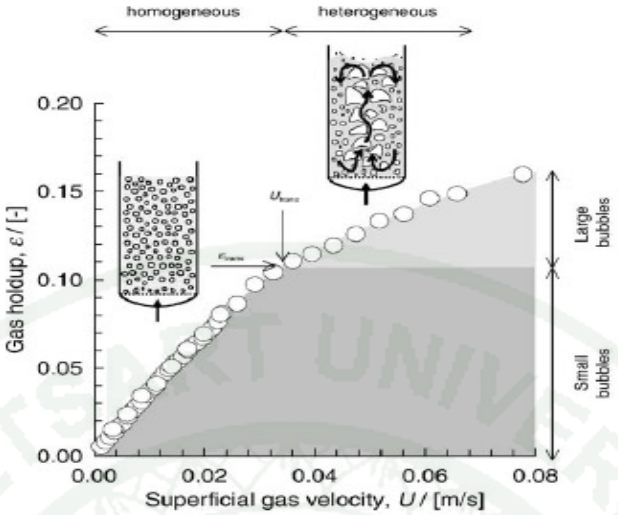

Figure 4 Schematic of experimental data on gas holdup in a 0.1m diameter bubble operating with the air–water system spanning both the homogeneous and heterogeneous flow.

Source: Krishna and Van Baten (2003)

2.3 Mass transfer coefficients, k_{Al}

The overall mass transfer rate per unit volume of the dispersion in a bubble column is governed by the liquid-side mass transfer coefficient, $k_l a$. In gas-liquid reactors, mass transfer from the gas to liquid phase most important goal of the process. The volumetric mass transfer coefficient is a key parameter in characterize, and design of both industrial stirred and non-stirred gas-liquid reactor. The determination of mass transfer parameters in bubble column reactors has been subject of numerous and publications (Shah *et al.,* 1982; Roberts *et al.,* 1984; Munz and Roberts, 1989; Deckwer and Shumpe, 1993). It was shown that the a priori design of bubble columns is still difficult due to the fact that the bubble properties (bubble size and shape, bubble velocity, and interfacial area) in gas liquid dispersions depend largely on reactor geometry, operating conditions, gas distribution, and physico-chemical properties of the two phases.

Akita and Yoshida (1973) performed the experimentation of various gas-liquid systems assuming total dispersion of the liquid phase and plug flow of the gas phase, and proposed the following dimensionless correlation

$$\frac{k_l a d_T^2}{D_{AB}} = 0.6\left(\frac{\mu_l}{D_{AB}}\right)^{0.5}\left(\frac{g d_T^2 \rho_l^2}{\sigma}\right)^{0.62}\left(\frac{g d_T^3 \rho_l^2}{\mu_l^2}\right)^{0.31}\varepsilon_g^{1.1} \qquad (5)$$

where d_T is a bubble column diameter, and a is an interfacial area.

Hikita *et al.* (1980) proposed another correlation, which also incorporates the gas viscosity as

$$\frac{k_l a v_g}{g} = 14.9 f\left(\frac{v_g \mu_l}{\sigma}\right)^{1.76}\left(\frac{\mu_l^4 g}{\rho_l \sigma^3}\right)^{-0.248}\left(\frac{\mu_{g\,l}^{\;2}}{\mu_l}\right)^{0.243}\left(\frac{\mu_l}{\rho_l D_l}\right)^{-0.604} \qquad (6)$$

In which f=1, for non-electrolytes (water, methanol, butanol, etc) and is a function of ionic strength in case of electrolyte solutions.

However, correlations of Hikita *et al.* (1980) (Equation 5) and Akita and Yoshida (Equation 6) were described the experimental data with errors of 25 to 37%. Therefore they proposed a new correlation using the Akita-Yoshida correlation as a basis. Since column diameter has a low influence on mass transfer coefficient, they have changed the characteristic length from the reactor diameter to the surface-to-volume mean bubble diameter, d_b, which has a more important role. The correlation obtained by a non- linear regression analysis is as follows:

$$\frac{k_l a d_b^2}{D_{AB}} = 0.62\left(\frac{\mu_l}{\rho_l D_{AB}}\right)^{0.5}\left(\frac{g d_T^2 d_b^2}{\sigma}\right)^{0.33}\left(\frac{g d_b^3 \rho_l^2}{\mu_l^2}\right)^{0.29}\left(\frac{V_g}{\sqrt{g d_b}}\right)^{0.68}\left(\frac{\rho_g}{\rho_l}\right)^{0.04} \qquad (7)$$

The d_b was assumed to be approximately constant (d_b = 0.003 m) as recommended by several authors.

2.4 Interfacial areas, $a_i^{'}$

Normally, k_{il} is calculated from $k_{il}a_i^{'}$ Hence, a correlation for $a_i^{'}$ is required, but the result may be subject to significant error. An expression for a_i given by Froment and Bischoff (1990) may be written

$$a_i^{'} = 2u_{sg}(\rho_l^3 g/\sigma^3)^{\frac{1}{4}} \tag{8}$$

2.5 Bubble diameter

The bubble diameter can be calculated using the equation proposed by Calderbank (1985). This correlation is the same as that for a mechanically agitated reactor. Another correlation for calculation of the bubble diameter was proposed by Akita and Yosida (1974)

$$\frac{d_B}{d_T} = 26\left(\frac{gd_T^2\rho_l}{\sigma_l}\right)^{-0.5}\left(\frac{gd_T^3\rho_l^2}{\mu_l^2}\right)^{-0.12}\left(\frac{u_g}{\sqrt{gd_T}}\right)^{-0.12} \tag{9}$$

Schulzke *et al.* (1998) experimentally and numerically studied of the dynamic behavior of bubble column reactor using two systems that is air-water and carbon dioxide absorption. For experiment conditions, superficial gas velocities ranged from 0.05 to 1 m/s and the superficial velocity of the liquid phase ranged from 0 to 0.15 m/s. The initial sodium hydroxide concentration varied from 0 to 1 mol/l and the inlet carbon dioxide mole fraction in gas phase varied from 0 to 10 %. The experimental values and the simulated results show good quantitative agreement not only for this example but for most experiments.

3. Mass transfer in Gas-Liquid Reaction

3.1 Model for mass transfer at gas-liquid interface

Consider the transport of gaseous species *A* from a bulk gas to a bulk liquid, in which it has a measurable solubility, because of a difference of chemical potential of *A* in the two phases (higher in the gas phase). The difference may be manifested by a difference in concentration of A in the two phases. At any point in the system in which gas and liquid phases are in contact, there is an interface between the phases. The two-film model (Whitman, 1923; Lewis and Whitman, 1924, Levenspiel, 1999) postulates the existence of a stagnant gas film on one side of the interface and a stagnant liquid film on the other, as depicted in Figure 5. The concentration of *A* in the gas phase is represented by the partial pressure (p_A) and that in the liquid phase by c_A. In figure 5, subscript *i* denote conditions at the interface. The δ_g and δ_L are the thicknesses of the gas and liquid films respectively. The interface is real, while the two films are fictitious, and are represented by the dashed lines in Figure 5; hence, δ_g and δ_L are unknown. In the two-film model, the following assumptions are made:

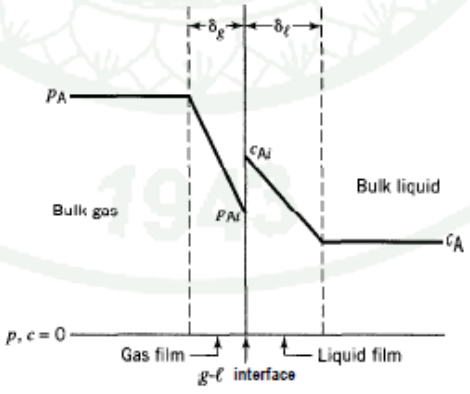

Figure 5 Schematic of two-film model (profiles) for mass transfer of *A* from gas phase to liquid phase (no reaction).

(a) The steady-state transport of A through the stagnant gas film is by molecular diffusion, characterized by the molecular diffusivity D_{Ag}. The rate of transport, normalized to refer to unit area of interface, is given by Fick's law

$$N_A = \frac{D_{Ag}(p_A - p_{Ai})}{RT\delta_g} = k_{Ag}(p_A - p_{Ai}) \quad (10)$$

where N_A is the molar flux of A, R the gas constant, T temperature, and k_{Ag} the gas-film mass transfer coefficient (Romanainen and salmi (1991, 1995); Levenspiel, 1999; Abhijart *et al.,* 2005) defined by

$$k_{Ag} = \frac{D_{Ag}}{RT\delta_g} \quad (11)$$

(b) Similarly, the transport of A through the liquid film is by molecular diffusion D_{Al} and the flux is the same as equations 11 and 12 at Steady-state) which can shown as follow

$$N_A = \frac{D_{Al}(c_{Ai} - p_{Ai})}{RT\delta_g} = k_{Al}(p_A - p_{Ai}) \quad (12)$$

where k_{Al} is the liquid-film mass transfer coefficient (Romanainen and salmi (1991, 1995) defined by

$$k_{Ag} = \frac{D_{Ag}}{\delta_l} \quad (13)$$

(c) There is equilibrium at the interface, which is another way of assuming that there is no resistance to mass transfer at the interface. The equilibrium relation may be expressed by means of Henry's law:

$$p_{Ai} = H_A c_{Ai} \tag{14}$$

where H_A is the Henry's law constant for species A.

3.2 Kinetic regime for two-film Model

The rate expressions developed in this section for gas-liquid systems, represented by reaction (Equation 15), are all based on the two-film model.

$$A(g) + B(l) \rightarrow C(l) \tag{15}$$

Since liquid-phase reactant B is assumed to be nonvolatile. The gas-phase reactant A must enter the liquid phase by mass transfer (see Figure 5). Reaction between A and B then takes place at some location within the liquid phase. At a given point, as represented in Figure 5, there are two possible locations: the liquid film and the bulk liquid. If the rate of mass transfer of A is relatively fast compared with the rate of reaction, then A reaches the bulk liquid before reacting with B. Conversely, for a relatively fast rate of reaction ("instantaneous" in the extreme), A reacts with B in the liquid film before it reaches the bulk liquid. Since the intermediate situation is also possible, we may initially classify the kinetics into three regimes which are reaction in bulk liquid only, reaction in liquid film only and reaction in both liquid film and bulk liquid, all of regime as shown in Figure 6.

The rates equation can result depending on the relative value of the constant k , k_g , k_l , the concentration ratio of reactants p_A / C_B and Henry's law constant. The eight special cases, each with its particular rate equation are from infinitely fast to very slow reaction, which can be divided eight cases, as follow

Table 2 Types of reaction for film theory

Cases	Types of reaction
A	Instantaneous reaction with low C_B
B	Instantaneous reaction with high C_B
C	Fast reaction in liquid film with low C_B
D	Fast reaction in liquid film with high C_B
E and F	Intermediate rate with reaction in the film and in the main body of liquid
G	Slow reaction in main body but with film resistance
H	Slow reaction, no mass transfer resistance

Source: Levenspiel (1999)

Case A Instantaneous reaction with low C_B

For case A, the rate of reaction between *A* and *B* is so high as to result in instantaneous reaction, then *A* and *B* cannot coexist anywhere in the liquid phase. The reaction is occurs at the liquid film. This is shown as a reaction plane as a Figure 6. At this point, C_A and C_B both become zero. Thus, the instantaneous rate of reaction at any moment in time can be calculated from Equation 16.

$$r_A'' = \frac{\frac{D_{Bl}}{D_{Al}}\frac{C_B}{b} + \frac{p_A}{H_A}}{\frac{1}{k_{Ag}a} + \frac{H_A}{k_{Al}a}} \tag{16}$$

where r_A'' is the rate of mass transfer of component *A*, H_A the Henry's law constant , k_{Ag} a gas phase mass transfer coefficient, k_{Al} a liquid phase mass transfer coefficient,

a a effective area, p_A a partial pressure of reactant A, $1/k_{Ag}a$ a gas film resistance, and $1/k_{Al}a$ a liquid film resistance.

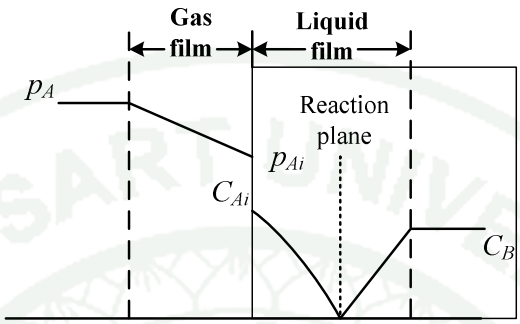

Figure 6 Schematic of instantaneous reaction rate for case A

Case B Instantaneous reaction with high C_B

In this case (Figure 7), the reaction will occur in interface of gas and liquid due to high concentration of *B*. The resistance in part of liquid can be neglected. The rate of mass transfer depends on the resistance in gas film only. The equation given by

$$-r''_A = k_{Ag} p_A \tag{17}$$

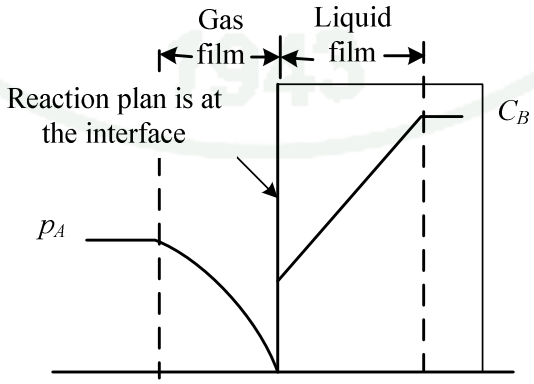

Figure 7 Schematic of instantaneous reaction with high C_B

Case C Fast reaction in liquid film with low C_B

The plane of reaction for case A now spreads into a zone of reaction in with *A* and *B* are both present. The reaction it fast enough so that this reaction zone remains totally within the liquid film. Thus no *A* enters the main body of liquid to react there. Since, the resistance of liquid is negligible. The concentration profiles as shown in Figure 8. The rate of this case can be written as:

$$r''_A = \frac{1}{\frac{1}{k_{Ag}a} + \frac{H_A}{k_{Al}a}} p_A \tag{18}$$

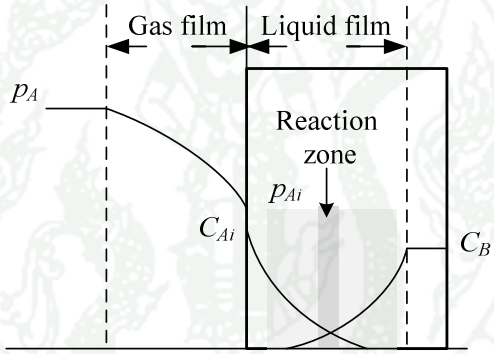

Figure 8 Schematic of fast reaction in liquid film with low C_B

Case D Fast reaction in liquid film with high C_B

This case can be considered pseudo first order rate with respect to *A*. For the special case, where C_B does not drop appreciably within the film. It can be taken to be constant throughout, and the second-order reaction rate (case C) simplifies to the more easily solve first-order expression. Thus the general rate expression as follow:

$$r''_A = \frac{1}{\frac{1}{k_{Ag}a} + \frac{H_A}{a\sqrt{D_A k C_B}}} p_A \tag{19}$$

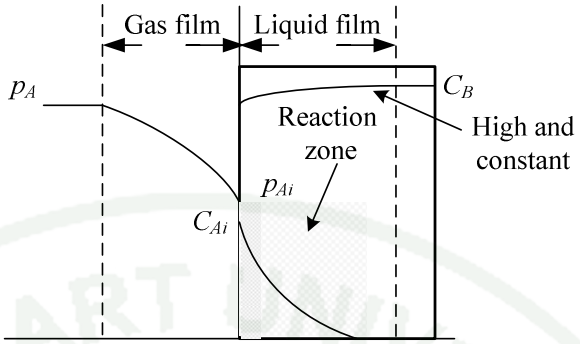

Figure 9 Schematic of fast reaction in liquid film with high C_B

Case E and F Intermediate rate with reaction in the film and in the main

Figure 10 show the intermediate rate with respect to mass transfer. The reaction is slow enough for some *A* to diffuse thought the film into the main body of the liquid. Consequently, a react both within the film and in the main body of the fluid. The general rate expression which has three resistances can be written as follow:

$$r''_A = \frac{1}{\frac{1}{k_{Ag}a} + \frac{H_A}{k_{Al}a} + \frac{H_A}{kC_B f_1}} p_A \qquad (20)$$

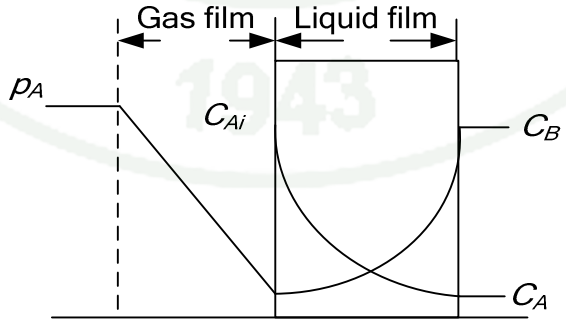

Figure 10 Schematic of intermediate rate with reaction in the film for case E

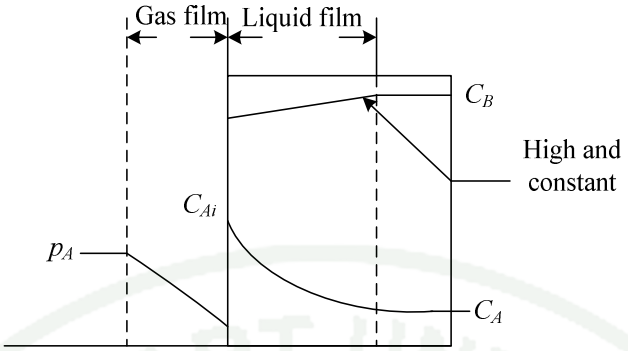

Figure 11 Schematic of intermediate rate with reaction in the film for case F

Case G Slow reaction in main body but with film resistance

In this case, the reaction is very slow as compare with mass transfer. This represents the somewhat curious case where all reactions occur in the main body of the liquid. However, the film still provides a resistance to the transfer of *A* into the main body liquid. Thus, three resistances enter into the rate expression as follow on equation (21)

Case H Slow reaction, no mass transfer resistance

For case H had shown infinitely slow reaction. The mass transfer resistance is negligible, the composition of *A* and *B* are uniform in liquid, and the rate is determined by chemical kinetic only that given by Equation (21)

$$r''_A = \frac{kf_1}{H_A} p_A C_B = kf_1 C_A C_B \qquad (21)$$

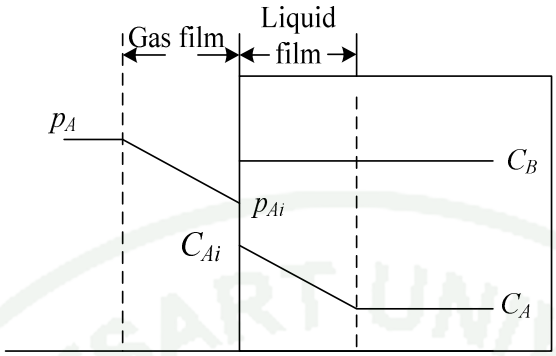

Figure 12 Schematic of Slow reaction in main the body of liquid for case G

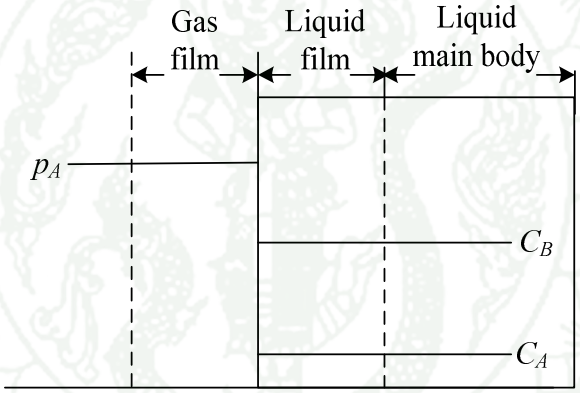

Figure 13 Schematic of Slow reaction, no mass transfer for case H

3.3 Absorption with Chemical Reaction

Let considered the case of a gas *A* which is absorbed by a liquid where it reacts irreversible with a dissolved reaction species *B*, according to the following chemical reaction:

$$A + \upsilon B \xrightarrow{k_1} P \tag{22}$$

A power-law kinetics rate from of $(m,n)^{th}$ order with respect to gas and liquid, respectively, is used. The two-film model then leads to the following differential equations for a simple irreversible reaction.

$$D_A \frac{d^2 C_A}{dx} = r \tag{23}$$

$$D_B \frac{d^2 C_B}{dx} = \upsilon r \tag{24}$$

where D_A and D_B are the molecular diffusion coefficient of A and B, C_A and C_B are the concentration of A and B in the liquid phase at the gas-liquid interface, r the rate of consumption of the gas by chemical reaction per unit liquid volume, ν the stoichiometry coefficient, and x the coordinate normal to the gas-liquid interface.

The rate of absorption can be calculated by general solution to the above set of differential equations. However, it is easier to classify the various regimes of absorption and to identify the controlling regime. This has some advantages when planning experiments. In order to show the various regimes for absorption of a gas in a reacting liquid, consider a $(m,n)^{th}$ order reaction whose rate then is given by

$$r = k_{mn} C_A^m C_B^n \tag{25}$$

The rate of absorption of the gas per unit gas-liquid interfacial area (R_{AS}) is given by the flux of the gas-liquid interface

$$R_{AS} = -D_A \left(\frac{dC_A}{dx} \right)_{x=0} \tag{26}$$

The normalization of the governing differential equations from Equations (25) and (26), following standard procedures, leads to the following dimensionless groups. The first group is Hatta number (Ha), which is the ratio of the maximum possible conversion in the liquid film to the maximum diffusional transport through the liquid film. It provides a measure of the extent of reaction in the film. The second group (q^*), which describes the movement of material within the liquid film, is visualized to occur by diffusion alone.

$$Ha = \left[\frac{2}{m+1} D_A k_{mn} (C_A^*)^{m-1} C_{Bl}^n \right]^{1/2} \tag{27}$$

and

$$q^* = \frac{C_{Bl} D_B}{\nu C_A^* D_A} \tag{28}$$

The famous Hatta number, *Ha*, is the main parameter which might be used to describe the regime in which the reaction is happening. The reaction regime can be fast, instantaneous or general (slow or moderately slow) as shown in Table 3. if the Hatta number is small, then the reaction is slow such that it will happen in the liquid film and it will continue in bulk liquid phase, However, if it is high, the reaction will be complete within in the liquid film and the concentration of the gas or key component will be zero at the edge of mass transfer film. For the case of an instantaneous reaction (a very high Hatta number), the gas and liquid reactants will react instantaneously as soon as they meet at a reaction plane inside the liquid film.

Table 3 Hatta number values with cases classification

Hatta number values	Cases
$Ha > 2$	Reaction occurs in liquid film cases A, B, C, and D.
$0.02 < Ha < 2$	In the intermediate region and the situation is more complex. cases E, F, G.
$Ha > 2$	the infinitely slow reaction case H.

Source: Levenspiel (1999)

This can be related to the Enhancement factor (*Ea*) by the following expression. The Enhancement factor (*Ea*) represents the ratio of observed rate of gas absorption to the maximum possible rate of gas-liquid mass transfer or, in the other words, the ratio of the actual rate of absorption with reaction to the rate of absorption without reaction.

$$Ea = \frac{R_{AS}}{k_L C_A^*} \tag{29}$$

It may be noted here that an alternative approach to the Enhancement factor (*Ea*) is to use the effectiveness factor, which is also known as the utilization factor. This is defined by the following expression (Froment and Bischoff, 1990; Kulkarni and Doraiswamy, 1975)

$$\eta_L = \frac{D_A (dC_A / dx)_{x=0} a}{k_{mn} \varepsilon_l (C_A^*)^m (C_{Bl})^n} \tag{30}$$

The Enhancement factor (Ea) given by Equation (29) is a function of the dimensionless groups Ha and q^* as defined earlier by Equation (27) and (28). If the reaction is an instantaneous reaction, the Enhancement factor (Ea) of an instantaneous reaction can be provided from the parameter q^*. If the Hatta number is far less than one ($Ha<1$), the reaction is slow enough that no appreciable reaction occurs in the gas-liquid film, but primarily occurs in the bulk of the liquid. The Hatta number is greater than one ($Ha>1$) for systems where appreciable reaction occurs in the liquid film. For this situation, the Enhancement factor (Ea) is generally shown as a plot of Hatta number with q^* as a parameter. An illustrative result is shown in Figure 14 for a $(1,1)$ order reaction.

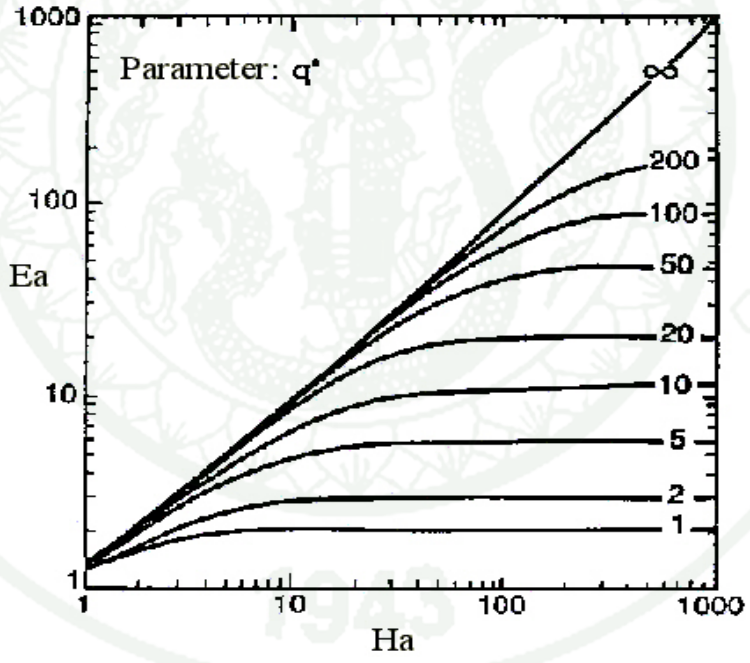

Figure 14 The Enhancement factor (Ea) verus Hatta number (Ha) with q^* as a parameter for a $(1,1)$ order reaction.

Several researchers and a lot of papers are devoted to study the mass transfer with chemical reaction using film theory. For fast first –order reactions, Hiroaka and Tanaka (1969) used the film theory to model chemical gas absorption.

Additionally, they used this model to study the effect of reaction rate on the concentration and temperature profiles and interfacial mass transfer rates of cyclohexane oxidation at 10 atm. Jozef Markos *et al.* (1998) have been simulated and experimented isothermal of gas-liquid reactor, both continuous and semi batch. The diffusion-reaction processes at gas-liquid interface, is based on the film model. They assumed that the model is steady state; isothermal conditions and reaction take place in liquid phase only. The dimensionless, steady state mass balance for generic i^{th} component is given by

$$\xi_i \frac{d\phi_{f,i}}{dx^2} = -Ha\sum_{j=1}^{N} \upsilon_j p_j R_j \qquad (31)$$

where ξ_i is the ratio of diffusivity, $\phi_{f,i}$ a dimensionless concentration in liquid film of component i, x a dimensionless film coordinate, and R_j a dimensionless of reaction rate. Furthermore, they obtained the computer code for the resulting of second order nonlinear differential equation. They applied their resulting for the example of catalytic oxidation and chlorination of *p*-xylene. They found that the simulation results agree with the experimental data.

Additionally, Hassen and Hubert (2003) studied the intermediate regime when a part of reaction occurs within the film and the bulk in bath conditions. The film theory is still used in the interface between gas and liquid. They found that, in a gas-liquid system, two steps control the overall reaction rates which are the mass transfer from the gas phase to liquid phase and chemical reaction in the liquid phase. Furthermore, this model was successfully tested during a series of experiments for fumaric acid ozonation in the bubble column.

Christine and Gabriel (2002) studied mass transfer with chemical reaction of slow regime using the film theory to describe mass transfer in the gas-liquid system; concentrations profiles in liquid film are represented schematically in Figure15. The system is isothermal and gas side mass transfer resistance is negligible

or gas *A* is pure, reactant *B* are non-volatile and steady state. The irreversible second order reaction has been chosen to study the influence of liquid phase hydrodynamics. They found that Danmkohler number and reaction rate parameters have important to consider the liquid hydrodynamics.

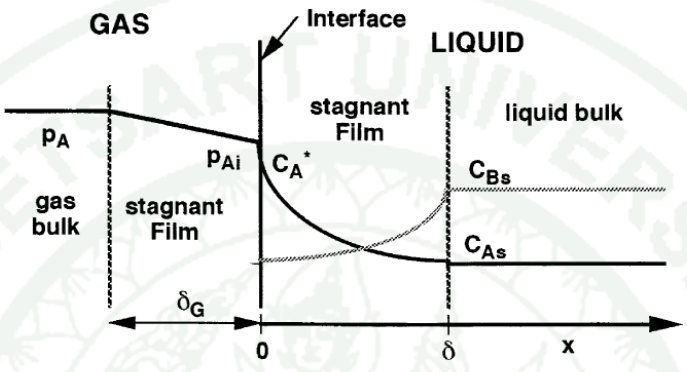

Figure 15 Mass transfer with chemical reaction: Concentration profiles in the diffusion film.

Abhijart *et al.* (2005) studied the mathematical and modeling of gas-liquid reactor using mixing cell model in co-current mode. The flow rate of gas and liquid throughout the reactors are constant. Additional, they represented the mathematical model in the bulk phase of gas and liquid and at the interface using film theory. The models applied for the gas liquid reaction of chlorination of butanoic acid and oxidation of cyclohexane which are industrially important system.

Juraj *et al.* (2007) obtained a non-equilibrium mathematical model of gas-liquid reactor. They presented the analysis of a CSTR with reactive separation for fast homogeneous chemical reaction in the liquid phase. To describe the vapor–liquid interface, the film model has been applied. They found that for the fast reactions, the liquid film can play an important role and can significantly influence the reactor behavior and the physical and chemical properties as well as the *V–L* equilibrium data for acetic acid esterification by ethanol have been used.

4. Model Accounting for Flow Pattern

Mixing Cell model

The mixing cell is useful to evaluate the performance of two or three phase reactor which has mixing characteristics intermediate to the ideal situations of plug flow and back mixing flow. This model is the mixing cell model where the actual reactor is portrayed as a number of completely backmixed reactors in series. The mixing cell model was developed based on the following assumptions, (1) the reactor has been visualized as consisting of N number of tanks in series, in each of which the liquid is completely mixed and the gas is in plug flow. The plug flow performance for whole reactor corresponds to $N = \infty$ or large while completely backmixed reactor corresponds to N=1. The intermediate values of N will correspond to liquid phase flow pattern between plug flows and perfectly mixed flow, (2) due to change in moles, the gas flow rate varies over the length of the reactor. Therefore, total gas phase balance has been considered in the current analysis, (3) the model can be used for co- and counter-current liquid flow. A schematic representation of the mixing cell model is shown in Figure 16.

Brahme *et al.* (1984) have been used the mixing cell model to simulate the hydrogenation of glucose and Jaganathan *et al.* (1987) proposed the hydrogenation of butynediol and the simulation has been used to predict the effect of various operating parameters on the reactor performance.

Carlos (2000) was modified the mixing cell model (MCM) for three phases reactor with significant back mixing in the liquid phase. Different phenomena are accounted for in the model: interfacial mass transfer limitations, adiabatic operation, phase distributions. All these effects are evaluated sequentially within repetitive cell unit.

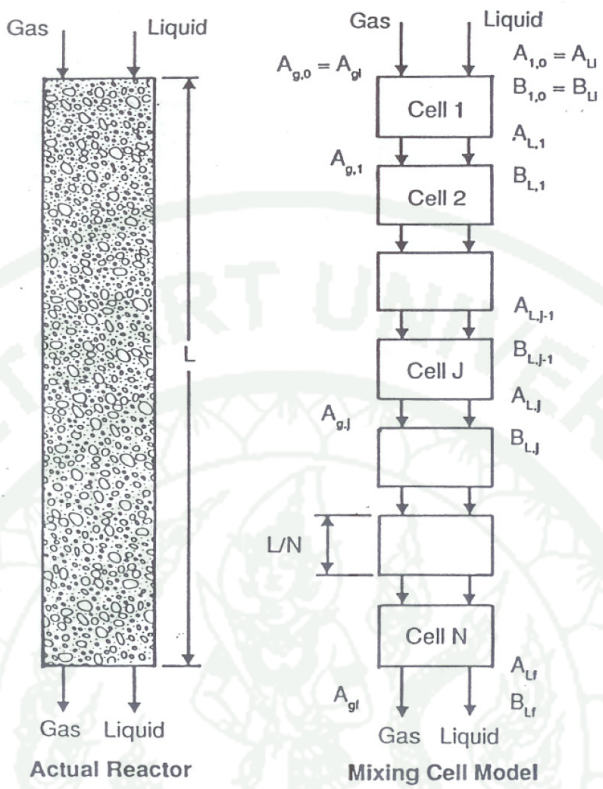

Figure 16 Schematic representation of mixing cell model

Axial Dispersion Model

The dispersion model is used to describe non ideal tubular reactors. In this model, there is an axial dispersion of the material, which is governed by an analogy to Fick's law of diffusion. This model applies to turbulent flow in pipes, laminar flow in long tubes, packed beds, shaft kilns, long channels, etc., (Levenspiel, 1999). Romanainen and salmi (1991, 1995) has been proposed dimensionless governing equations a single component in an axial dispersion reactor of bubble column which can be shown as

Liquid phase

$$\frac{d^2 n_i^b}{dX^2}\frac{(1-\varepsilon_g)}{Pe_L}-\frac{dn_i^b}{dX}+\sum_{j=1}^{NR} V(1-\varepsilon_g)\upsilon_j R_j^b+\alpha N_i^f\Big|_{Z=\delta_m}=0 \qquad (32)$$

Gas phase

$$\frac{d^2 n_i^g}{dX^2}\frac{(\varepsilon_g)}{Pe_g}-\frac{dn_i^g}{dX}+aN_i^f\Big|_{Z=0}=0 \qquad (33)$$

where Pe_L and Pe_g are Peclet number in liquid phase and gas phase respectively, and X is high of reactor.

5. Method for Solving Differential Equation

The boundary element method is a numerical computational method of solving linear partial differential equations which have been formulated as integral equations (i.e. in boundary integral form). It can be applied in many areas of engineering and science including fluid mechanics, acoustics, electromagnetics, and fracture mechanics. The integral equation may be regarded as an exact solution of the governing partial differential equation which can be used again to calculate numerically the solution directly at any desired point in the interior of the solution domain. The boundary element method is often more efficient than other methods, including finite elements, in terms of computational resources for problems where there is a small surface/volume ratio. Conceptually, it works by constructing a "mesh" over the modelled surfacet which shown as Figure 17. Boundary element formulations typically give rise to fully populated matrices. This means that the storage requirements and computational time will tend to grow according to the square of the problem size.

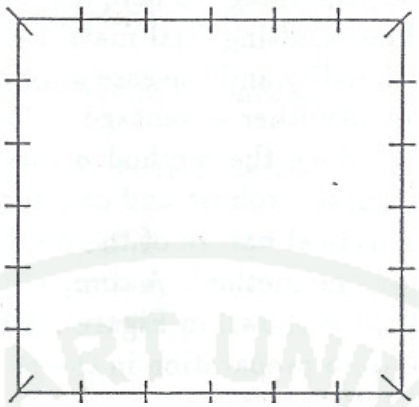

Figure 17 Schematic of boundary element discretization of an arbitrary two dimensional.

Ramachandran (1991) has been used the boundary integral element method for solving the solution of the linear diffusion-reaction equation in two dimensions. In this method the dimensionality of the problem is reduced by one by choosing the modified zero-order Bessel function of the second kind as the weighting function. The method can be extended to three-dimensional problems with the associated benefits of reduction in dimensionality. A number of examples are presented to illustrate the method. One such case study presented is the calculation of catalyst effectiveness factor in trickle beds under conditions of partial wetting.

Lesage *et al.* (1999) has been applied the boundary element method to solve highly non-linear differential equations describing hydrodynamics and liquid/solid mass transfer at the wall of a packed-bed reactor with single-phase liquid flow. It is based on the boundary integral element concepts where both the dependent variable and its gradient become the primary variables. The mass transfer experimental measurements, obtained for four different Schmidt numbers, are in good agreement with the computed predictions when uniform velocity profiles are used.

Ramachandran (2005) has been proposed the Boundary integral method to solve a system of differential equations with a convection-diffusion operator and a

nonlinear rate term for each equation. The operator part can be eliminated by using an inverse formulation by a proper choice of the weighting function for each differential equation. This reduces the problem to an integral formulation which is then solved by approximating the dependent variables by cubic osculation. The method has been demonstrated to a packed bed reactor with heat and mass dispersion and for a counter current heat exchanger.

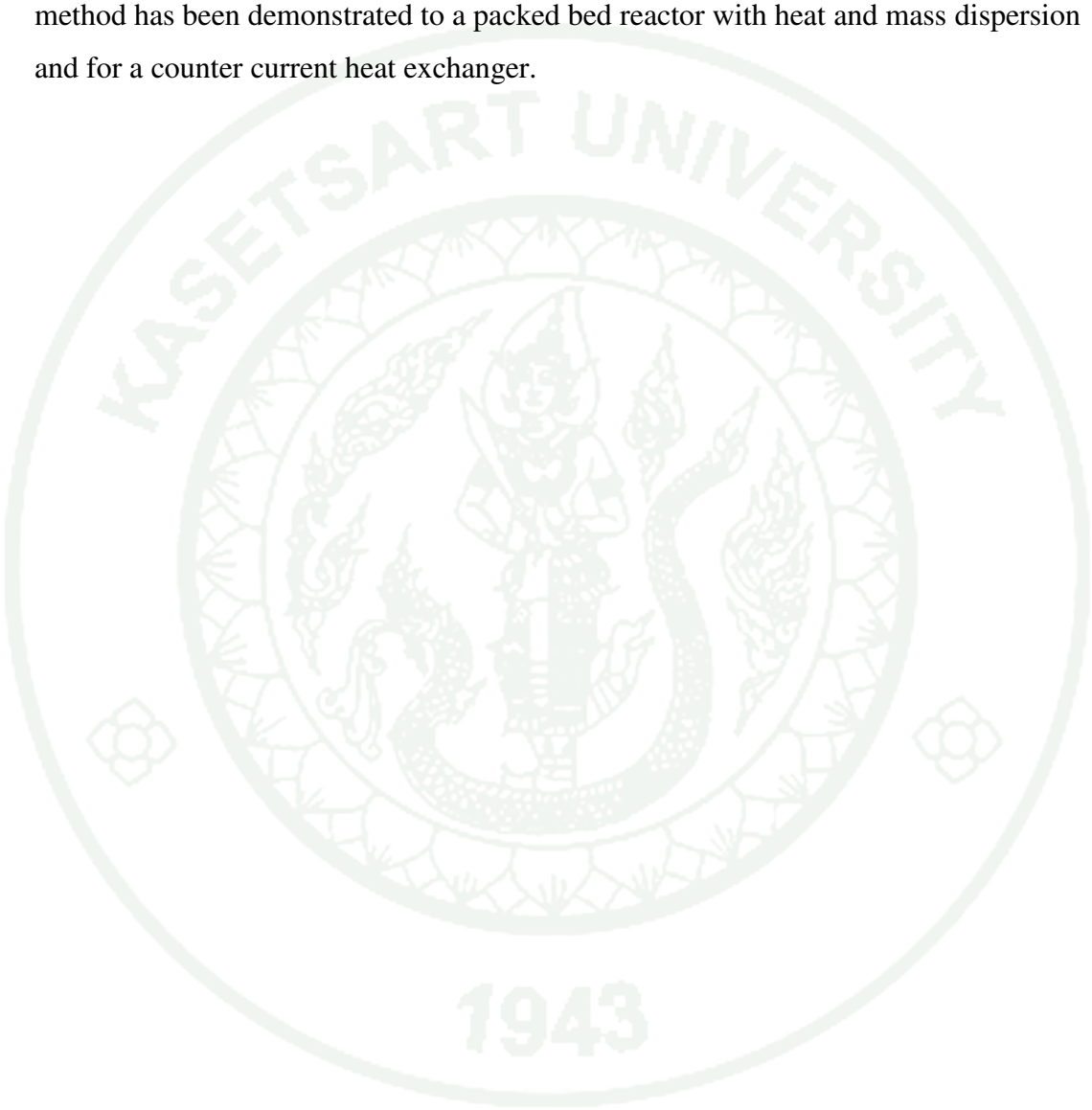

MATERIAL AND METHODS

Material

The program code was written in Matlab and complied in a computer Pentium III MMX 500HZ.

Methods

This research develops a mathematical model for gas-liquid reactor using film theory. This model is tested in three case studies which are absorption of CO_2-NaOH, H_2S-Fe^{3+} (EDTA) reaction, and CO_2-Na_2CO_3 reaction. These three cases represent the very fast, intermediate and slow reaction regimes. In this work is carried out in four sections. Section 1 is to develop of mathematical models for the coupling of mixing cell in the bulk of gas and liquid phases in co-current and counter current mode. Section 2 is developed of mathematical models for the reactor model. Section 3 is to solve of mathematical models by the Boundary Element method (BEM). This section indicated that how the film model can be solved by using boundary element method and it then show how the reactor model can be often solved simply by modifying the boundary condition of the film model. Last section, (4) the applied of the model to case study and Lo-cat process. The details of these sections are show as follow:

1. Mathematical Models for CSTR Gas and Liquid Reactors

In a general gas-liquid reactor, reaction occurs only in the liquid phase. Development of mathematical model was done in two parts. The first part involves heat and mass balances of all components in each phase, i.e., gas and liquid phases. The second one deals with heat and mass transfer and chemical reaction in the film. The reactor can be operated in either co-current or counter-current mode. The details are as follow.

1.1 Mathematical Model: Heat and Mass Balances in Bulk Phases

Heat and mass balances in bulk phases of a gas- liquid reactor are obtained in co-current and counter-current modes using the mixing-cell approach. In the mixing-cell model, the number of mixing-cell is used to indicate the flow behavior within the reactor. If the number of mixing cells approaches to one, the flow in the reactor is complete mixed (i.e., a CSTR) which has high degree of mixing. If the number of the mixing cells approaches to infinity, it has low degree of mixing in contrast CSTR (i.e.,a plug flow reactor). Figure 18 shows the general of the mixing-cell model in the co-current and counter-current modes. In the mixing-cell model, the actual reactor is portrayed as a number of mixing cells of completely backmixed reactors connected in series. The mixing cells number for gas and liquid phases are not necessary to be equal depending on each phase behavior. The assumptions for the heat and mass balances are: (1) the gas-liquid system is at steady state; (2) the reaction only takes place in liquid phase; (3) in each cell, the gas and liquid phases are well mixed; and (4) the volumetric liquid flow rate is constant.

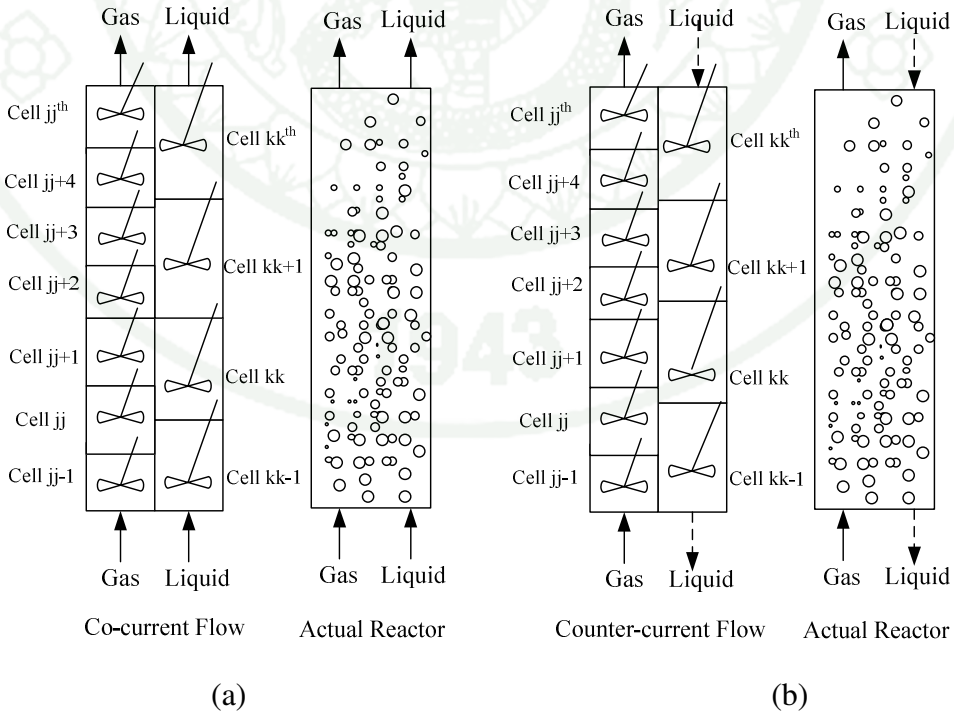

Figure 18 Diagram of mixing-cell model in co-current and counter-current modes.

In this work, between gas and liquid phases, there are gas film and liquid film. Figure 19 shows one cell, jj^{th} cell, of the mixing-cell model. This special case, the mixing cell number of gas and liquid are equal. The mass balance for gas and liquid bulk phases can be developed as follows.

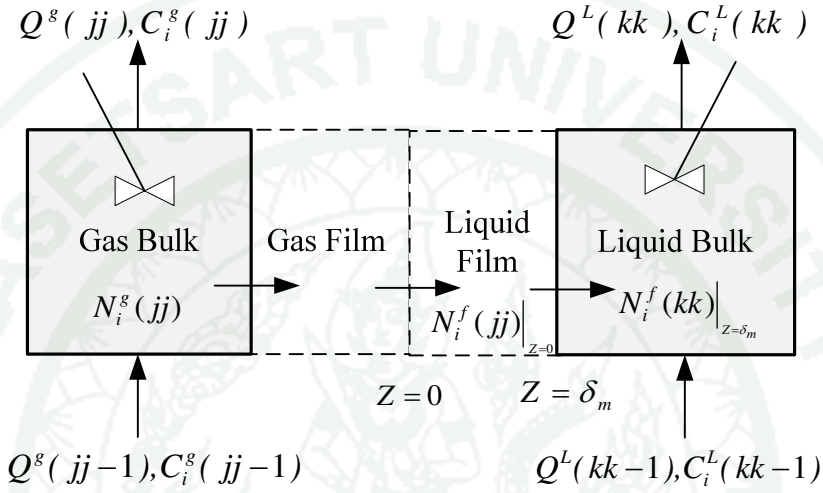

Figure 19 Diagram of one cell of mixing-cell model. The $Z=0$ and $Z=\delta_m$ are the positions of gas-liquid and liquid film-liquid bulk interfaces respectively.

Mass balance in gas phase

The control volume for mass balance in gas bulk is shown in Figure 20. The mass balance for component i in gas bulk of the mixing cell jj, is written in Equation 34. The right hand side indicates the molar flow rates of the inlet and outlet streams respectively, and the left hand side represents the molar flow rate of gas from gas bulk into gas film.

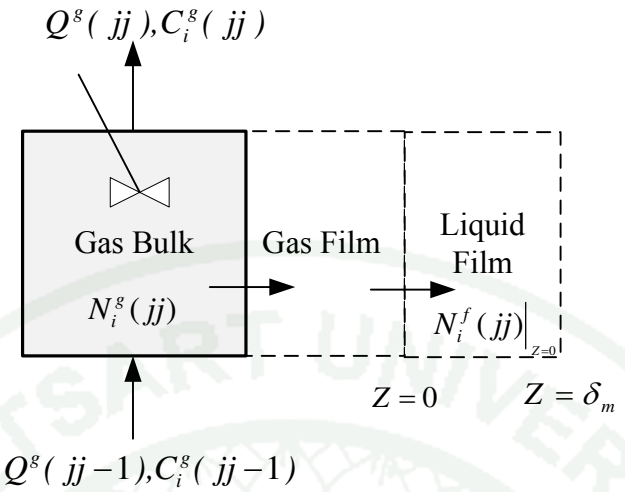

Figure 20 Diagram of mass balance in gas phase. Control volume for gas bulk is shown in shaded area.

$$aV_{cell}N_i^g(jj) = n_i^g(jj-1) - n_i^g(jj) \tag{34}$$

where a is an interfacial area per volume of reactor, V_{cell} a volume of a mixing cell, N_i^g an interfacial molar flux of component i in gas phase, and n_i^g the molar flow rate of component i in gas phase. The molar flow rate is defined as

$$n_i^g = Q_i^g C_i^g \tag{35}$$

where Q_i^g is a volumetric flow rate of gas feed and C_i^g the molar concentration of component i in gas phase.

From the assumption, the reactions take place in the liquid phase only. Thus, the molar fluxe from gas bulk is equal to the interfacial molar flux from the gas film at the gas-liquid interface.

$$N_i^g(jj) = N_i^f\big|_{Z=0}(jj) = -D_i \frac{dC_i^f(jj)}{dZ}\bigg|_{Z=0} \tag{36}$$

The N_i^f and C_i^f are the interfacial molar flux and molar concentration of species i in the liquid film respectively. The mass balance for the species i in gas bulk of the jj^{th} mixing cell is written as follows:

$$-aV_{cell}D_i\left.\frac{dC_i^f(jj)}{dZ}\right|_{Z=0} = Q^g(jj-1)C_i^g(jj-1) - Q^g(jj)C_i^g(jj) \qquad (37)$$

where D_i is defined as molar liquid phase diffusivity of component i.

The gas phase mass balance given by Equation (37) can be formulated into dimensionless form as follows:

$$f^g(jj-1)c_i^g(jj-1) - f^g(jj)c_i^g(jj) + \left[\frac{\alpha_{gL}}{N_g}\right]\gamma_{Fi}s_i\left.\frac{dc_i^f(jj)}{d\xi}\right|_{\xi=0} = 0 \qquad (38)$$

where c_i^g is dimensionless of gas phase concentration defined as

$$c_i^g = \frac{C_i^g}{C_{i,ref}^g} \text{ and } c_i^f = \frac{C_i^f}{C_{i,ref}} \qquad (39)$$

where $C_{i,ref}^g$ is the reference gas phase reactant concentration and $C_{i,ref}$ a reference liquid concentration ($C_{i,ref} = C_{i,ref}^g / H_{i,ref}$). $H_{i,ref}$ the reference Henry's law constant for species i, N_g the mixing cell number of gas phase, and f^g the dimensionless of flow rate of gas ($f^g = Q^g / Q_{ref}^g$)The dimensionless film thickness is defined as that $\xi = Z/\delta_m$. The parameters appearing in Equation 38 are defined as follows:

The Damkohler number for mass transfer is

$$\alpha_{gL} = \frac{aV_{cell}k_L}{u_{ref}^L A_r} \tag{40}$$

where k_L is a liquid side mass transfer coefficient based on concentration driving force, u_{ref}^L is the reference superficial velocity of liquid phase being liquid feed reference, and A_r is a cross section area of the reactor. The effective gas to liquid flow rate ratio is written as

$$\gamma_{Fi} = \frac{u_{ref}^L}{u_{ref}^g H_{i,ref}} \tag{41}$$

and s_i is the diffusivity ratio.

$$s_i = \frac{D_i}{D_{ref}} \tag{43}$$

where D_{ref} is the diffusivity of chosen reference (key) component.

Mass balance in liquid phase

The control volume for mass balance in liquid bulk in co-current mode shows in Figure 21. The mass balance for component i in liquid phase of the mixing cell kk^{th}, is written in Equation 45. where the first term in the left hand side of Equation 43 represents the mass flux of component i coming from the liquid film and the two terms in the right hand side indicate the molar flow rate of the liquid inlet and outlet respectively, and the last term is the consumption by chemical reaction in the bulk of liquid phase,

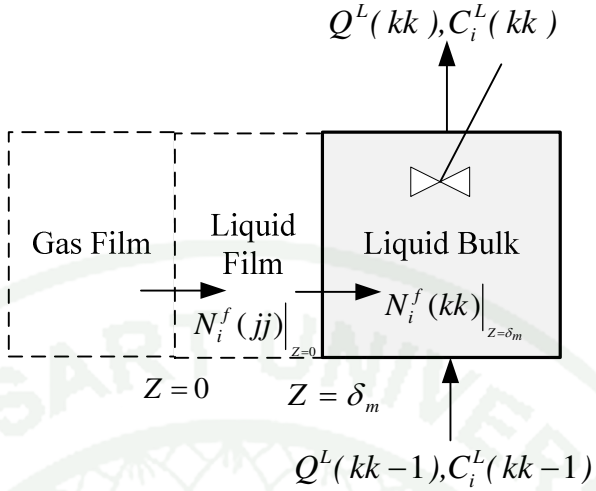

Figure 21 Diagram of mass balance in liquid phase. Control volume for liquid bulk in co-current mode is shown in shaded area.

The mass balance of gas bulk in co-current mode at the steady state conditions can be written as follow:

$$-aV_{cell} N_i^f\Big|_{Z=\delta_m}(kk) = aVD_i \frac{dC_i^f(kk)}{dZ}\Big|_{z=\delta_m}$$
$$= n_i^L(kk-1) - n_i^L(kk) - \sum_{j=1}^{NR} V(\varepsilon_L - a\delta_m)\nu_{ji} R_j^b \tag{43}$$

where $N_i^f\big|_{Z=\delta_m}$ is the mass flux at δ_m again given by Fick's law, ε_L the liquid phase hold up, ν_{ji} a stochiometry of component i in reaction j, and R_j^b a function for reaction j in liquid bulk. The molar flow rate of component i in liquid phase, n_i^L, is written as

$$n_i^L = Q_i^L C_i^L \tag{44}$$

where Q_i^L is a volumetric flow rate of the component i in liquid phase and C_i^L the molar concentration of component i in liquid phase.

The rate function for reaction j in liquid bulk, R_j^b, is written as

$$R_j^b = k^L C_A^L C_B^L \tag{45}$$

where k^L is reaction rate constant, The rate constant in Equation (47) can be written as a product of temperature independence term.

$$k^L = k_{ref} \exp\left[\frac{Ea}{R}\left[\frac{1}{T^L} - \frac{1}{T_{ref}}\right]\right] \tag{46}$$

Substituted Equation (47) into Equation (46) and rearranging, the liquid phase mass balance given by Equation (45) can be formulated into dimensionless form as follows:

$$s_i \frac{\alpha_{gL}}{N_g} \frac{dc_i^f(kk)}{d\xi}\bigg|_{\xi=1} = f_i^L(kk-1)c_i^L(kk-1) - f_i^L(kk)c_i^L(kk) - \frac{1}{\omega_i}\sum_{j=1}^{NR} \upsilon_{ji} \frac{M_j}{N_l} r_j^b \, exp(\gamma(1 - \frac{1}{\theta^L(kk)})) \tag{47}$$

where f_i^L is dimensionless liquid flow rate, c_i^L the concentration of component i in liquid phase, ω_i the ratio of the reference liquid phase reactant concentration (liquid feed condition) to the reference gas phase reactant concentration (gas feed condition), $\omega_i = C_{i,ref} / C_{ref}$, N_l the mixing cell number of liquid. The kinetic parameter of reaction j, M_j, appearing in Equation 47 is written as

$$M_j = \frac{V_{cell}(\varepsilon_L - a\delta_m)R_j^{ref}}{Q_L^{ref} C_{ref}} \tag{48}$$

where $r_j^b = R_j^b / R_j^{ref}$ is the dimensionless representation of the rate function.

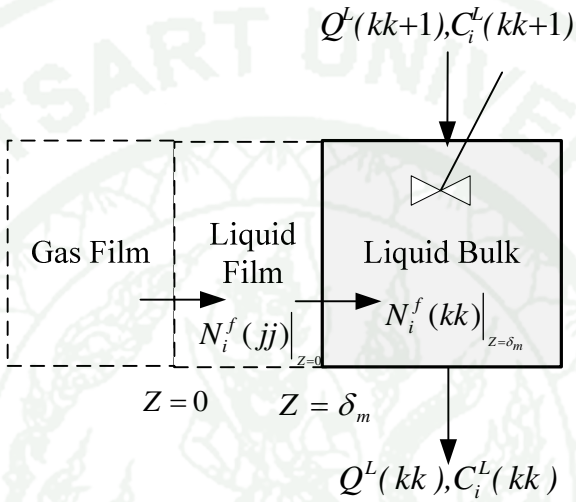

Figure 22 Diagram of mass balance in liquid phase. Control volume for liquid bulk in counter-current mode is shown in shaded area.

The counter current mode is the two flows move in opposite directions which the gas phase flows upwards and the liquid phase flows downwards. The control volume for mass balance of the liquid bulk is shown in Figure 22. The equation for gas phase in counter current mode is the same as co-current mode while the equation for liquid phase is difference. The mass balance equation for counter current mode is written as follow:

$$aV_{cell} D_i \left.\frac{dC_i^f(kk)}{dZ}\right|_{z=\delta_m} = n_i^L(kk+1) - n_i^L(kk) - \sum_{m=1}^{NR} V_{cell}(\varepsilon_L - a\delta_m)\nu_m R_m^b \tag{49}$$

The dimensionless mass balance in liquid phase in counter-current mode can be formulated as follow:

$$s_i \frac{\alpha_{gL}}{N_g} \frac{dc^f(kk)}{d\xi}\bigg|_{\xi=1} = f_i^L(kk+1)c_i^L(kk+1) - f_i^L(kk)c_i^L(kk) - \frac{1}{\omega_i}\sum_{j=1}^{NR} \upsilon_{ji} \frac{M_j}{N_l} r_j^b \, exp(\gamma(1-\frac{1}{\theta^L(kk)})) \quad (50)$$

1.1.3 Heat balance in gas phase

The control volume for heat balance in gas bulk is shown in Figure 23.

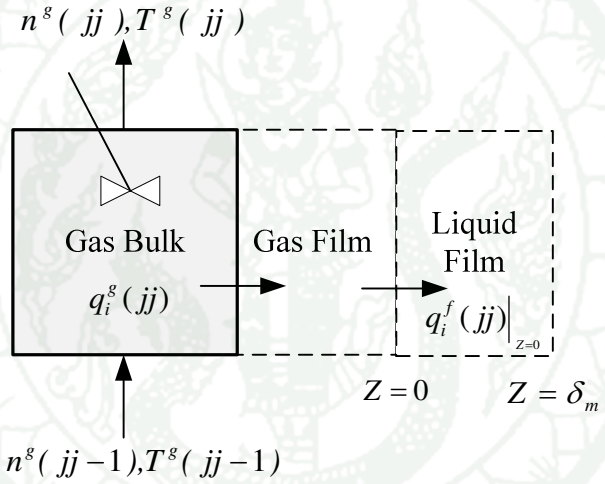

Figure 23 Diagram of heat balance in gas phase. Control volume for gas bulk in co- current mode is shown in shaded area.

The steady state heat balance of gas-liquid reactor is shown in Equation (51). The first term of Equation (51) represents the heat fluxes of the gaseous component transferred from bulk gas to gas film. The two terms in the right hand side indicate the heat rate of the liquid inlet and outlet respectively. The heat fluxes from the gas bulk are transferred into gas film which can be written as

$$aV_{cell}q^g = m^g(jj-1)\overline{C}_p^g T^g(jj-1) - m^g(jj)\overline{C}_p^g T^g(jj) \quad (51)$$

where T^g is a temperature in gas phase, $\overline{C}_p^g$ an average heat capacity of gas phase, and m^g a mass flow rate of gas phase.

Assuming mixing cell model, and no reaction in gas phase, the heat flux from gas bulk is equal to heat flux at the interface (Z=0). $q^g = q^f\big|_{Z=0}$ the net rate of heat conduction in bulk of gas to interfacial flux to the liquid given by Fourier's law as

$$q^f(jj)\big|_{z=0} = -\kappa \frac{dT^f(jj)}{dZ} \tag{52}$$

The heat balance for gas phase of mixing is written as follows

$$-aV_{cell}\kappa \frac{dT^f(jj)}{dZ} = m^g(jj-1)\overline{C}_p^g T^g(jj-1) - m^g(jj)\overline{C}_p^g T^g(jj) \tag{53}$$

where $q^f\big|_{Z=0}$ is the heat flux at the interface which can be described by Fourier's law. Furthermore, where κ is an average thermal conductivity of gas phase, and the dimensionless equation for gas phase heat balance can be formulated as

$$s_g \left.\frac{d\theta^f(jj)}{d\xi}\right|_{\xi=0} = \theta^g(jj-1) - \frac{f^g(jj-1)}{f^g(jj)}\theta^g(jj-1) \tag{54}$$

θ^g is a dimensionless gas phase temperature

$$\theta^g = \frac{T^g}{T^g_{ref}} \text{ and } \theta^f = \frac{T^f}{T^g_{ref}} \tag{55}$$

s_g is the dimensionless of heat transfer term for gas phase

$$s_g = \frac{aV_{cell}\kappa}{m_g \delta_m \overline{C_p^g}} \tag{56}$$

Heat balance in liquid phase

The control volume for heat balance in liquid bulk in co-current and counter current modes shown in are show in Figure 24 and 25, respectively. The heat balance of liquid phase for co- current flow is given by Equation 58.

$$-aVq_i^f(kk)\Big|_{Z=\delta_m} = aV\kappa \frac{dT^f(kk)}{dZ}\Big|_{z=\delta_m} = m_i^L(kk-1)\overline{C}_P T^L(kk-1)$$
$$-m_i^L(kk)\overline{C}_P T^L(kk) - \sum_{j=1}^{NR} V_{cell}(\varepsilon_L - a\delta_m)\nu_{ji} R_j^b(-\Delta H_{r,j}) \tag{57}$$

where m_i^L is defined as mass flow rate of liquid phase, The dimensionless liquid heat balance equation can be written as

$$\alpha_{gL} Le \frac{d\theta^f(kk)}{d\xi}\Big|_{\xi=1} = \theta^L(kk-1) - \frac{f^L(kk)}{f^L(kk-1)}\theta^L(kk)$$
$$-\frac{1}{\omega_i}\sum_{j=1}^{NR} B\nu_{ji} M_j r_j^b \exp\left[\gamma\left(1-\frac{1}{\theta^L(kk)}\right)\right] \tag{58}$$

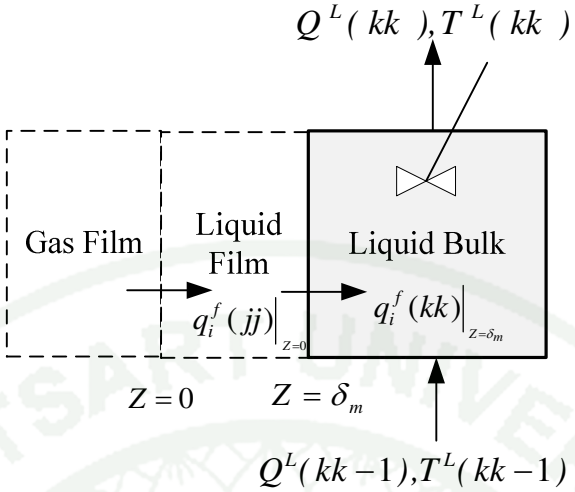

Figure 24 Diagram of heat balance in liquid phase. Control volume for liquid bulk in co-current mode is shown in shaded area.

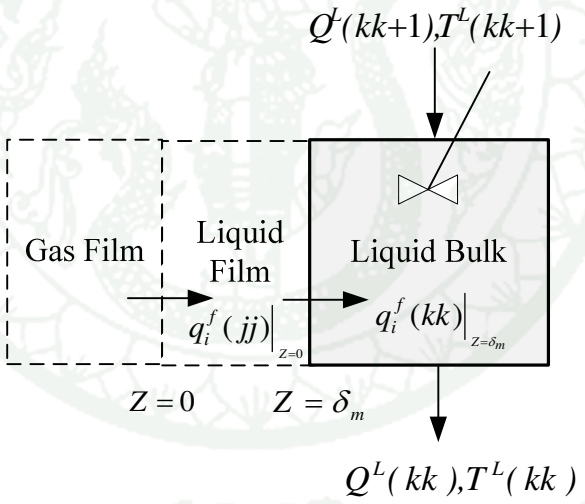

Figure 25 Diagram of heat balance in liquid phase. Control volume for liquid bulk in counter-current mode is shown in shaded area.

The heat balance of liquid phase for counter current flow is given by

$$-aVq_i^f(kk)\Big|_{Z=\delta_m} = aV\kappa\frac{dT^f(kk)}{dZ}\Big|_{z=\delta_m} = m_i^L(kk+1)\overline{C}_p^L T^L(kk+1) - m_i^L(kk)\overline{C}_p^L T^L(kk) - \sum_{j=1}^{NR} V_{cell}(\varepsilon_L - a\delta_m)\nu_{ji}R_j^b(-\Delta H_{r,j}) \quad (59)$$

The dimensionless liquid heat balance equation can be written as

$$\alpha_{gL}Le\frac{d\theta^f(kk)}{d\xi}\Big|_{\xi=1} = \theta^L(kk+1) - \frac{f^L(kk)}{f^L(kk-1)}\theta^L(kk) - \frac{1}{\omega_i}\sum_{j=1}^{NR} B\nu_{ji}M_j r_j^b \exp\left[\gamma\left(1-\frac{1}{\theta^L(kk)}\right)\right] \quad (60)$$

where Le is the Lewis number ($Le = \lambda_L / \rho_L C_p^L D_{ref}$) and B the heat of reaction parameter defined as

$$B = -\frac{\Delta H_r C_{ref}}{\rho_L C_p^L T_{ref}} \quad (61)$$

1.2 Mathematical Model: Film Model

In this section, the mathematical model of gas-liquid reaction at the interface using film theory is presented together with the heat and mass balance in liquid film including the boundary conditions at the interface of gas-liquid($Z = 0$) and at liquid film-liquid bulk (Z = δ_m).

Mass balance in liquid film

The steady state mathematical model in liquid film based on the film theory is developed. For the liquid film with simultaneous reaction and diffusion according to Fick's second law, the equation of mass transfer between the gas and liquid phase is described based on the film model is written as

$$D_i \frac{d^2 C_i^f}{dZ^2} = -\sum_{j=1}^{NR} v_{ji} R_j \tag{62}$$

where v_{ji} is a stoichiometric coefficient of species i in any reaction j, R_j the rate of consumption by chemical reaction per unit liquid volume, and Z the coordinate normal to the gas-liquid interface.

The dimensionless steady state mass balance for component i is given by

$$\frac{d^2 c_i^f}{d\xi^2} = \frac{1}{s_i \omega_i} \sum_{j=1}^{NR} v_{ji} Ha_j^2 r_j \tag{63}$$

where c_i^f is a dimensionless concentration ($c_i^f = C_i^f / C_{i,ref}$), ξ a dimensionless distance in the film ($\xi = Z/\delta_m$), Ha_j is the Hatta number for reaction j ($Ha_j^2 = \delta_m^2 R_j(C_{i,ref}) / D_{ref} C_{ref}$), NR is the total number of reactions studied in the model, and r_j is a dimensionless rate for j reaction.

The boundary conditions for mass balance in liquid film

The equation of mass transfer between gas and liquid phase (Eq. (64)) in liquid film is non-linear second order differential equation. Two boundary conditions are required to solve this equation. The applicable conditions are the conditions at the

interface (Z = 0) and at the boundary between the liquid film and liquid bulk (Z = δ_m).

Boundary condition at Z = 0

As mentioned above, to solve the film model, interface molar fluxes are needed. The mass flux of components from gaseous phase enters into liquid. From the assumption, the reaction takes place only in liquid film so that the molar fluxes in the gas phase are equal to molar flux at the interface (Z = 0),
Thus

$$N_i^g = N_{i,Z=0}^f \tag{64}$$

The driving force between the concentrations in the gas bulk and at the interface (Z = 0) is written as

$$N_i^g = k_{g,i}(p_{g,i} - p_{i,Z=0}) \tag{65}$$

where $k_{g,i}$ is the gas phase mass transfer coefficient for species i, $p_{g,i}$ is the partial pressure of component i in the gas bulk and $p_{i,Z=0}$ is an interfacial partial pressure of component i at the interface (Z = 0). The mass flux at the interface is described by Fick's law equation.

$$N_{i,Z=0}^f = -D_i \frac{dC_{i,Z=0}^f}{dZ} \tag{66}$$

where $C_{i,Z=0}^f$ is defined as concentration of component i at the interface (Z = 0). From Equation (66), the interfacial partial pressure ($p_{i,Z=0}$) is related to interfacial liquid concentration. It can be described by Henry's law. The Henry's law is used to describe the equilibrium relationship between the liquid concentration and vapor concentration. At equilibrium, the partial pressure of a gas above a liquid is

proportional to the concentration of the chemical in the liquid. Henry's law expressed as

$$p_{i,Z=0} = H_i C^f_{i,Z=0} \tag{67}$$

where H_i is the Henry's law constant which can be related to the Henry's constant $H_{ref,i}$ based on a reference temperature T_{ref} and is written as:

$$H_i = H_{ref,i} h\left(\theta_{\xi=0}\right) \tag{68}$$

where $\theta_{\xi=0}$ is the dimensionless interfacial temperature and $h\left(\theta_{\xi=0}\right)$ is defined as the temperature dependency function. Thus,

$$h(\theta) = exp\left[\gamma_{si}\left(1-\frac{1}{\theta}\right)\right] \tag{69}$$

the activation parameter for solubility is written as:

$$\gamma_{si} = \frac{-\Delta H_{si}}{RT_{ref}} \tag{70}$$

and the activation parameter for vaporization is written as

$$\gamma_v = \frac{-\Delta H_V}{RT_{ref}} \tag{71}$$

where ΔH_{si} is the heat of solution, ΔH_V is the heat of vaporization, and R is the gas constant. The dimensionless equation corresponding to Equations (65)-(69) can be formulated as

$$Bi_{m,i}(c^{*}_{g,i} - h(\theta^{f}_{\xi=0})c^{f}_{i,\xi-0}) = -\left.\frac{dc^{f}_{i}}{d\xi}\right|_{\xi=0} \tag{72}$$

where $Bi_{m,i}$ is the Biot number for mass transfer, $c^{*}_{g,i}$ is a concentration in gas phase, $c^{f}_{i,\xi-0}$ is the concentration at the interface ($\xi = 0$), The Biot number for gas phase mass transfer, $Bi_{m,i}$ was defined as

$$Bi_{m,i} = \frac{\delta_m H_{i,ref} k_g}{D_i} \tag{73}$$

the concentration in gas phase, $c^{*}_{g,i}$, is obtained as

$$c^{*}_{g,i} = \frac{C_{g,i}}{C_{i,ref}} = \frac{p_{g,i}}{H_{ref,i} C_{ref,i}} \tag{74}$$

If the condition is in the case of non-volatile components, $Bi_{im,i}$ is zero. Then boundary condition at $\xi = 0$ reduces to the no mass flux condition so that Eq (73) is written as

$$\left.\frac{dc^{f}_{i}}{d\xi}\right|_{\xi=0} = 0 \tag{75}$$

Boundary condition at $\xi = 1$

The concentration at the boundary condition $\xi = 1$ or the concentration at the interface between liquid film and liquid bulk is equal to concentration in the bulk of liquid. The dimensionless of concentration at the boundary condition $\xi = 1$ can be written as

$$c^{f}_{i,\xi=1} = c^{b}_{i} \tag{76}$$

where $c^{f}_{i,\xi=1}$ is the dimensionless of concentration at the boundary condition $\xi = 1$ and c^{b}_{i} the dimensionless of concentration in the bulk of liquid, $C^{i}_{b} / C_{ref,i}$.

Heat balance in liquid film

The heat transfer in the liquid film is given by

$$\lambda_{L}\left(\frac{d^{2}T^{f}}{dZ^{2}}\right) = \sum_{j=1}^{NR}(-\Delta H_{r})R_{j} \tag{77}$$

where λ_{L} is the liquid thermal diffusivity, T^{f} the temperature in liquid film and ΔH_{r} is a heat of reactions. The dimensionless formula for heat balance was obtained:

$$\frac{d^{2}\theta^{f}}{d\xi^{2}} = -\sum_{m=1}^{NR} Ha^{2}\beta r \tag{78}$$

where θ^{f} is a dimensionless temperature in liquid film and β the heat of reaction parameter for the *j* reaction is written as

$$\beta = \frac{(-\Delta H_{r,j})D_{ref}C_{ref}}{\lambda_{L}T_{ref}} \tag{79}$$

where T_{ref} is the reference temperature for normalization.

Boundary condition at Z =0

Boundary condition at Z =0 for heat transfer is described in Equation (78). The Fourier's law conductive heat flux equals the summation of three heats which are heat convection, heat of solution and heat of condensation respectively.

$$-\lambda_L\left(\frac{dT^f_{(j)}}{dZ}\right)=h_g(T^g-T^f_{Z=0})+(-\Delta H_{si})\left(-D_i\frac{dC^f_{i,(j)}}{dZ}\right)_{Z=0}+(-\Delta H_V)\left(-D_i\frac{dC^f_{i,(j)}}{dZ}\right)_{Z=0} \tag{80}$$

where h_g is the heat transfer coefficient of gas phase, ΔH_s a heat of solution, and ΔH_V the heat of evaporation. The dimensionless of equation is given by Equation (84)

$$-\left(\frac{d\theta^f}{d\xi}\right)_{\xi=0}=Bi_H(\theta^g-\theta^f_{\xi=0})-\sum_{i=1}^{Ns}\beta_{si}\left(\frac{dc_i^f}{d\xi}\right)_{\xi=0} \tag{81}$$

where Bi_H is the Biot number for heat transfer, $\theta^f_{\xi=0}$ the dimensionless temperature at the interface ($\xi = 0$), and β_{si} a parameter of heat of solution at interface.

As mention above, the dimensionless quantities are defined.

Biot number for heat transfer, $Bi_H=\dfrac{h_g\delta_m}{\lambda_L}$ (82)

Dimensionless temperature at the interface, $\theta=\dfrac{T}{T_{ref}}$ (83)

Parameter of heat of solution at interface, $\beta_{si}=\dfrac{(-\Delta H_{si})D_iC_{i,ref}}{\lambda_L T_{ref}}$ (84)

Boundary condition at $Z = \delta_m$

The boundary condition at $Z = \delta_m$ is obtained from the fact that the heat transfer thickness is larger than the mass transfer film thickness. Therefore there is the temperature gradient at the distance of $Z = \delta_m$ to δ_h. The left hand side of Equation (82) is heat of conduction term and the right hand side is heat of convection between phases

$$q^f_{Z=\delta_h} = -\lambda_L \frac{T^L - T^f_{Z=\delta_m}}{\delta_h - \delta_m} \tag{85}$$

The heat flux at $Z = \delta_m$ is conducted by Furrier's law, is written as

$$q^f_{Z=\delta_h} = -\lambda_L \frac{dT^f}{dZ} \tag{86}$$

Therefore Equation (86) can be formulated as follow

$$-\lambda_L \frac{dT^f}{dZ} = -\lambda_L \frac{T^L - T^f_{Z=\delta_m}}{\delta_h - \delta_m} \tag{87}$$

The dimensionless format $Z = \delta_m$ is formulated as

$$(L_w^{(1/2)} - 1)\left(\frac{d\theta}{d\xi}\right)_{\xi=1} = \theta^f_{\xi=1} - \theta^L \tag{88}$$

where δ_h is the film heat transfer and L_w, Lewis is the ratio of film thickness of mass to film thickness of heat transfer, $L_w = \left(\frac{\delta_h}{\delta_m}\right)^2$.

2. Reactor model

The reactor model can be directly incorporated in boundary element method which the Equation (38) and film boundary condition can be combined to obtain modified boundary conditions for gas phase at $\xi = 0$ (Equation (72)).

$$B^*_{im,i}(c^g_i(jj) - f^g(jj)h_i(\theta^f_{\zeta=0})c^f_{i,\xi=0}(jj) = -\left.\frac{dc^f_{i,}(jj)}{d\xi}\right|_{\xi=0} \tag{89}$$

where $B^*_{im,i}$ is a modified Biot number defined as following:

$$Bi^*_{im,i} = \frac{Bi_{m,i}}{(f^g(jj) + \alpha_{gL}\gamma_{Fi}s_i Bi_{m,i})} \tag{90}$$

Note that $Bi^*_{m,i}$ takes into account directly the concentration change in the gas phase for each cell. The boundary condition (Equation (100)) is directly in terms of the known inlet gas concentration. Once the BEM film model is solved with this modification, the outlet concentration of gas phase can be calculated as

$$c^g_i(jj) = \frac{c^g_i(jj-1)f^g(jj-1) + \alpha_{gL}\gamma_{Fi}B_{im,i}h\left(\theta^f_{\xi=0}\right)c^f_{i,\xi=0}(jj)}{(f^g(jj) + \alpha_{gL}\gamma_{Fi}s_i B_{im,i})} \tag{91}$$

In a similar manner Equations (54) and (81) for gas phase heat balance and the boundary condition for gas temperature can be combined to give a composite boundary condition for the film temperature equation. The resulting equation is

$$-\left(\frac{d\theta^f(jj)}{d\xi}\right)_{\xi=0} = Bi^*_H(\theta^g(jj-1) - \theta^f_{\xi=0}(jj)) - \sum_{i=1}^{Ns}\beta_{si}\left(\frac{dc^f_i(jj)}{d\xi}\right)_{\xi=0} \tag{92}$$

where

$$Bi_H^* = \frac{Bi_H}{(1 + Bi_H S^g)} \tag{93}$$

The boundary condition, at $\xi = 1$, the liquid phase mass balance (Equation 47) and the liquid film boundary conditions can be combined to obtain modified boundary conditions for all the liquid phase species. The reactor model is written as (see Appendix A)

$$s_i \frac{\alpha_{gl}}{N_L} \frac{dc_i^f(j)}{d\xi}\bigg|_{\xi=1} + (1 + \frac{1}{\omega_B}\frac{M}{N_L}k_2)c_B\big|_{\xi=1} + \frac{1}{\omega_A}\frac{M}{N_L}k_1 c_A\big|_{\xi=1} = \frac{1}{\omega_A}\frac{M}{N_L}k_3 + c_i^L(j-1) \tag{94}$$

The equation (58) and (88) for liquid phase heat balance and the boundary condition for liquid temperature can be combined to give a composite boundary condition for the film temperature equation. The resulting equation is

$$\left[(\frac{\alpha_{gL}}{N_L}Le\right| + (L_w^{(1/2)} - 1)\Big]\left(\frac{d\theta_{(j)}}{d\xi}\right)_{\xi=1} + (1 + Bv\frac{M}{N_L}k_4)\theta\big|_{\xi=1} - Bv\frac{M}{N_L}k_1 c_A\big|_{\xi=1} - Bv\frac{M}{N_L}k_2 c_B\big|_{\xi=1} = -Bv\frac{M}{N_L}k_3 + Bv\frac{M}{N_L}k_5 + \theta^L(j\text{-}1) \tag{95}$$

3. Numerical Approach

In previous section, the mathematically of the bulk phase and film balance have been develop. In the co-current mode, the bulk phase mass balance equations are coupled to mass balance for gas and liquid film through the interface fluxes of the component also call the gas-liquid reactor model. The reactor model in Equation (89-95) can be solving using the boundary element method. The details show as follow

Boundary Element Method (BEM)

Second order ordinary differential equation (2^{nd} ODE) in the liquid film is solved by Boundary Element Method (BEM). In this method, the boundary concentration conditions at both ends ($\xi = 0$ and $\xi = 1$) of liquid film are required**.** The boundary element method is suitable for solving the non-linear partial differential equation so that the equation in film model as Equation (63) can be written as

$$\frac{d^2 c_k}{d\xi^2} = f_k(c_1, c_2, ..., c_M) \tag{96}$$

where *c* is the concentration and temperature, *k* denoting equations number index; *k* =1 to *M* with *M* being the total number of differential equations. The function f_k is the forcing function for the *k*th equation and this is in general the function of all dependent variables $c_1, c_2, ..., c_M$. The problem is representative of diffusion with reaction in a multicomponent mixture. Thus, the LHS of Equation (96) is proportional to the net rate of diffusion species *k*, while the f_k term on the RHS is quantity proportional to the net rate of consumption of this species by various chemical processes taking place in the system. The dependent variable c_k will therefore be also referred to as the concentration of species *k*. the total number of species present in the system is then *M*.

In the liquid film thickness, from $\xi = 0$ to 1, is discrete to n subdomain and $n+1$ nodes as shown in Figure 4. The range of each of subdomain (h) is defined from the left end point of subdomain, a, to right end point, b, of the same subdomain.

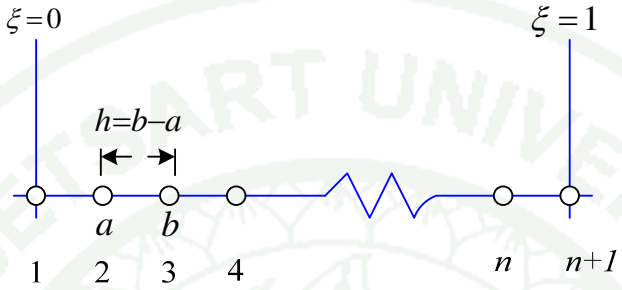

Figure 26 Illustration of Boundary Element Method in the liquid film for i^{th} species.

The boundary conditions are specified at the end point of the interval for all the dependent variables. The domain can be assumed as $\xi = 0$ to $\xi = 1$ without loss of generality and we can express the boundary conditions as follow:

Boundary condition at $\xi = 0$ is specified in the following manner

$$a_{1k} p_{1k} + a_{2k} c_{1k} = a_{3k}; \qquad k = 1, M \tag{97}$$

where the point $\xi = 0$ is given the nodal subscript 1; thus where p_{1k} is defined as the gradient of species k at point $\xi = 0$, c_{1k} is defined as concentration or temperature at $\xi = 0$, and a_{1k}, a_{2k}, and a_{3k} are the constant that specified in this point for species k. Similarly, boundary condition at $\xi = 1$ is represented as:

Boundary condition at $\xi = 1$

$$b_{1k} p_{(n+1)k} + b_{2k} c_{(n+1)k} = b_{3k} \tag{98}$$

where the point $\xi = 1$ is given the nodal subscript, $n+1$. Thus, $p_{(n+1)k}$ is defined as the gradient of species *k* at point $\xi = 1$, c_{1k} is defined as concentration or temperature at $\xi = 1$ and b_{1k}, b_{2k}, and b_{3k} are the constant that specified in this point for species *k* while the boundary condition $\xi = 1$.

Consider again the solution of forcing function (f_k) using the method of quasilinearization which is written as

$$f_k = f_k^* + \sum_{i=1}^{m} \left\{ \frac{\partial f_k}{\partial \mathrm{c_i}} \bigg|^* c_i - c_i^* \right\} \tag{99}$$

where c_i^* stand for the average value of concentration of species *i* over a given element at the current level of iteration. Also, the partial derivatives in the above equation are evaluated at these assumed average concentrations of the various species. Equation (99) can be expressed as:

$$f_k = f_k^* + \sum_{i=1}^{m} \frac{\partial f_k}{\partial c_i} \bigg|^* c_i - \sum_{i=1}^{m} \frac{\partial f_k}{\partial c_i} \bigg|^* c_i^* \tag{100}$$

where the 'linearized rate constants' are defined over a particular subdomain as:

$$K_{1k} = f_k^* - \sum_{i=1}^{m} \frac{\partial f_k}{\partial c_i} \bigg|^* c \tag{101}$$

$$K_{2k} = \frac{\partial f}{\partial c_i} \bigg|^* \tag{102}$$

With these approximations, Equation (96) for species *k* can be expressed within each subdomain as:

$$\frac{d^2c_k}{d\xi^2} = K_{1k} + \sum_{i=1}^{m} K_{2ki}c_i \tag{103}$$

The weighted residual formulation of Equation (103) over a subinterval (*a*,*b*) is:

$$\int_a^b G\frac{d^2c_k}{d\xi^2} = \int_a^b G\left[K_{1k} + \sum_{i=1}^{m} K_{2ki}c_i\right]d\xi \tag{104}$$

The term on the left hand side of Equation (104) is integrated by parts twice and two weighting function G_1 and G_2 are defined as follows:

$$G_1 = \xi\text{-}a \tag{105}$$

$$G_2 = b\text{-}\xi \tag{106}$$

In order to evaluate the integral term containing c_i on the RHS of Equation (104) we construct an osculating polynomial for c_i each subdomain. This polynomial is defined in terms of nodal values and the gradients at *a* and *b* by the following equation:

$$c_i = (b-a)\varphi_1 p_{ai} + \varphi_2 c_{ai} + (b-a)\varphi_3 p_{bi} + \varphi_4 c_{bi} \tag{107}$$

where the first subscript of Equation (110) refers to the nodes (*a* or *b*) while the second subscript denotes the species (*i*) under consideration. The osculating polynomials φ_i (*i* = 1 to 4) as shown in Table 4.

Table 4 The osculating polynomials

Basis functions, φ_i	Osculating polynomials
1	$\eta - 2\eta^2 + \eta^3$
2	$1 - 3\eta^2 + 2\eta^3$
3	$-\eta^2 + \eta^3$
4	$3\eta^2 - 2\eta^3$

The integral terms on the RHS of Equation (115) can be evaluated as follows:

$$\int_a^b G_1 c_i d\xi = \frac{1}{30} h^3 p_{ai} + \frac{3}{20} h^2 c_{ai} - \frac{1}{20} h^3 p_{bi} + \frac{7}{20} h^2 c_{bi} \tag{108}$$

$$\int_a^b G_1 K_{1k} d\xi = \frac{h^2}{2} K_{1k} \tag{109}$$

$$\int_a^b G_2 c_i d\xi = \frac{1}{30} h^3 p_{ai} + \frac{7}{20} h^2 c_{ai} - \frac{1}{30} h^3 p_{bi} + \frac{3}{20} h^2 c_{bi} \tag{110}$$

$$\int_a^b G_2 K_{1k} d\xi = \frac{h^2}{2} K_{1k} \tag{111}$$

These relationships are now substituted into Equation (104) to provide two equations corresponding to the discretized representation of the k^{th} equation. This k^{th} equation can be compacted by using the Kronecker delta notation. This is convenient from a computer programming point of view. Thus, for the subinterval, the discretized version of the k^{th} equation is:

$$\sum_{i=1}^{M} \left[H_{11i} p_{ai} + H_{12i} c_{bi} + H_{13i} p_{bi} + H_{14i} c_{bi} \right] = h^2 \frac{K_{1k}}{2} \tag{112}$$

$$\sum_{m=1}^{M}\left[H_{21i}p_{ai}+H_{22i}c_{ai}+H_{23i}p_{bi}+H_{24i}c_{bi}\right]=h^2\frac{K_{1k}}{2} \qquad (113)$$

where the element level coefficient matrix for species i in the k^{th} equation are defined as follows:

Table 5 Element level coefficient matrix for species i in the k^{th} equation

Weighting function equation	Coefficient matrix for species i in the k^{th}
First weighting function, $\xi - a$	$H_{11i} = -\frac{1}{30}h^3K_{2ki}$
	$H_{12i} = \delta_{ki} - \frac{2}{30}h^2K_{2ki}$
	$H_{13i} = \frac{1}{20}h^3K_{2ki} + h\delta_{ki}$
	$H_{14i} = -\delta_{ki} - \frac{7}{20}h^2K_{2ki}$
Second weighting function, $b - \xi$	$H_{21i} = -\frac{1}{20}h^3K_{2ki} - \mathrm{h}\delta_{\mathrm{ki}}$
	$H_{22i} = -\delta_{ki} - \frac{7}{20}h^2K_{2ki}$
	$H_{23i} = \frac{1}{30}h^3K_{2ki}$
	$H_{24i} = \delta_{ki} - \frac{3}{20}h^2K_{2ki}$

There are $2M$ equations of the above type for each subinterval. The equations are assembled together with the boundary conditions to form the global matrix. The Equations (112) and (113) are applicable to each subdomain. These are collected together along with boundary condition into the global matrix. The resulting global matrix is shown in Table 6 for the particle case of four subdomains ($N = 3$).

The solution of this matrix gives the concentration and gradient of all species at all nodal points. These value are, however, based on the quasilinear rate constants, based on assume the average concentration for each species over each subdomain. Thus, the solution is iterated using the new average value until convergence is achieved. The detail of developing of program code in matlab tool for solving BEM is described in section 3.

Table 6 Matrix structure of the final assembled equation for 3 species ($i = 3$), 2 subdomain ($n = 2$), and 3 nodes ($p = 3$)

Equation	Species (i)	node 1						node 2						node 3					
		p_{11}	c_{11}	p_{21}	c_{21}	p_{31}	c_{32}	p_{12}	c_{12}	p_{22}	c_{22}	p_{32}	c_{32}	p_{13}	c_{13}	p_{23}	c_{23}	p_{33}	c_{33}
B.C. $\xi = 0$ Equation (89) and (92)	1	*	*	0	0	0	0	0	0	0	0	0	0	0	0	0	0	0	0
	2	0	0	*	0	0	0	0	0	0	0	0	0	0	0	0	0	0	0
	3	0	0	0	0	*	*	0	0	0	0	0	0	0	0	0	0	0	0
Boundary Element Method: Equation (112)	1,2 and 3	*	*	*	*	*	*	*	*	*	*	*	*	0	0	0	0	0	0
Boundary Element Method: Equation (112)	1,2 and 3	*	*	*	*	*	*	*	*	*	*	*	*	0	0	0	0	0	0
Boundary Element Method: Equation (112)	1,2 and 3	*	*	*	*	*	*	*	*	*	*	*	*	0	0	0	0	0	0
Boundary Element Method: Equation (113)	1,2 and 3	0	0	0	0	0	0	*	*	*	*	*	*	*	*	*	*	*	*
Boundary Element Method: Equation (113)	1,2 and 3	0	0	0	0	0	0	*	*	*	*	*	*	*	*	*	*	*	*
Boundary Element Method: Equation (113)	1,2 and 3	0	0	0	0	0	0	*	*	*	*	*	*	*	*	*	*	*	*
B.C. $\xi = 1$ Equation (94) and (95)	1	0	0	0	0	0	0	0	0	0	0	0	0	*	*	0	*	0	*
	2	0	0	0	0	0	0	0	0	0	0	0	0	0	*	*	*	0	*
	3	0	0	0	0	0	0	0	0	0	0	0	0	0	0	0	0	0	0

3. Developing of Program Code in Matlab Tool for Solving BEM

The developed mathematical model in the form of a nonlinear second order ordinary differential equation was solved by the numerical BEM as shown above. In this section, a program code in MatLab tool will be developed to solve the equations. The first step to solve this problem is assumed the average concentration or temperature and gradient of concentration or temperature then using these values to construct the global matrix and solve. The iterative solution can be enumerated as follows:

The global matrix on Table1 can be enumerated as follow:

1. Assume an average concentration for each subinterval
2. Based on this average concentration compute the value of constant term in the linearized k^{th} equation (K_{1k}) and coefficient of c_m (K_{2ki}) for each subinterval and coefficient in the subdomain discretization (H_{11i} , etc.)
3. Collect the equations for each subinterval into global matrix.
4. Include the boundary condition at $\xi = 0$ and $\xi = 1$ as two additional equations into the global matrix.
5. Solve the global matrix by any standard routine for linear equation solver.
6. Check whether the assumed average concentrations are close to calculate values within a specified tolerance. If so, the solution has coverage. Otherwise the iteration are repeated starting at step 1 until convergence within a specified tolerance is obtained.

The flow chart for calculation in the mixing cell model for co-current and counter current are show in the Figure 27 and 28.

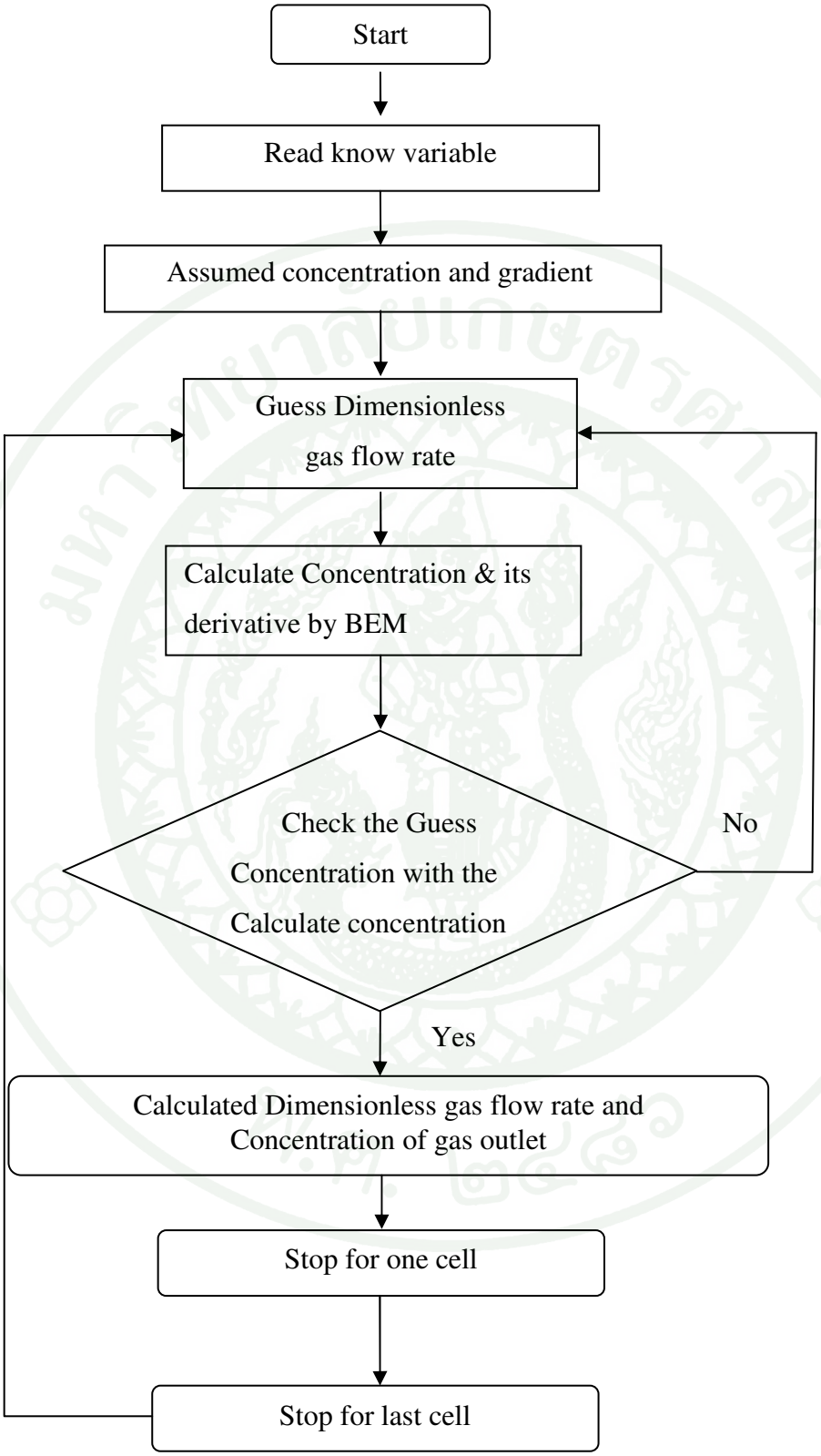

Figure 27 Flow chart for calculation in the mixing cell in co-current mode

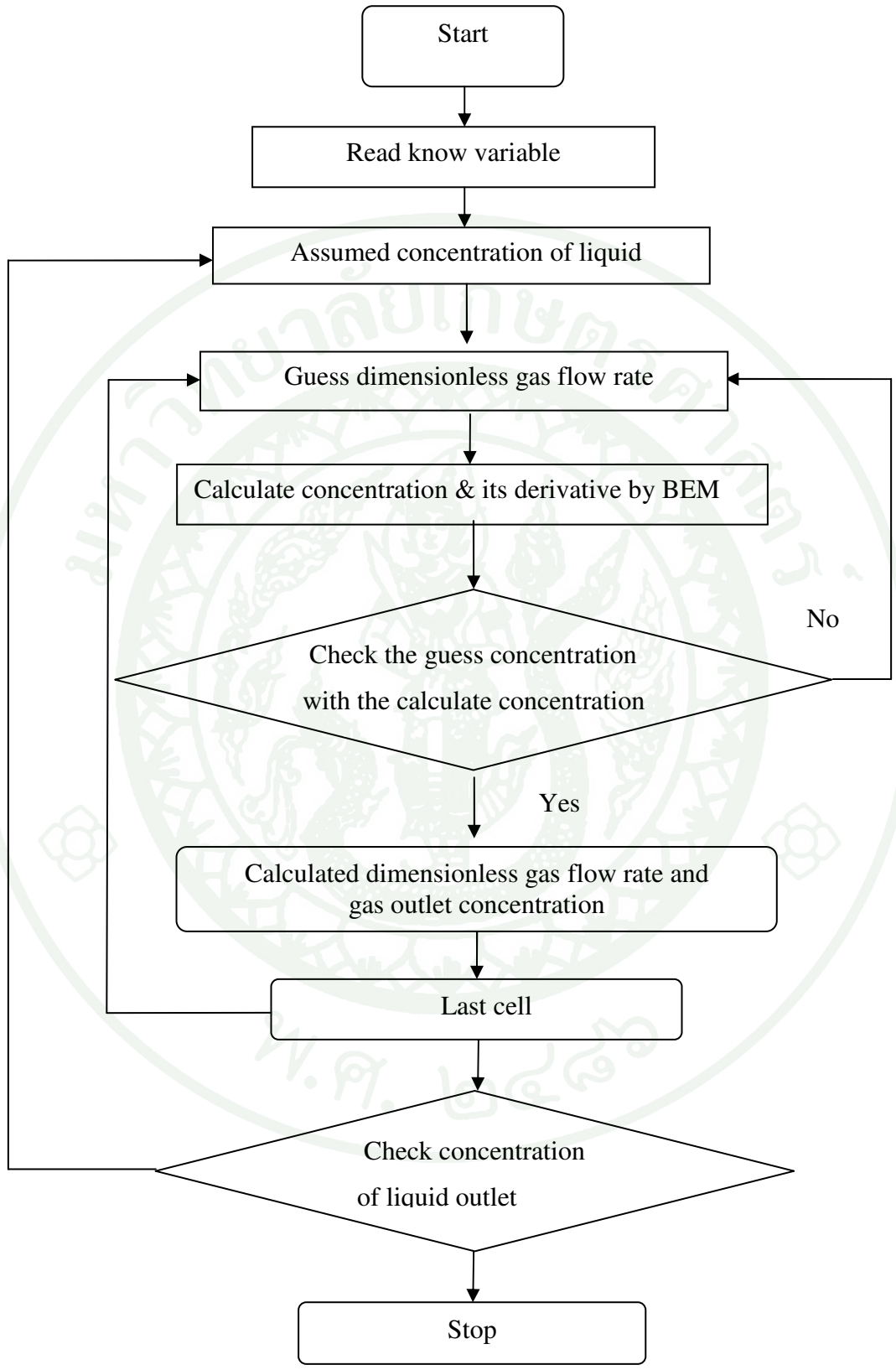

Figure 28 Flow chart for calculation in the mixing cell in counter-current mode

4. Simulation of Gas-Liquid Reactions

A. CO_2-NaOH systems.

The reaction mechanism of the chemisorptions of carbon dioxide in an aqueous solution of sodium hydroxide is important industrial gas-liquid reaction which is a second order irreversible reaction. Consider the following reaction scheme,

$$CO_2(g) + 2NaOH(l) \longrightarrow Na_2CO_3(l) + H_2O(l) \qquad (114)$$

where the dissolved gaseous species (CO_2) reacts with the NaOH to form sodium carbonate (Na_2CO_3) and water (H_2O). The features of gas-liquid reactor, operating conditions and kinetics, diffusion, and solubility parameters used for chemisorptions of carbon dioxide in an aqueous solution of sodium hydroxide are shown in Tables 7-9. The reactor type is packed column.

Table 7 The features of paked column reactor in CO_2-NaOH reaction.

Feathers	Value	Reference
Diameter (m)	0.87	
High (m)	1.015	
Volume of reactor (m^3)	0.604	
Gas hold up	0.9	Danckwert (1970)
Interfacial area (m^{-1})	100	Danckwert (1970)

Table 8 Operating conditions for NaOH and CO_2 system.

Operating conditions	Value
Superficial gas velocity (m/s)	$6.1x10^{-2}$
Superficial liquid velocity (m/s)	$1.29x10^{-3}$
Pressure (Pa)	$1.1018x10^{5}$
Temperature (K)	298
Partial pressure of CO_2 (Pa)	10^{5}
Concentration of liquid feed reactant (mol/m^3)	500

Table 9 Kinetics, Diffusion, and Solubility Parameters for CO_2 and NaOH system.

Parameters	Value	Reference
Rate constant (m^3/mol s)	10	Levenspiel (1999)
Henry's law constant (Pa m^3/mol)	2,500	Levenspiel (1999)
Gas phase mass transfer coefficient (m/s)	$1 x10^{-6}$	Perry and Green (1997)
Liquid phase mass transfer coefficient(m/s)	$1 x10^{-4}$	Levenspiel (1999)
Diffusion coefficient in liquid of CO_2 (m^2/s)	$1.8x10^{-9}$	Levenspiel (1999)
Diffusion coefficient in liquid of OH^- (m^2/s)	$3.06x10^{-9}$	Levenspiel (1999)
Diffusion coefficient in liquid of CO_3^{2-} (m^2/s)	$0.923 x10^{-9}$	Ebrahimi et al. (2003)

B. H_2S-Fe^{3+} (EDTA) reaction

Lo-Cat is a gas treating process that removes hydrogen sulfide out of gas streams and converts to solid sulfur. In this process, H_2S and chelated iron Fe^{3+} (EDTA) solution are used as a reactant. The features of gas-liquid reactor, operating conditions, and kinetics, diffusion, and solubility parameter used in the reaction of H_2S-Fe^{3+}(EDTA) are listed in Tables 10-12.

A simple representation of the reaction is

$$H_2S(g) + 2Fe^{3+}(EDTA)(l) \longrightarrow 2H^+ + S(s) + 2Fe^{2+}(l) \qquad (115)$$

The reaction rate is a second order irreversible process and its rate is given by

$$r = kC_{H_2S}C_{Fe^{3+}} \qquad (116)$$

Table 10 The features of paked column reactor for reaction of H_2S-Fe^{3+}(EDTA).

Features	Value	Reference
Diameter (m)	0.108	
Volume of reactor (m^3)	$7.32x10^{-3}$	
Gas hold up	0.050	Limtrakul *et al.* (2005)
Interfacial area (m^{-1})	1,700	Perry and Green (1997)

Table 11 Operating conditions for H_2S-Fe^{3+}(EDTA) system.

Operating conditions	Value
Superficial gas velocity (m/s)	$9x10^{-2}$
Superficial liquid velocity (m/s)	$1.0x10^{-2}$
Partial pressure of H_2S (Pa)	3,000
Concentration of liquid feed (mol/m^3)	20
Temperature (K)	298
Pressure (Pa)	$1.1018x10^5$

Table 12 Kinetics, Diffusion, and Solubility Parameters for H_2S-Fe^{3+} (EDTA) system.

Parameters	Value	Reference
Rate constant (m^3/mol·s)	9	Deberry (1993)
Henry's law constant (Pa·m^3 / mol)	1,950	Deberry (1993)
Gas phase mass transfer coefficient (m/s)	$3x10^{-4}$	Perry and Green (1997)
Liquid phase mass transfer coefficient (m/s)	$6x10^{-4}$	Perry and Green (1997)
Diffusion coefficient in liquid of H_2S (m^2/s)	$1.44x10^{-9}$	Wubs (1994)
Diffusion coefficient in liquid of Fe^{3+} (EDTA)	$5.4x10^{-10}$	Wubs (1994)
Diffusion coefficient in liquid of Fe^{2+} (EDTA)	$5.4x10^{-10}$	Wubs (1994)
Diffusion coefficient in liquid of H^+	$9.311x10^{-10}$	Ebrahimi et al. (2003)

C. CO_2-Na_2CO_3 reaction

The absorption of CO_2 in carbonate solution has been examined extensively (Nysing and Kramers, 1958; Danckwerts, 1970; Hikita *et al.,* 1976; Danckwerts and Savage, 1982; Lopez, 1991; Sharma, 1996) and the chemistry of the process is well understood. Furthermore, it is well-accepted that the reaction is second order with respect to the carbonate concentration. When CO_2 permeates across the liquid film into carbonate solution, carbonate ion is partially converted stoichiometrically The features of gas-liquid reactor, operating conditions, and kinetics, diffusion, and solubility parameter used in the reaction of CO_2-Na_2CO_3 are listed in Tables 13-15. The mechanism of the CO_2-Na_2CO_3 reaction is written as:

$$CO_2(g) + CO_3^{2-}(l) + H_2O \longrightarrow 2HCO_3^- \qquad (117)$$

The reaction rate is a second order process and its rate is given by

$$r = kC_{CO_2}C_{CO_3^{2-}} \quad (118)$$

Table 13 The feathers of gas-liquid reactor for CO_2-Na_2CO_3 reaction

Feathers	Value
Diameter (m)	0.046
High (m)	0.25
Volume of reactor (m^3)	$1.66x10^{-3}$
Gas hold up	0.05
Interfacial area (m^{-1})	1,700

Table 14 Operating conditions for CO_2-Na_2CO_3 reaction

Operating conditions	Value
Superficial gas velocity (m/s)	$3.0x10^{-2}$
Superficial liquid velocity (m/s)	$6.67x10^{-3}$
Pressure (Pa)	$1.0x10^5$
Temperature (K)	298
Partial pressure of CO_2 (Pa)	10^5
Concentration of liquid feed reactant (mol/m^3)	600

Table 15 Kinetics, Diffusion, and Solubility Parameters for CO_2-Na_2CO_3 reaction.

Parameters	Value	Reference
Rate constant ($m^3/mol{\cdot}s$)	$1.95x10^{-2}$	Dehouche and Lieto (1995)
Henry's law constant ($Pa{\cdot}m^3/mol$)	3663	Dehouche and Lieto (1995)
Gas phase mass transfer coefficient (m/s)	$3x10^{-5}$	Dehouche and Lieto (1995)
Liquid phase mass transfer coefficient (m/s)	$6x10^{-4}$	Doraiswamy and Sharma (1984)

Table 15 (continued)

Diffusion coefficient in liquid of CO_2 (m^2/s)	$1.8x10^{-9}$	Levenspiel (1999)
Diffusion coefficient in liquid of CO_3^{2-} (m^2/s)	$9.3x10^{-10}$	Dehouche and Lieto (1995)
Diffusion coefficient in liquid of HCO_3^- (m^2/s)	$9.3x10^{-10}$	Ebrahimi *et al.* (2003)

RESULTS AND DISCUSSION

In this section, illustrates the simulation results of gas-liquid reactions. In this research, the mixing characteristic in gas and liquid phase in each cell are assumed to be well- mixed. The heat and mass transfer in the liquid film are described based on the film theory. In co-current and counter modes, the fluxes at the interface of the film theory are then directly used as the link to the reactor model. These models were solved by boundary element method. The solution of the reactor model can be predicted the performance of gas-liquid reactor. This research work involves studying the performance of the gas-liquid reactor in co-current and counter current modes. The the mathematical models were applied for three cases studies which are the reaction of CO_2 and NaOH, H_2S and Fe^{3+} (EDTA), and CO_2 and Na_2CO_3. These studied can be divided into six parts. Firstly, the effects of mass transfer on the reaction regimes. Second, concentration profile along with the column length. Third, the effect of the flow types on the conversion which are the effect of mixing cell number. Fourth, the effect of the operating mode on conversion. Fifth, prediction the Enhancement factor. Finally, study the performance of gas-lift Lo-Cat process.The simulation result shown as follow:

1. Effect of Mass Transfer and Kinetic Reaction on Reaction Regimes

The reaction regime in the reactor can be identified by considering the concentration profile along the liquid film thickness. The fast or slow reaction is indicated by the concentration profile of gaseous reactant dissolved in the liquid film. If the gaseous reactant is used up in the liquid film, the fast reaction takes place. Additionally, if gaseous reactant is consumed both liquid film and liquid bulk. The intermediate regime is takes place. On the other hand, if the gaseous reactant concentration is nearly constant along the thickness, the slow reaction takes place. The concentration profiles of each species along liquid film thickness for each reaction are shown in Figures 29-34. The concentration of the dissolved gas at the gas-liquid interface ($\xi = 0$) is related to the solubility of gas reactant in liquid phase.

The concentration of liquid reactant at the end of liquid film ($\xi = 1$) is identical to the concentration in liquid bulk. Various types of reactions are investigated such as the reactions of CO_2 and NaOH, H_2S and Fe^{3+} (EDTA), and CO_2 and Na_2CO_3.

A.CO_2-NaOH reaction

The mechanism of the CO_2-NaOH reaction is written as:

$$CO_2(g) + 2NaOH(l) \longrightarrow Na_2CO_3 + H_2O$$

The concentration profiles as a function of liquid film thickness at the bottom and the top of the reactor in co-current and counter modes for CO_2 –NaOH reaction are shown Figure 29-31.

Figure 29 shows the concentration profiles as a function of liquid film thickness in co-current mode. It was found that at the bottom of the reactor, the concentration of CO_2 is sharply reduce from $\xi = 0$ to $\xi = 1$ and used up at 0.8, on the other hand, the concentration of NaOH is increased along with the liquid film thickness. At the top of the reactor, the concentration profile of CO_2 is similar in that of the bottom of reactor and used up at $\xi = 0.4$ although the magnitude is reduced significantly. The concentration of NaOH is slightly increased with liquid film at the top.

Figure 30 shows the concentration profiles as a function of liquid film thickness in a counter current mode. It was found that at the bottom of the reactor, the concentration of CO_2 is reduced from $\xi = 0$ to $\xi = 0.65$ and used up at $\xi = 0.65$. The results was similar to those in a co-current mode. While the concentration profile of NaOH is increased with the liquid film thickness. At the top of reactor, the concentration of CO_2 is used up at $\xi = 0.4$ and the concentration of NaOH is higher near the feed condition. It can be concluded that are in chemisorptions of CO_2-NaOH reaction in both co-current and counter current modes are in fast reaction regime since

CO_2 is used up in the liquid film. Therefore, there is no reaction and mass transfer resistance in the main body of liquid. The chemical kinetic step controls the rate of reaction in the liquid film. Thus, the liquid hold up is not important. This reaction needs large interfacial area. Mechanically agitated contactors are suitable for this reaction scheme. Because the values of effective interfacial area provided by mechanically agitated contactors are generally relative high.

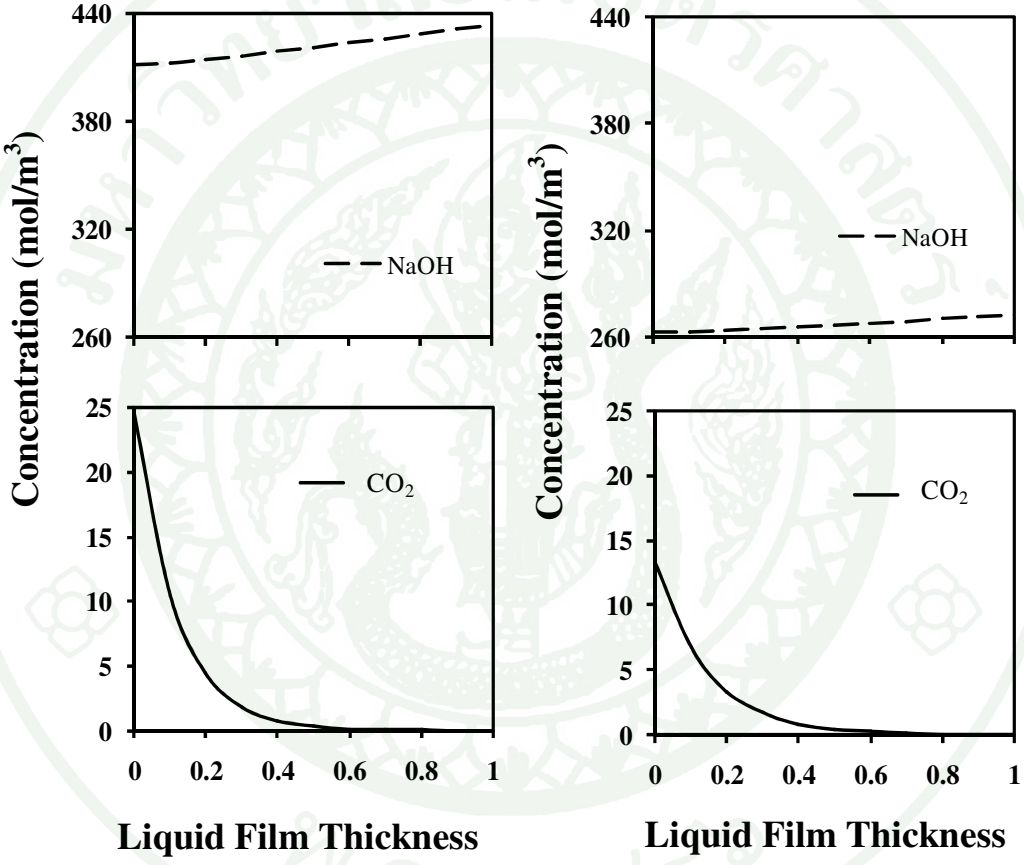

(a) at the bottom of reactor (b) at the top of reactor

Figure 29 Concentration profile as a function of liquid film thickness for CO_2-NaOH reaction in co-current mode.

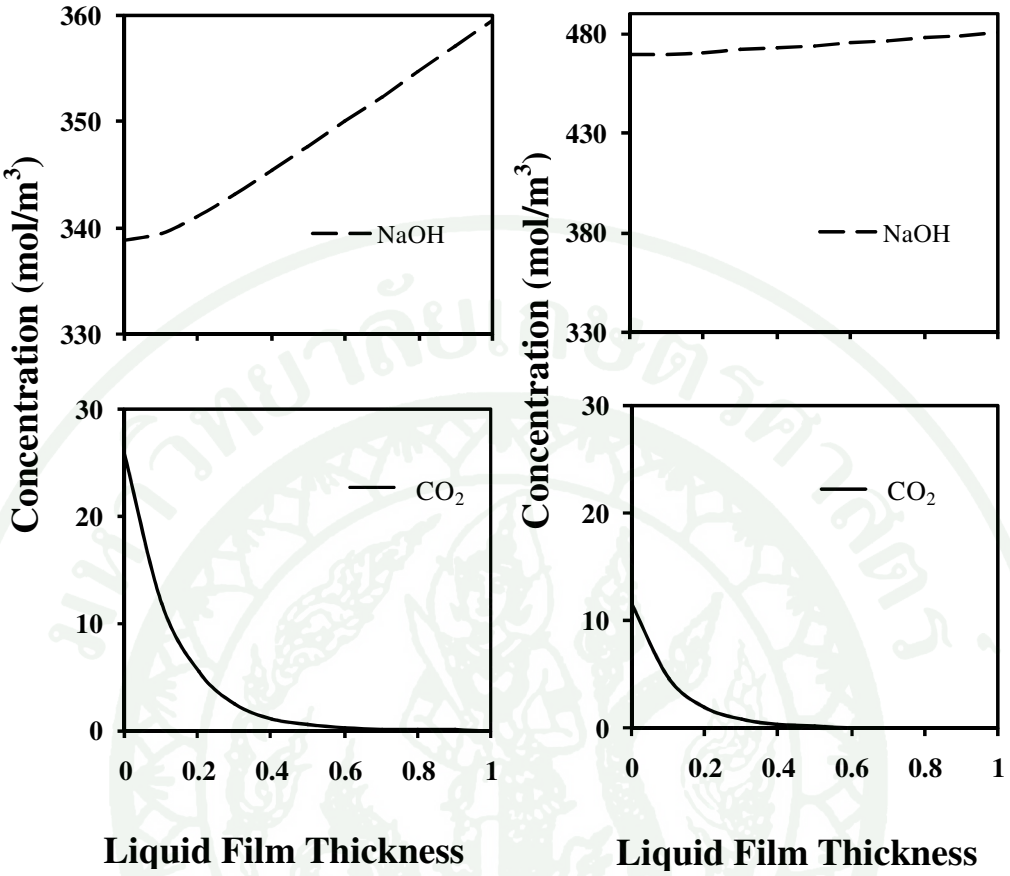

(a) at the bottom of reactor (b) at the top of reactor

Figure 30 Concentration profile as a function of liquid film thickness for CO_2-NaOH reaction in counter current mode.

B. H_2S-Fe^{3+}(EDTA) reaction

The mechanism of the H_2S-Fe^{3+} (EDTA) reaction is written as:

$$H_2S(g) + 2Fe^{3+}(EDTA)(l) \longrightarrow 2H^+ + S + 2Fe^{2+}$$

The concentration profiles as a function of liquid film thickness at the bottom and the top of the reactor in co-current and counter current modes for H_2S-Fe^{3+} (EDTA) reaction are shown in Figures 31-32.

In this reaction scheme, the concentration profiles as a function of liquid film thickness in a co-current mode for H_2S-Fe^{3+} (EDTA) reaction are shown in Figure 31. At the bottom of the reactor, the concentration of H_2S is not completely used in the liquid film. The reaction occurs both liquid film and liquid bulk. The concentration of Fe^{3+} (EDTA) is nearly constant from $\xi = 0$ to $\xi = 1.0$. At the top of the reactor, the concentration profile of H_2S is similar to that at the bottom of reactor. The concentrations of Fe^{3+}(EDTA) is nearly constant with liquid film thickness. Thus, it can be concluded that this reaction scheme is in the intermediat rate regime. The chemical reaction and mass transfer control the rate. Both interfacial area and liquid hold up should be high. The mechanically agitated contactors and bubble columns will be suitable.

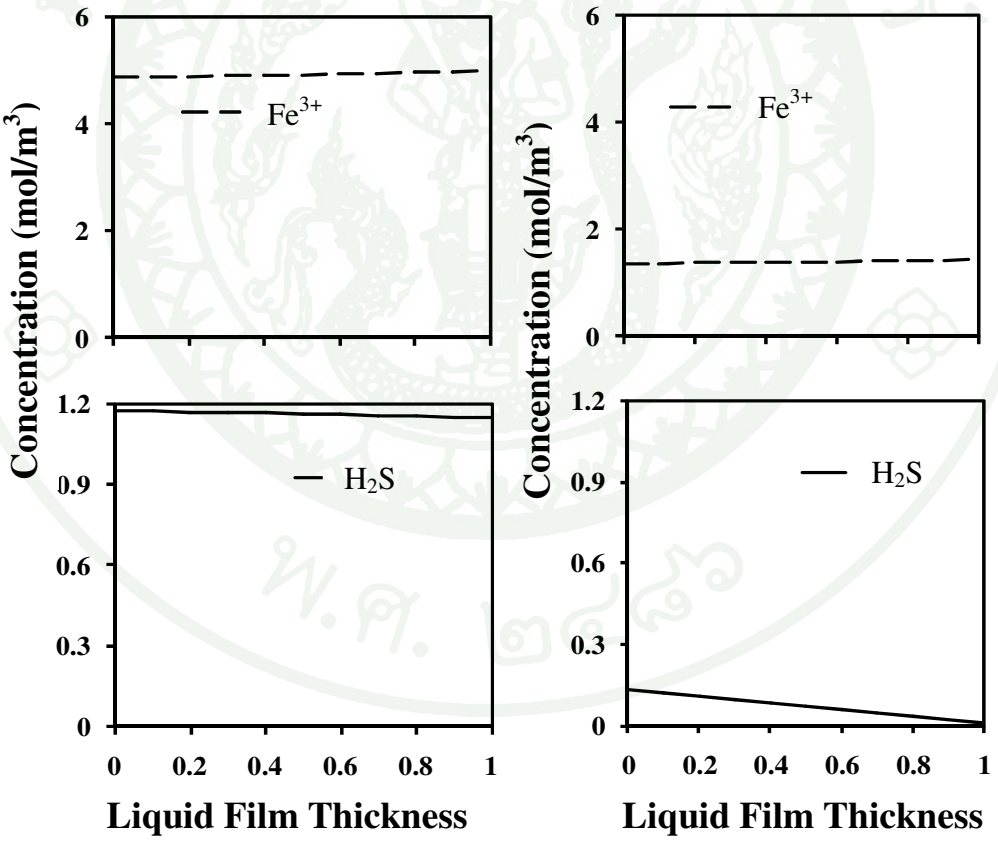

(a) at the bottom of reactor (b) at the top of reactor

Figure 31 Concentration profile as a function of liquid film thickness for H_2S-Fe^{3+} (EDTA) reaction in co-current mode.

Figure 32 shows the concentration profiles as a function of liquid film thickness in a counter current mode. It was found that at both bottom and top of the reactor, the concentration profiles of H_2S are mostly used up in the liquid film thickness. This reaction scheme is fast. Therfore, this reaction scheme is chemical kinetic control in liquid film. A packed tower and stirred tank are proper for this reaction scheme. Although, the feed concentrations, type of reactor for co-current and counter current modes are the same the regime for these two modes of operation are different. This migh me due to difference in concentration profiles.

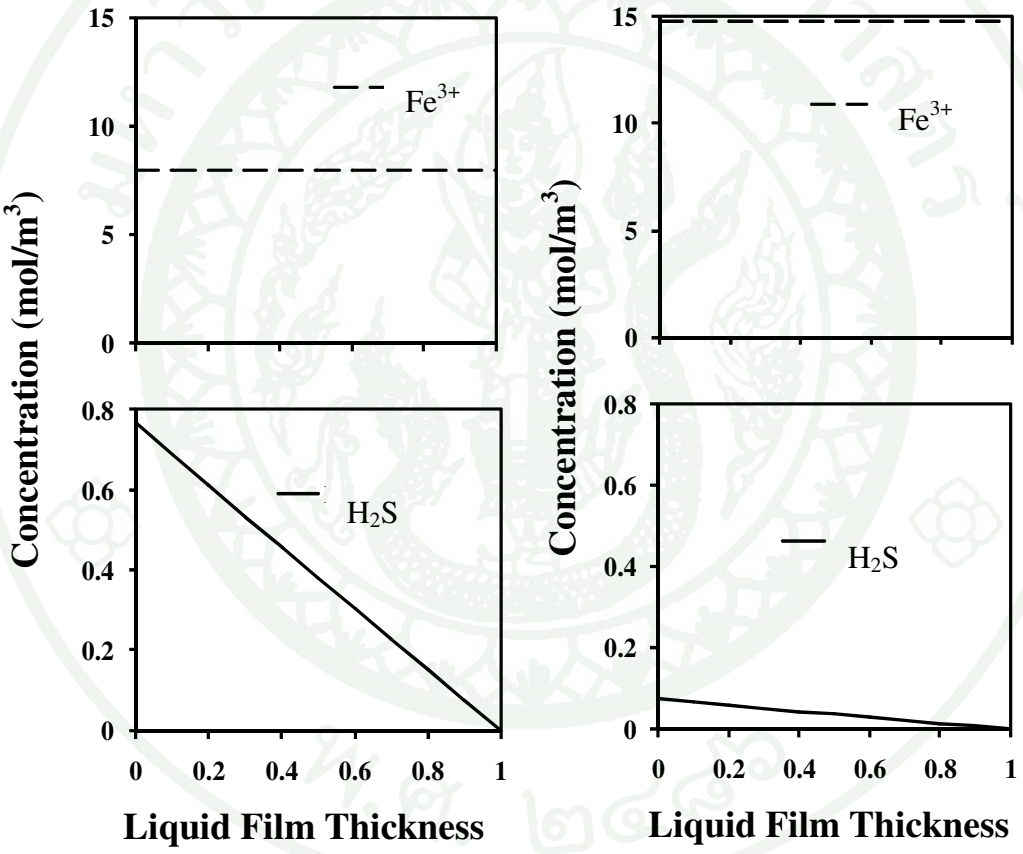

(a) at the bottom of reactor (b) at the top of reactor

Figure 32 Concentration profile as a function of liquid film thickness for H_2S-Fe^{3+} (EDTA) reaction in counter current mode**.**

C. CO_2-Na_2CO_3 reaction

The mechanism of the CO_2-Na_2CO_3 reaction is written as:

$$CO_2(g) + CO_3^{2-}(l) + H_2O \longrightarrow 2HCO_3^-$$

The concentration profiles as a function of liquid film thickness at the bottom and top of the reactor in co-current and counter current modes for CO_2-Na_2CO_3 reaction are shown in Figures 33-34.

Figure 33 shows the concentration profiles as a function of liquid film thickness in co-current mode for CO_2-Na_2CO_3 reaction. It was found that the bottom of the reactor, the concentrations of CO_2 and CO_3^{2-} are almost constant along with liquid film thickness. At the top of the reactor, the concentration profiles of CO_2, and CO_3^{2-} are similar to those in the bottom of the reactor. It can be concluded that this reaction scheme is a slow reaction. Here, the mass transfer resistant is negligible and the reaction rate is determined by chemical kinetic alone. Therefore, the reaction needs a large bulk liquid volume. A bubble reactor is suitable for this reaction in which the gas is dispersed in the liquid phase at the bottom through a gas distributor. Since the liquid hold up is large and the liquid residence time can be varies over a wild range.

Figure 34 shows the concentration profiles as a function of liquid film thickness in a counter current mode. It was found that at both bottom and top of the reactor. CO_2 is completely used in the end of liquid film which is contrast the result in a co-current mode. A counter current mode gives higher mass transfer than that of co-current mode. Thus the reaction regime shifts to a fast reaction. The results are similar to those of CO_2-NaOH and H_2S- Fe^{3+}(EDTA) reactions**.** This reaction needs large interfacial area. A packed tower and stirred tank can be used.

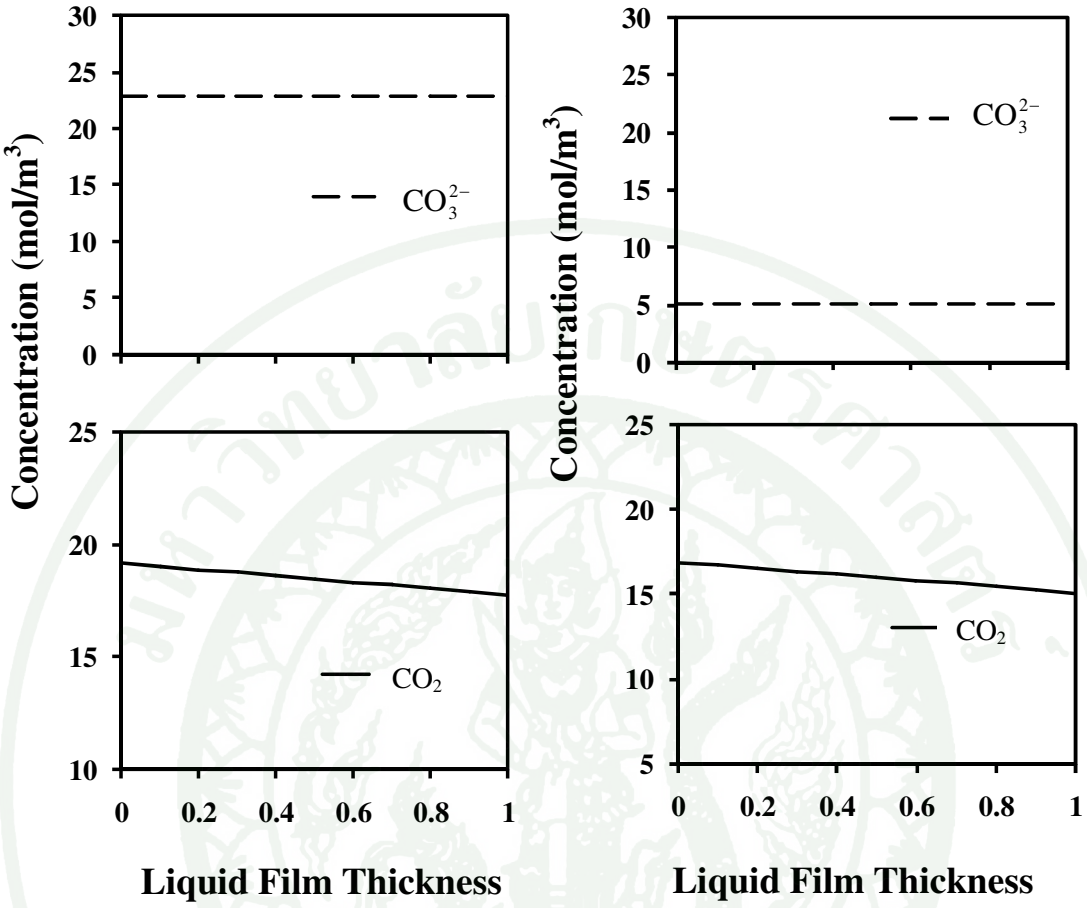

(a) at the bottom of reactor (b) at the top of reactor

Figure 33 Concentration profiles as a function of liquid film thickness for CO_2-Na_2CO_3 reaction in co-current mode.

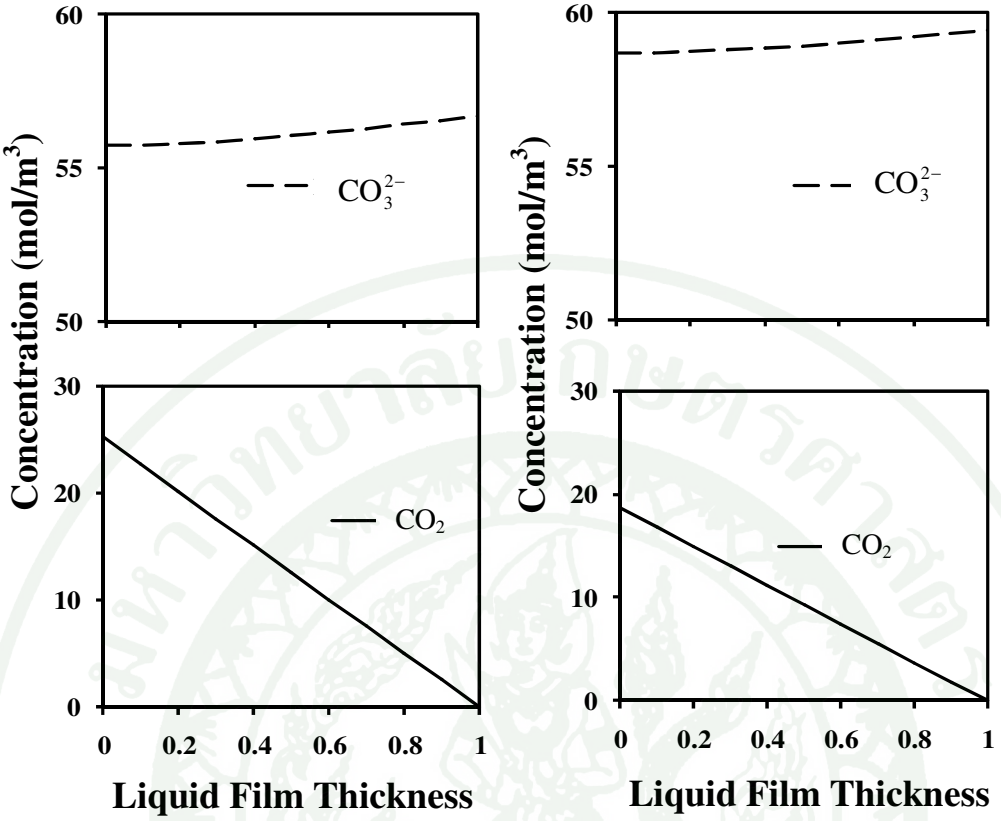

(a) at the bottom of reactor (b) at the top of reactor

Figure 34 Concentration profiles as a function of liquid film thickness for CO_2-Na_2CO_3 reaction in counter-current mode.

2. Concentration Variation along Column Length

The information of concentration profile of each species along column length indicates the nature of reaction and tendency in the reactor performance. The concentrations of all species along reactor length (dimensionless) for each reaction are shown in Figures 35-37. Various types of reactions are investigated which are the CO_2 and NaOH, H_2S and Fe^{3+} (EDTA), and CO_2 and Na_2CO_3 reaction**.**

A. CO_2-NaOH reaction

In the reaction of CO_2-NaOH, the partial pressure of CO_2 is 10^5 Pa, the Henry's law constant of CO_2 at the reference temperature is 2500 Pa·m^3/mol and the concentration of NaOH used in this system is 500 mol/m^3. The concentration profiles as a function column length in co-current and counter current modes for CO_2- NaOH reaction are shown in Figure 35 (a) and (b), respectively.

Figure 35 (a) and (b) shows the concentration profiles as a function of reactor length for CO_2-NaOH reaction in co-current and counter current mode. It was found that in both co-current and counter current modes the concentration of CO_2 decreases with column length while the concentrations of Na_2CO_3 are increases. On the other hand, in a counter current mode the concentration of NaOH is high at the top of reactor and then, its decreases from the top of reactor to the bottom. Because the concentration of NaOH is fed at the top of reactor.

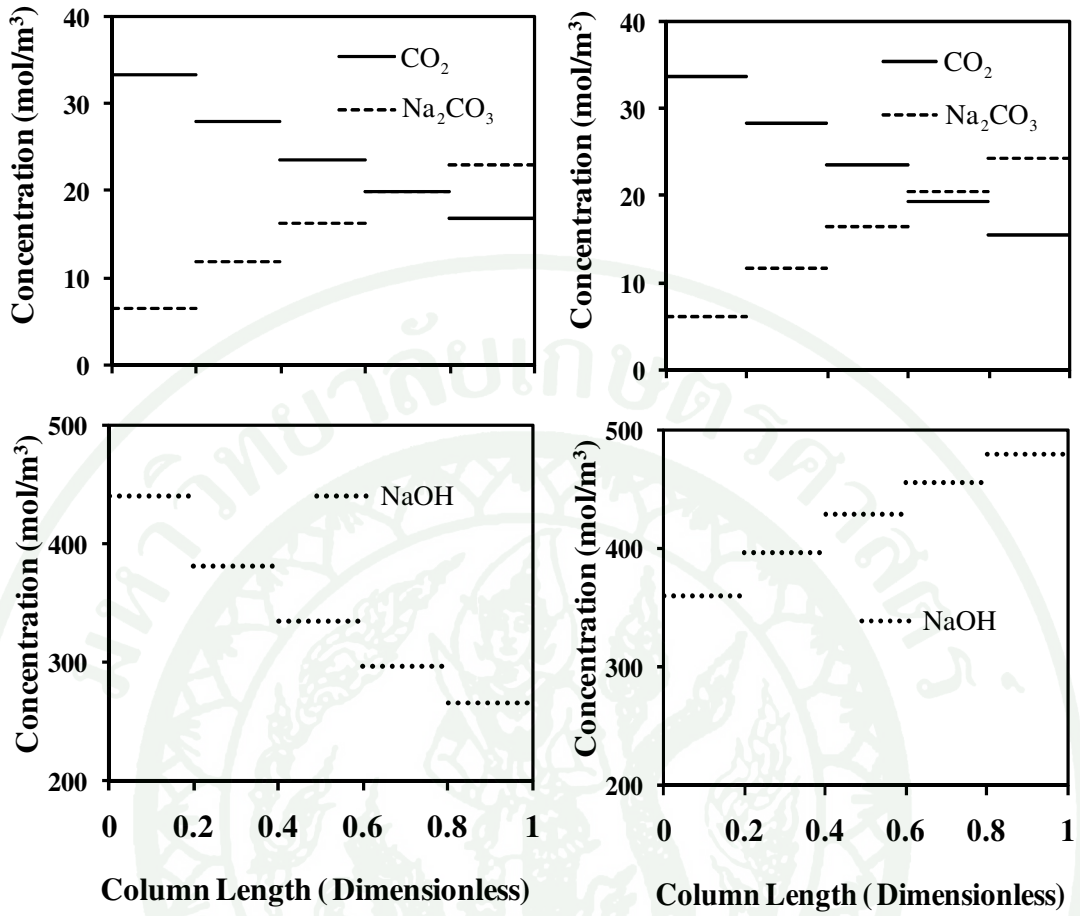

Figure 35 Concentration profiles as a function of reactor length for CO_2-NaOH reaction in co- current (a) and counter-current modes (b).

B. H_2S-Fe^{3+}(EDTA) reaction

The reaction of H_2S-Fe^{3+} (EDTA), the partial pressure of H_2S is 3,000 Pa, the Henry's law constant of H_2S at the reference temperature is 1950 Pa·m^3/mol and the concentration of Fe^{3+} (EDTA) used in this system is 20 mol/m^3. The concentration profiles as a function column length in co-current and counter current modes for H_2S-Fe^{3+} (EDTA) reaction are shown in Figures 36 (a) and (b) respectively.

Figures 36 (a) and (b) show the concentration as a function of reactor length for H_2S-Fe^{3+} (EDTA) reaction in co-current and counter current mode. It can be seen that the concentrations of both reactants (H_2S and Fe^{3+} (EDTA)) decrease along the reactor length. On the other hand, the concentration of products H^+ and Fe^{2+}, suddenly increases along the reactor length until $Z/L = 0.8$ and then, it slightly increases near the top of the reactor due to small amount of liquid reactant. Futhermore, in a counter current mode, concentration of liquid reactant increases with column length and high at the top of reactor due to near the feed condition.

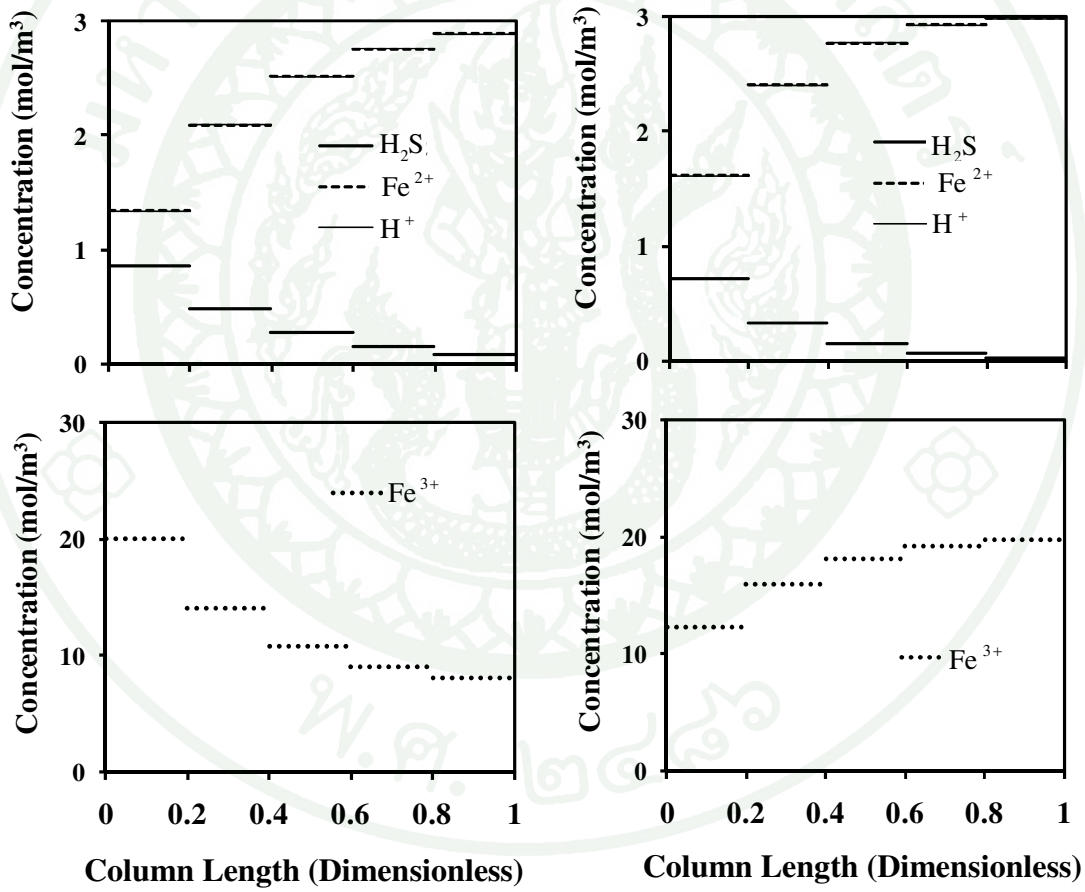

Figure 36 Concentration profile as a function of reactor length for H_2S-Fe^{3+} (EDTA) reaction in co- current (a) and counter current modes (b).

C. CO_2-Na_2CO_3 reaction

The reaction of CO_2-Na_2CO_3 reaction, the partial pressure of CO_2 is 10^5 Pa, the Henry's law constant of CO_2 at the reference temperature is 3,663 $Pa \cdot m^3/mol$ and the concentration of Na_2CO_3 used in this system is 60 mol/m^3. The concentration profiles as a function column length in co-current and counter current modes for CO_2-Na_2CO_3 reaction are shown in Figures 37 (a) and (b) respectively.

Figure 37(a) and (b) shows the concentration profiles as a function of column length for CO_2-Na_2CO_3 reaction in co-current and counter current modes. It can be seen that the concentration profile of gas phase reactance (CO_2) suddenly decreased along with the column length. The concentration of product HCO_3^-, sharply increases along the reactor length until $Z/L = 0.6$ and then, it slightly increases near the top of reactor. This similar to the reaction of H_2S-Fe^{3+} (EDTA).

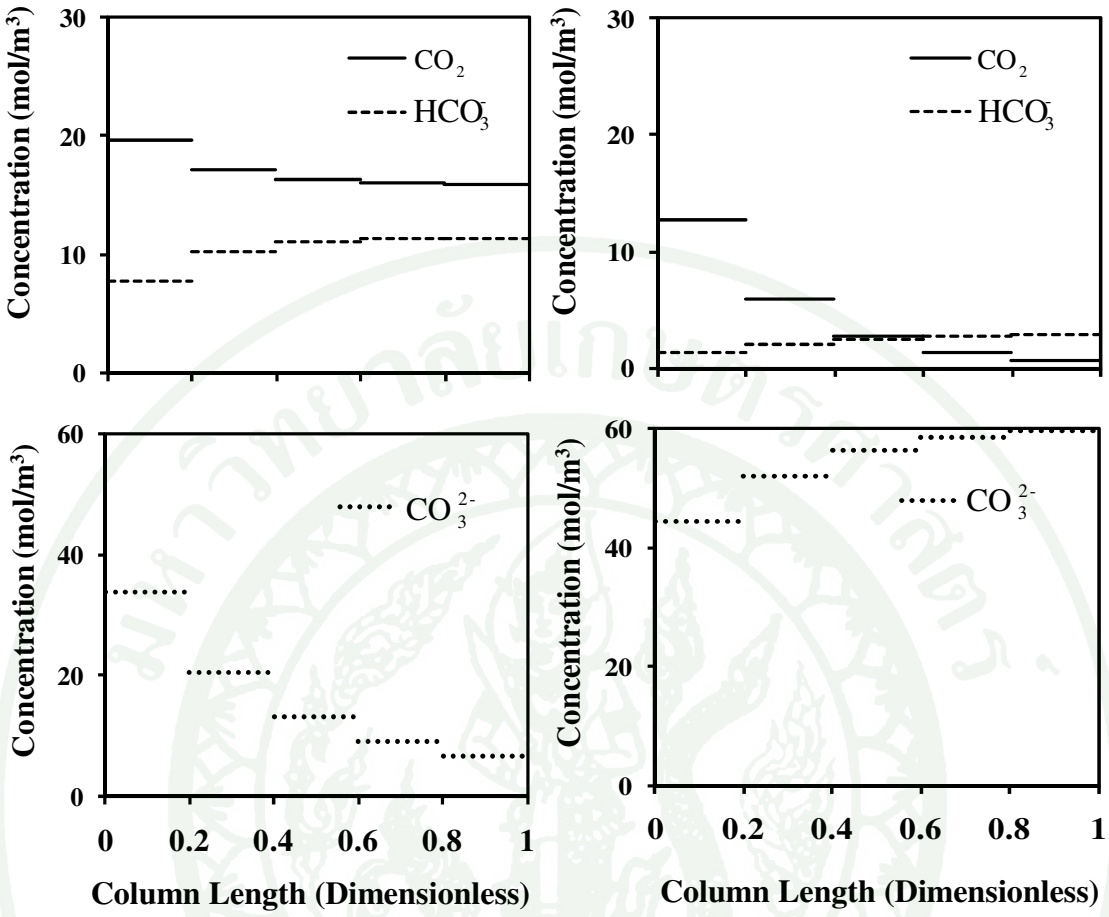

(a) co-current mode (b) counter current mode

Figure 37 Concentration profile as a function of reactor length for H_2S-Fe^{3+} reaction in a co- current (a) and a counter current modes (b).

3. Effect of the Mixing Cell number on Reactor Performance

In this section, the performance of the reactor operated with co-current and counter current modes were obtained. In each cell the flow is assumed to be well mixed. The number of mixing cell of gas and liquid are equal. The conversion profiles of gas and liquid reactants, along the reactor length as a function of number of mixing cell for the chemisorptions of cabon dioxide into aqueous solution of sodium

hydroxide, H_2S into aqueous solution of Fe^{3+} (EDTA), and CO_2 into aqueous solution of Na_2CO_3 are shown in Figures 38-43.

A. CO_2-NaOH reaction

The effect of mixing cell number was carried out in a reactor volume of 0.604 m^3 with a column length to diameter ratio of 1.17. The gas and liquid superficial velocities are $6.1x10^{-2}$ and $1.29x10^{-3}$ m/s, respectively. The corresponding liquid residence time (τ) is 788 s. Figures 38-39 show the conversion profiles along with reactor length as a function of number of mixing cells for CO_2-NaOH reaction in co-current and counter current modes.

Figure 38 shows the conversion profiles of CO_2 and NaOH along the reactor length as a function of number of mixing cell for a second-order irreversible chemical reaction of CO_2-NaOH in a co-current mode. It was found that the conversion of CO_2 and NaOH for one cell system (N=1) is constant along the column length. The flow pattern for this reactor shows a complete mixed flow which is the pattern for a CSTR (Continuous-Stirred Tank Reactor). When the number of mixing cells is more than one (N >1), the reactor behavior begins to deviate from the pattern of CSTR. The conversion profile of CO_2 and NaOH are increased along the reactor length. The larger is the number of mixing cells; the higher is the conversions of gas and liquid phase reactants.

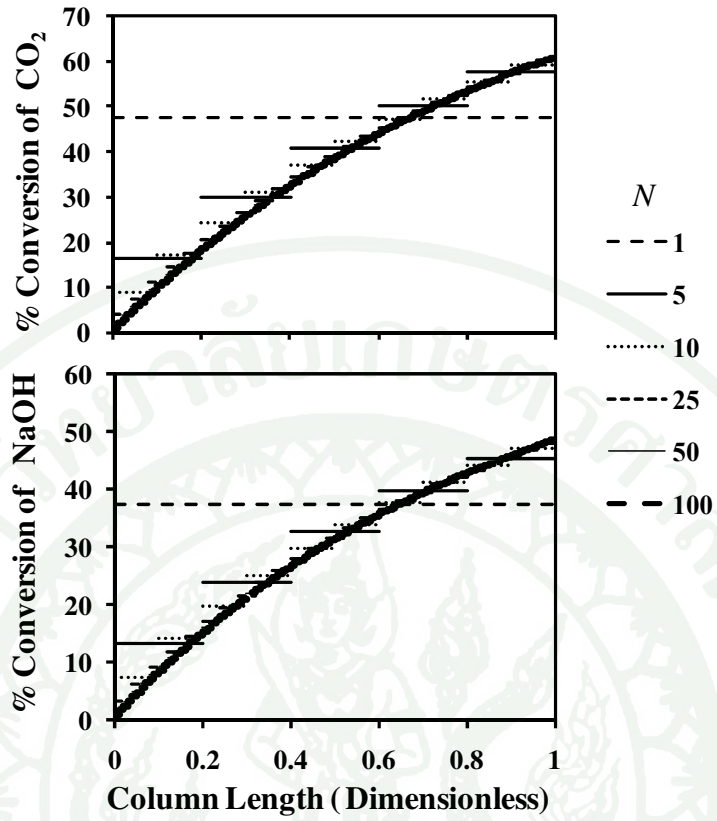

Figure 38 Conversion profiles as a function of the number of mixing cells for CO_2-NaOH reaction in co-current mode.

Figure 39 shows the conversion profile of CO_2 and NaOH along the reactor length as a function of mixing cell number for CO_2-NaOH reaction in a counter current mode. The results are similar to those in a co-current mode. The conversion profiles of CO_2 are increased when the number of mixing is more than one (N>1). The reactor behavior begins to deviate from the pattern of CSTR. The flow pattern is closed to plug flow when number of mixing cell more than 25 (N>25). On the other hand, the conversion profiles of NaOH decreases along the reactor length because at the bottom of the reactor, the solubility of CO_2 is high and reacts with low concentration of NaOH caused by high NaOH consumption.

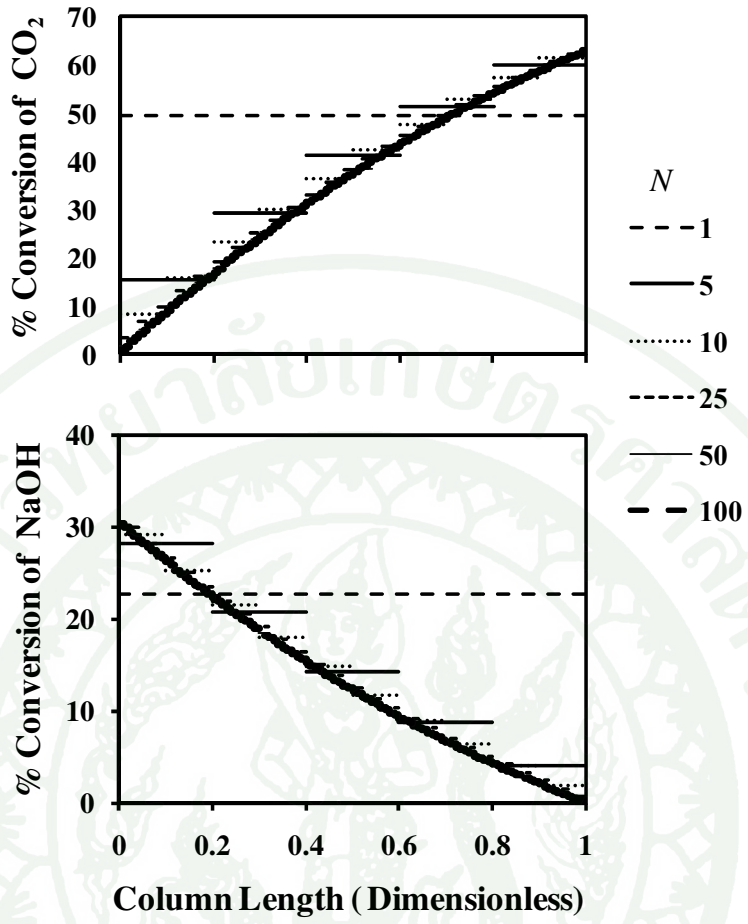

Figure 39 Conversion profiles as a function of the number of mixing cells for CO_2-NaOH reaction in counter current mode.

B. H_2S-Fe^{3+} reaction

The effects of mixing cell number were carried out in a reactor volume of $1.8x10^{-3}$ m^3 with a column length to diameter ratio of 1.82. The gas and liquid superficial velocities are $9x10^{-2}$ and $1.0x10^{-2}$ m/s, respectively. The corresponding liquid residence time (τ) is 19.67s. Figures 40-41 show the conversion profiles along reactor length as a function of number of mixing cells for H_2S-Fe^{3+}(EDTA) reaction in co-current and counter current modes.

Figure 40 shows the effect of mixing cell number on the conversion profiles of H_2S and Fe^{3+}(EDTA) along the reactor length in a co-current mode. It was

found that the conversion of H_2S and Fe^{3+}(EDTA) for one cell system (N=1) is constant along the column length. When the number of mixing cell is more than 1 (N >1). The reactor behavior deviates from the pattern of CSTR. The conversion profile at the mixing cell number of 100 (N =100) is not much different than that at the mixing cell number of 25 (N =25). It can be concluded that the behavior in this reactor is closed to plug flow reactor at the number of mixing cells more than 25 (N >25).

Figure 41 shows the conversion profile of H_2S and Fe^{3+} (EDTA) as a function of column length in a counter current mode. The conversion profiles of H_2S is increased along the column length when number of cell more than one ($N>1$). This result is similar to that in the co-current mode. However, the conversion of $Fe^{3+}$is decreased along the column length. The flow pattern is closed to plug flow when number of mixing cell more than 25 (N>25).

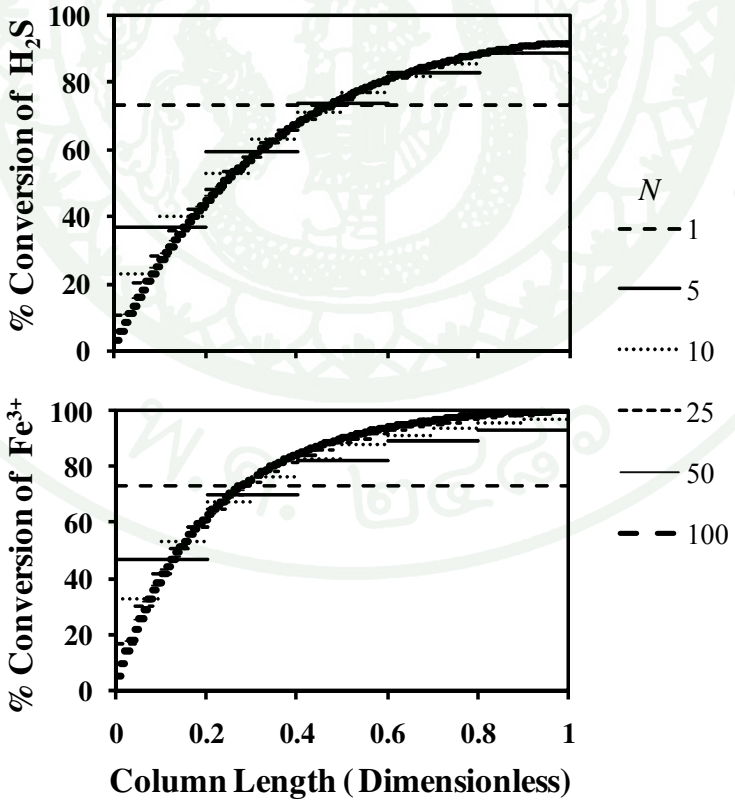

Figure 40 Conversion profiles as a function of the number of mixing cells for H_2S-Fe^{3+}(EDTA) reaction in co-current mode.

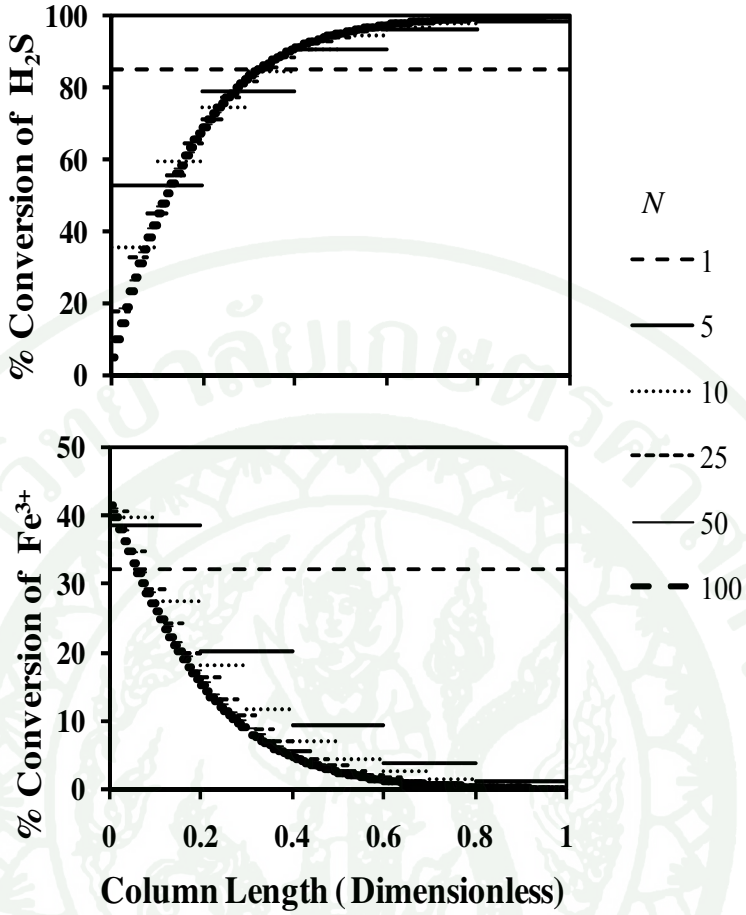

Figure 41 Conversion profiles as a function of the number of mixing cells for H_2S-Fe^{3+}(EDTA) reaction in counter current mode.

C. CO_2-Na_2CO_3 reaction

The effect of number of mixing cells was carried out in a reactor volume of 1.66×10^{-3} m^3 with a column length to diameter ratio of 5.43. The gas and liquid superficial velocities are 3×10^{-2} and 6.67×10^{-3} m/s, respectively. The corresponding liquid residence time (τ_L) is 271 s. Figures 42-43 show the conversion profiles along reactor length as a function of number of mixing cells for CO_2-Na_2CO_3 reaction in co-current and counter current modes.

The effect of mixing cell number on the conversion profile of CO_2-Na_2CO_3 reaction along the reactor length in a co-current mode is shown in Figure 42. It was found that the conversions of CO_2 and Na_2CO_3 are constant along the column length for one cell system (N=1). When the mixing cell number more than 10 (N >10), the conversion profiles of CO_2 are closed to be those of plug flow. The conversion profile at the mixing cell number of 100 (N =100) is not much different than that at the mixing cell number of 10 (N =10). It can be concluded that the conversion profiles in this reactor is closed to plug flow reactor at the number of mixing cells more than 10 (N >10).

Figure 43 shows the conversion profiles of CO_2 and Na_2CO_3 as a function of column length in a counter current mode. The conversion of Na_2CO_3 is decreased along the column length when number of cell more than one ($N>1$). This result is similar to that in the co-current mode. However, the conversion of Na_2CO_3 is decreased along the column length. The flow pattern is closed to plug flow when number of mixing cell more than 25 (N>25).

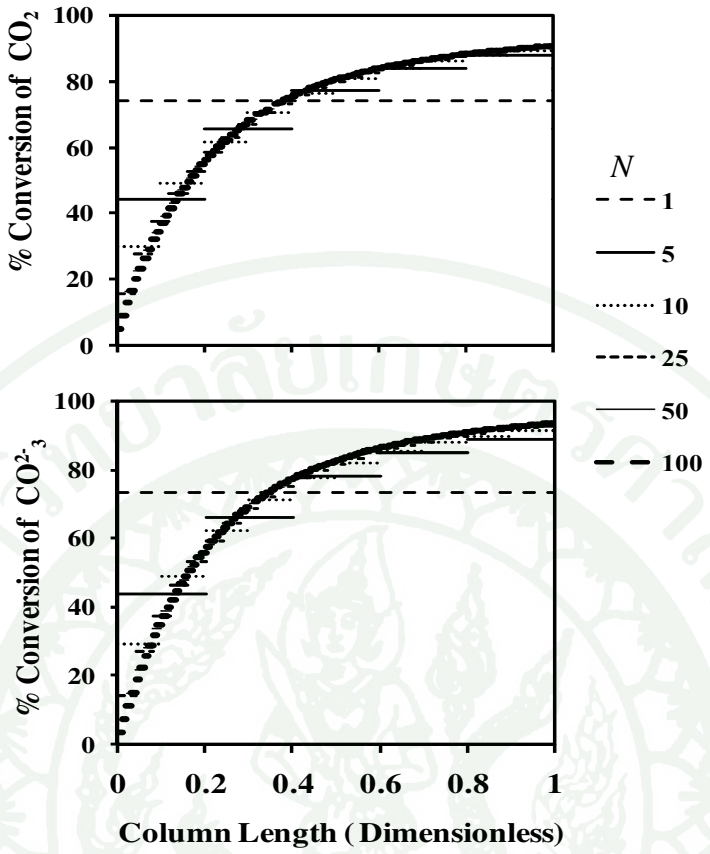

Figure 42 Conversion profiles as a function of the number of mixing cells for CO_2-Na_2CO_3 reaction in co-current mode.

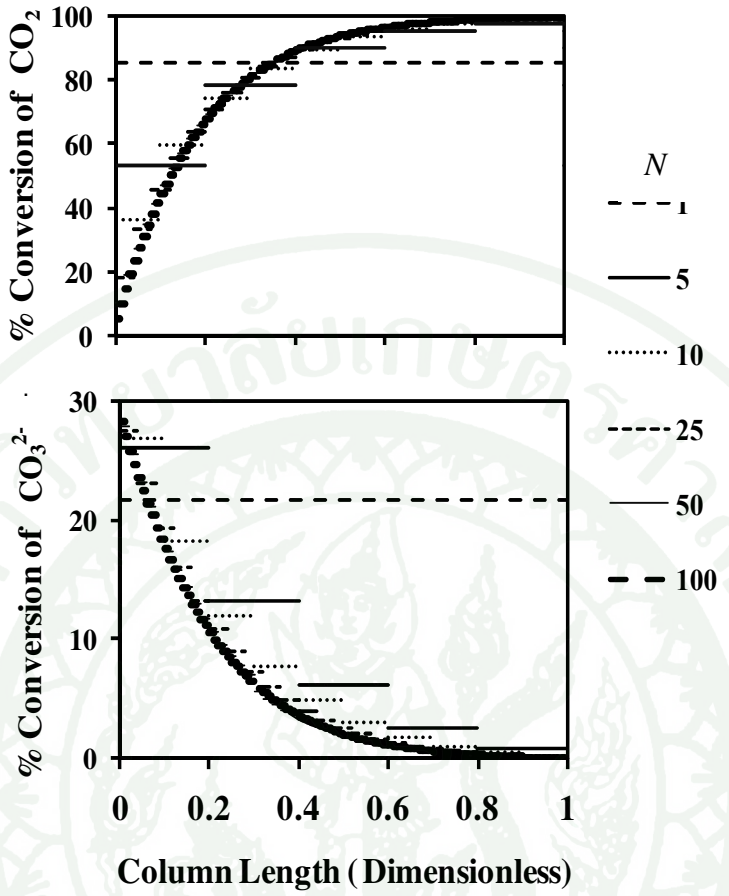

Figure 43 Conversion profiles as a function of the number of mixing cells for CO_2-Na_2CO_3 reaction in a counter current mode.

4. Effect of the Operating Mode on Reactor Performance

This section studies the effect of the operating mode on the reactor performance. Co-current and counter modes were studied. In a co-current mode, two flows of gas and liquid move upwards in the same direction while in a counter current mode two flows move in opposite directions in which the gas phase flows upwards and the liquid phase flows downwards. The mixing cells in numbers are set to be five and twenty-five cells for both gas and liquid phases. The effect of operating mode on the reactor performance for various reactions such as the CO_2 and NaOH, H_2S and Fe^{3+} (EDTA), and $CO_2$and Na_2CO_3 reactions are shown in Figures 44-46.

A. CO_2-NaOH reaction

The effect of the operating mode on the performance of the reactor for chemisorptions of cabon dioxide into aqueous solution of sodium hydroxide is shown in Figure 44 (a) and (b). Figure 44 (a) shows the conversions of the reactants, CO_2 and NaOH. The number of mixing cell is set to be five cells. It can be seen that the conversion of CO_2 in a counter-current mode gives higher conversion than that in co-current mode. Because a counter current mode gives higher driving force for mass transfer than that of a co-current mode. This leads to higher mass transfer. On the other hand, the co-current mode gives higher conversion of NaOH than that in counter current mode because the concentration of gas is low at the top of the reactor. Thus gas phase reactants are slightly soluble in the liquid phase so that the consumption of NaOH is low. Futhermore, the conversion of CO_2 is not significantly difference in both modes because at small mixing cell number the flow behavior is closed to a mixed flow. Figure 44(b) shows the effect of the operating mode on the performance of the reactor using twenty-five (N=25) mixing cell numbers. The result is similar to that at five of mixing cell number (N=5). In addition, the conversion of CO_2 at twenty-five mixing cell numbers in a counter current mode is higher than that of a co-current mode most of the reactor lenght. This due to large mixing cell number leading to higher driving force of mass transfer.

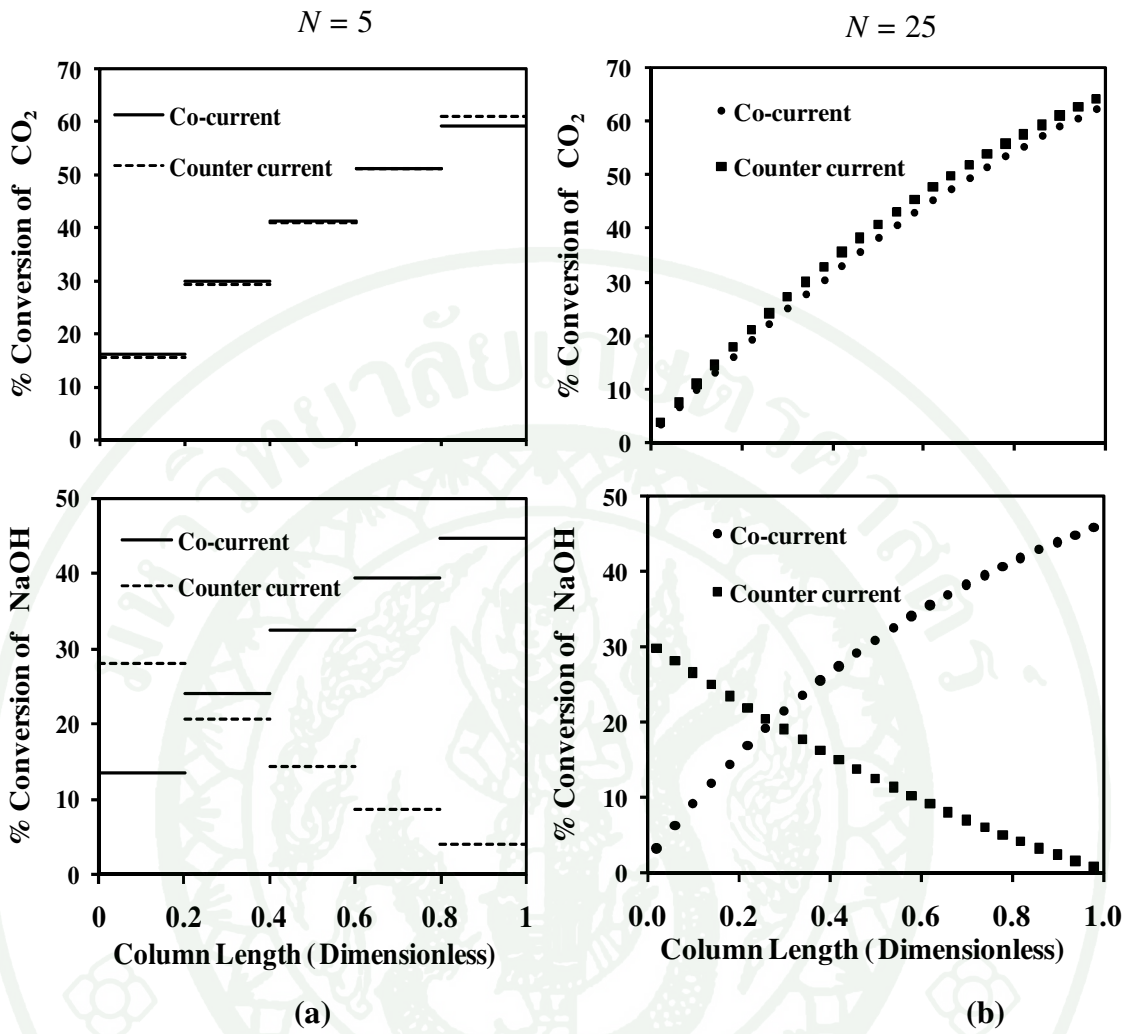

Figure 44 The effect of operating mode on the conversion CO_2 and NaOH in a co-current and counter current modes for mixing cell number N=5 (a) and N=25 (b).

B. H_2S-Fe^{3+}(EDTA) reaction

The effect of the operating mode on the performance of the reactor for the reaction of H_2S-Fe^{3+}(EDTA) is shown in Figure 45(a) and (b). The conversion of H_2S at the exit in the counter-current mode is higher than that in a co-current mode due to higher mass transfer than that in a counter-current mode. This is similar to that in the first case study, CO_2-NaOH reaction. On the other hand, the co-current mode gives higher conversion of Fe^{3+}(EDTA) than that in the counter current mode

due to the slightly soluble of gas in the liquid phase at the top of the reactor. At the number mixing cell number of 25 (N=25), the conversion of H_2S in a counter current mode is still higher than that of co-current mode along column length.

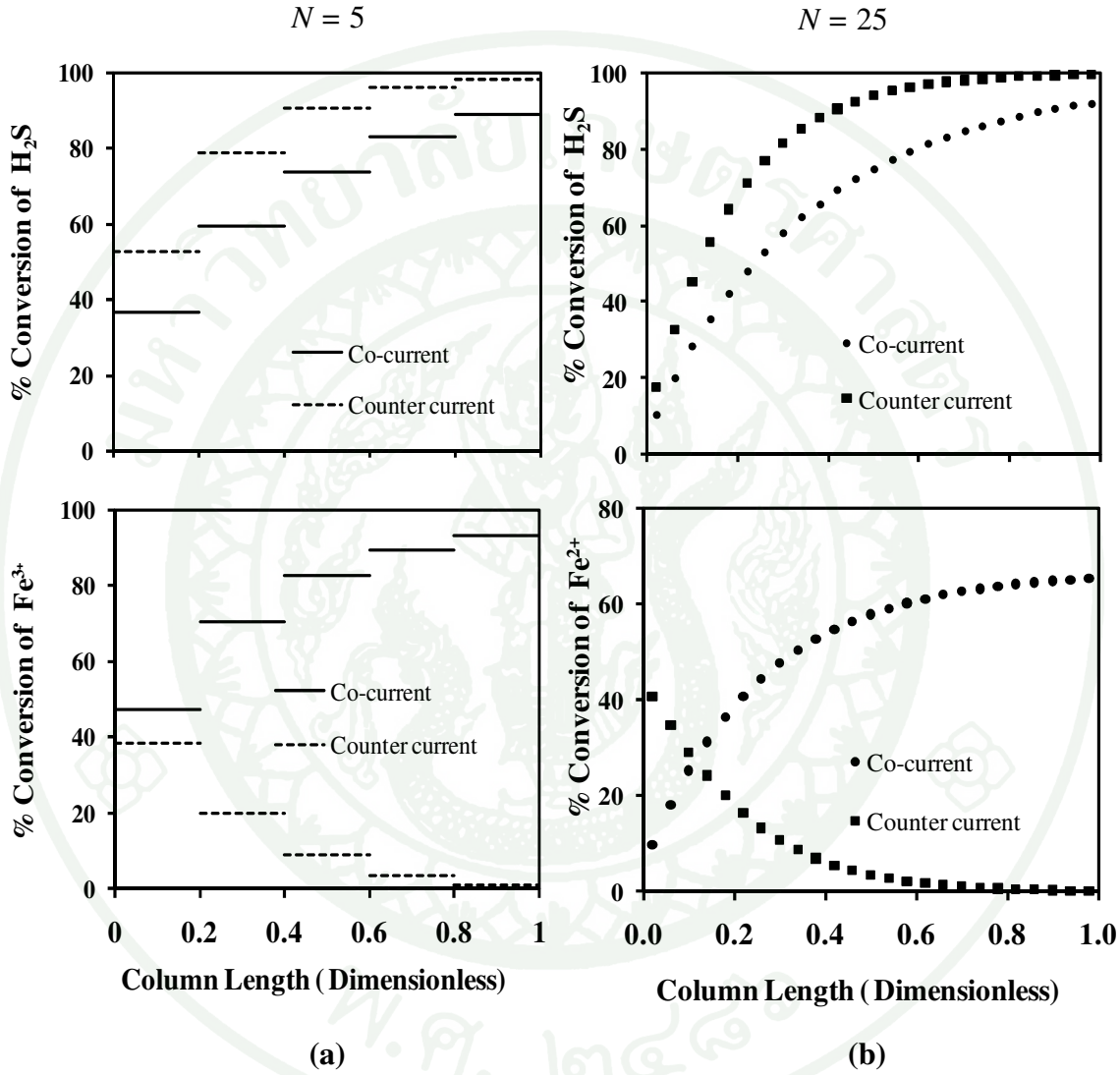

Figure 45 Effect of operating mode on the conversion of H_2S-Fe^{3+}(EDTA) reaction for co-current and counter current modes for mixing cell number N=5 (a) and N=25 (b).

C. CO_2-Na_2CO_3 reaction

The effect of the operating mode on the performance of the reactor for the chemisorptions of CO_2-Na_2CO_3 reaction is shown in Figure 46 (a) and (b). From the reaction scheme, it can be seen that on the bottom of reactor the conversion of CO_2 for N=5 and N=25 both in co-current and counter current modes is not different much, but at the top of reactor the conversion of CO_2 in counter current mode gives higher conversion than that of co-current mode. This result is similar early two cases, CO_2-NaOH and H_2S-Fe^{3+} (EDTA) reactions, that is a counter-current mode gives higher conversion than that in a co-current mode.

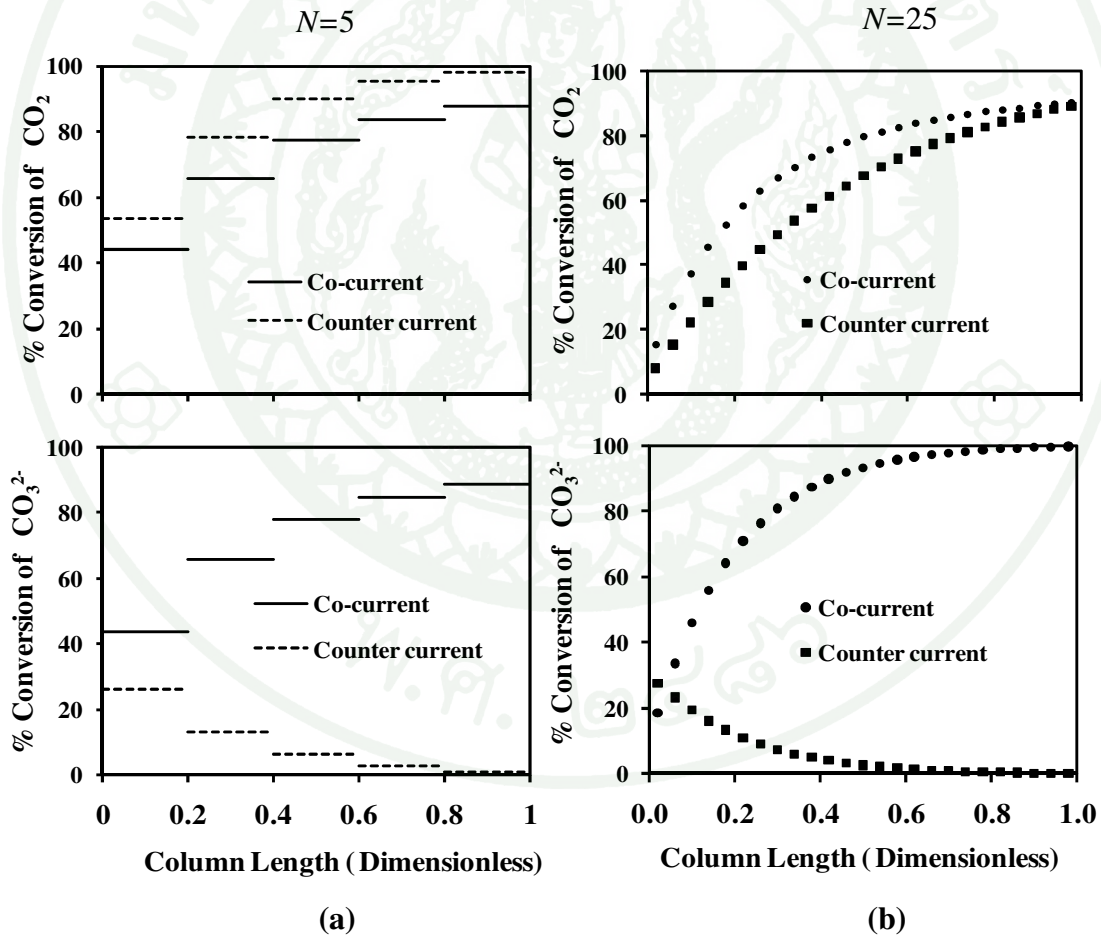

Figure 46 Effect of operating mode on the conversion CO_2-Na_2CO_3 reaction for co-current and counter current modes for mixing cell number N=5 (a) and N=25 (b).

5. Prediction Enhancement Factor (*Ea*)

This section studies the effect of the mixing cell on the Enhancement factor in the co-current and counter current modes. The gas-liquid reactions mainly occur in gas absorption processes, in which the reaction is applied as a means of accelerating the absorption. The reactions invoved in these absorption processes may be fast, intermediate, or slow reactions. The reaction regime was shown in Section 3 (mass transfer in gas-liquid reactions). For a fast reactions, Hatta Number (*Ha*) is large; it is often justified to consider the reaction to be completed in the film. However, some important industrial gas-liquid reaction which is a slow reaction, quite often the Hatta Number (*Ha*) is much smaller than one. There are many researches which study the relationship of Hatta Number (*Ha*) versus Enhancemen factor (*Ea*) as shown in Figure 21. Enhancement factor (*Ea*) is a parameter used to evaluate the expression rate of reaction, which is useful for reactor design. Enhancement factor (*Ea*) is defined as the ratio of the rate of taking up of gaseous reactant when reaction occurs to the rate of taking up of gaseous reactant for straight mass transfer. Various types of reactions are investigated which are the gas liquid reactions of CO_2-NaOH, H_2S-Fe^{3+} (EDTA) and CO_2-Na_2CO_3. The enhancement factor (*Ea*) profiles along the reactor length as a function of number of mixing cells are shown in Figures 47-52.

A. CO_2-NaOH reaction

The simulation condition for studying the effect of mixing cell on the Enhancement factor in co-current and counter current mode. This section the numbers of mixing cell for gas and liquid phases are equal. Figure 47 shows the enhancement factor profiles along reactor length as a function of number of mixing cells for CO_2-NaOH reaction.

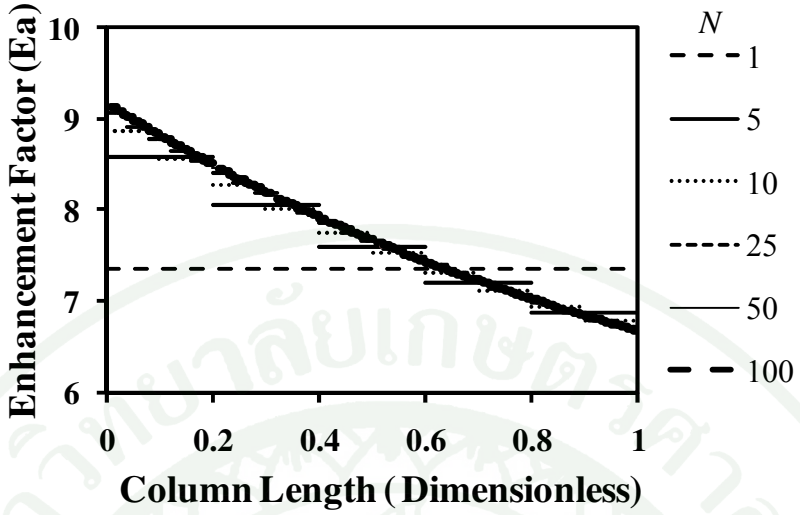

Figure 47 Enhancement factor along the reactor length as a function of the number of mixing cells for CO_2-NaOH reaction in a co-current mode.

The enhancement factor (*Ea*) of the system with the number of mixing cell of 1 ($N = 1$), which has complete mixed flow is constant at 7.36 along the column length. Enhancement factor (*Ea*) decreases along the column length when the number of mixing cells is more than one. Because the concentration of liquid reactanct is decreased leading to lower Hatta number.Thus, the reaction rate is slower. At the number of mixing cells more than 25 ($N > 25$), the enhancement factor (*Ea*) profiles do not change with the number of mixing cells. The lowest enhancement factor (*Ea*) at the number of mixing cells of 100 ($N = 100$) is 6.68. Enhancement factor (*Ea*) increases with decreasing number of mixing cell. The enhancement factors (*Ea*) for all the number of mixing cell are more than one and depend on the concentration of reactant. As shown in the previous section, it was found that increasing number of mixing cells, the concentration of reactant decreases. Thus, the lower concentration of reactant leads to lower enhancement factor (*Ea*). Therefore, at the outlet of the reactor the enhancement factor for the number of mixing cells of 100 ($N = 100$) is smallest and the CSTR obtains the greatest enhancement factor (*Ea*). Addionally, the Enhacement factor is more than one. The fast reaction ocurrs

.

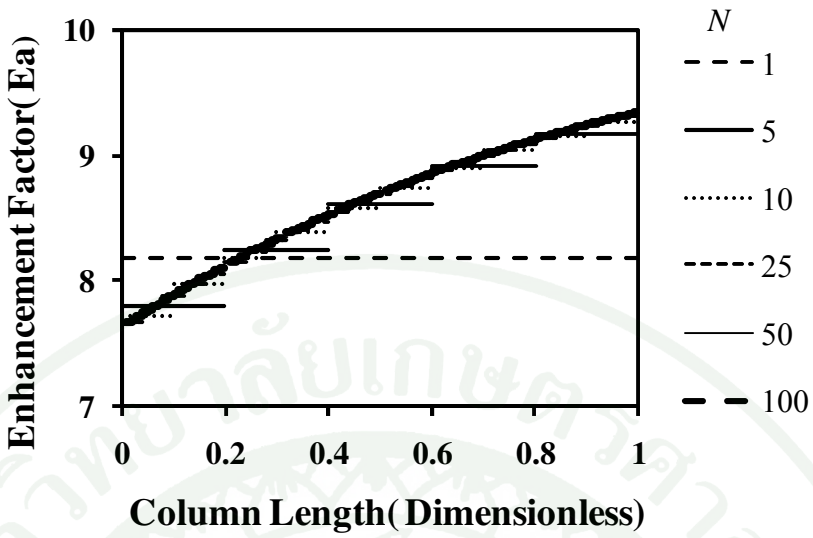

Figure 48 Enhancement factor along the reactor length as a function of the number of mixing cells for CO_2-NaOH reaction in a counter current mode.

The enhancement factor (*Ea*) along the rector length as a function of mixing cell number for CO_2-NaOH reaction in a counter current mode is shown in Figure 48. The enhancement (*Ea*) factor of this system with a complete mixed flow (the number of mixing cell =1) is constant at 8.18 along the column length. When the mixing cell number is more than one ($N > 1$), the enhancement factor increases along the column length. Enhancement factor (*Ea*) increases with increasing number of mixing cells due to higher concentration of NaOH. High concentration of liquid phase reactant leads to high enhancement factor. At the mixing cell number more than ten ($N > 10$), the enhancement factor do not change with the number of mixing cells.

B. H_2S-Fe^{3+} (EDTA) reaction

Figures 49-50 show the enhancement factor profiles along with the column length as a function of number of mixing cells for H_2S-Fe^{3+} (EDTA) reaction in co-current and counter current modes.

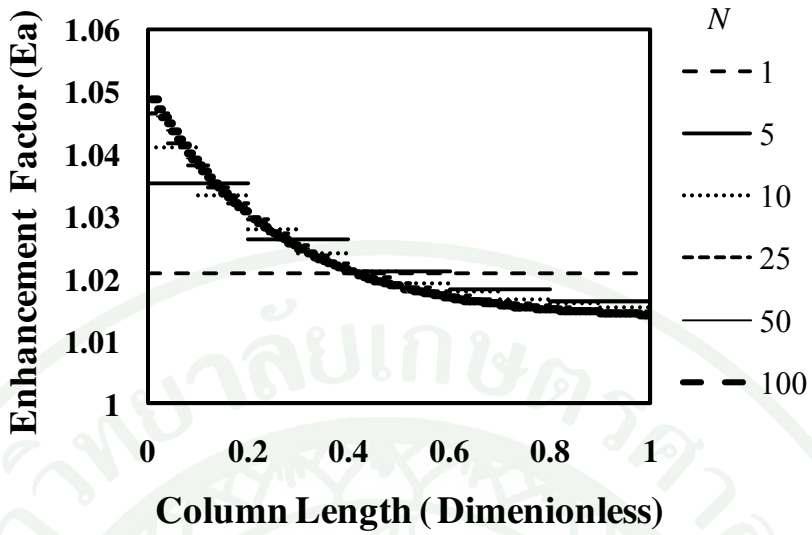

Figure 49 Enhancement factor along the column length as a function of mixing cells number for H_2S-Fe^{3+} (EDTA) reaction in a co-current mode.

Figure 49 shows enhancement factor (*Ea*) along the reactor length as a function of number of the mixing cells for H_2S-Fe^{3+} (EDTA) reaction in a co-current mode. It was found that the enhancement factor of the system with the mixing cell of one ($N = 1$) is constant at 1.023 along the column length. Enhancement factor (*Ea*) gradually decreases along the column length when the number of mixing cells is more than one ($N > 1$). At the number of mixing cells more than 50 ($N > 50$), the enhancement factors (*Ea*) profiles do not change with the number of mixing cells. The lowest enhancement factor (*Ea*) for the number of mixing cells of 100 ($N = 100$) is 1.016 at the top of column. The effect of the number of mixing cells for this reaction scheme is similar in that of CO_2-NaOH reaction. Enhancement factor (*Ea*) increases with decreasing the number of mixing cell. Enhancement factors (*Ea*) for all number of mixing cells is slightly more than one and depends on the concentration of reactant. It was found that increasing the number of mixing cell, the concentration of reactant decreases as shown in the previous section. Thus, the high concentration of reactant leads to high Enhancement factor (*Ea*).

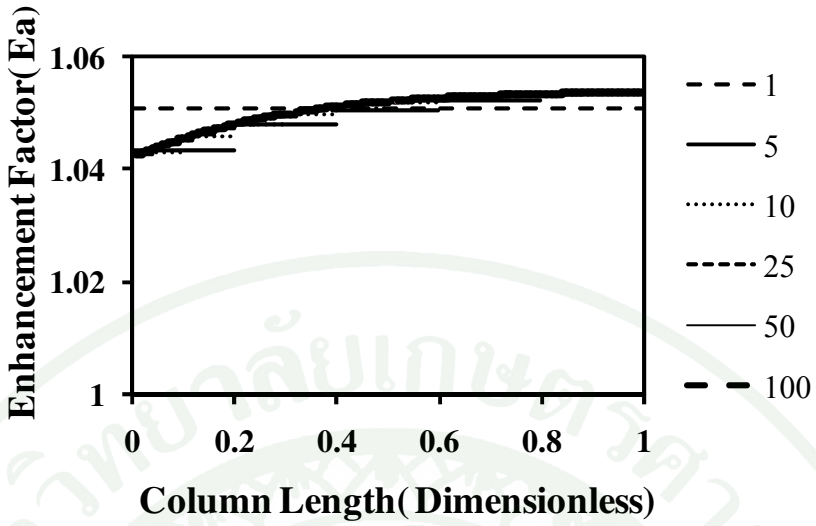

Figure 50 Enhancement factor along with the column length as a function mixing cells number for H_2S-Fe^{3+} (EDTA) reaction in counter current mode.

The enhancement factor (*Ea*) along column length as a function of mixing cell number for H_2S-Fe^{3+} (EDTA) reaction in a counter current mode is shown in Figure 50. The enhancement (*Ea*) factor of this system for a complete mixed flow is constant at 1.051 along the column length. When the mixing cell number is more than one ($N > 1$), the enhancement factor is increased along with the column length, and nearly constant at column length of 0.6 (The enhancement factor is not different from that at the number of mixing cell of 10. Enhancement factors (*Ea*) for all number of mixing cells depends on the concentration of reactant. Thus, the high concentration of reactant leads to high Enhancement factor (*Ea*).

C. CO_2-Na_2CO_3 reaction

Figure 51-52 show the enhancement factor profiles along with the column length as a function of number of mixing cells for CO_2-Na_2CO_3 reaction in co-current and counter current modes.

The enhancement factor (*Ea*) along column length as a function of mixing cell number for CO_2-Na_2CO_3 reaction in a co-current mode is shown in Figure

51. The enhancement (*Ea*) factor of this system is constant at 0.45 along the column length. When the mixing cell number is more than one ($N > 1$), the enhancement factor decreases along column length. Enhancement factor (*Ea*) increases with increasing the number of mixing cells.With the number of mixing cell above 50 (*N*>50) the enhancement factor does not depend on the number of mixing cell. The enhancement factor for this reaction is in slow regime.

The enhancement factor (*Ea*) along the rector length as a function of mixing cell number for CO_2-Na_2CO_3 reaction in a counter current mode is shown in Figure 52. The Enhancement (*Ea*) factor of this system is constant at 1.16 along the column length. This is similar to that for CO_2-NaOH reaction. When the mixing cell number is more than one ($N > 1$), the enhancement factor increases along column length, the enhancement factor is does not change with number of mixing cellwhen *N* is large than 10 ($N > 10$). Enhancement factor (*Ea*) increases with increasing number of mixing cells due to higher concentration of CO_2-Na_2CO_3 reaction at the top of reactor compared to that at the bottom of the reactor.

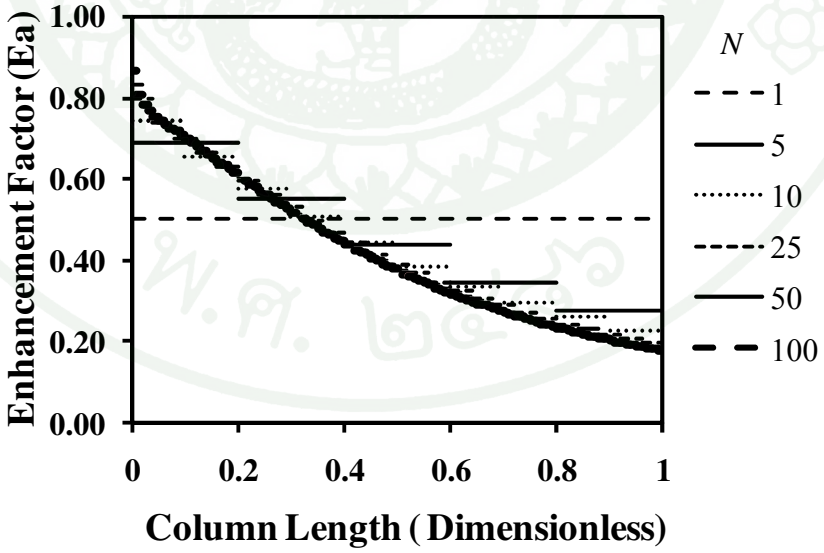

Figure 51 Enhancement factor along with the column length as a function mixing cells number for CO_2-Na_2CO_3 reaction in co-current mode.

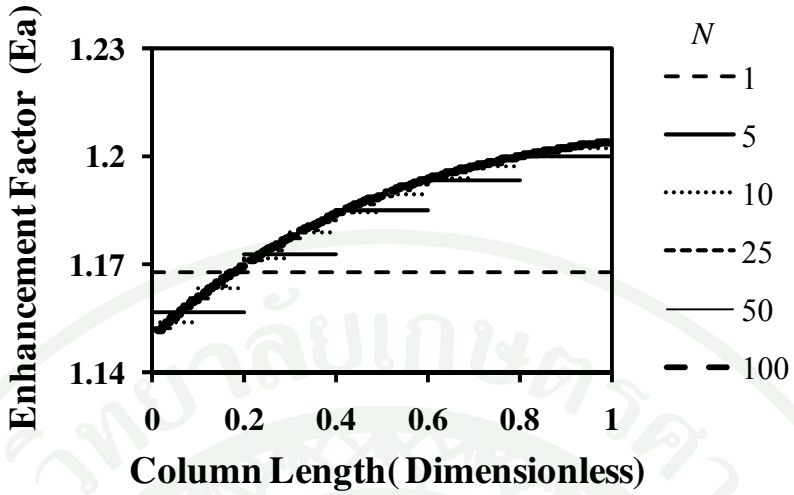

Figure 52 Enhancement factor along with the column length as a function mixing cells number for CO_2-Na_2CO_3 reaction in counter-current mode.

6. The Lo-Cat process

This section shows an application of the model to industrially importance case study which is Lo-Cat process. This research work involves the study of the performance of the Lo-Cat gas-lift reactor and the effects of operating conditions on the H_2S removal efficiency. The Lo-Cat process is a liquid phase oxidation. The Lo-Cat process can be divided into two steps, the reaction and the regeneration steps. These two steps occur in a gas-lift reactor as shown in Figure 53.

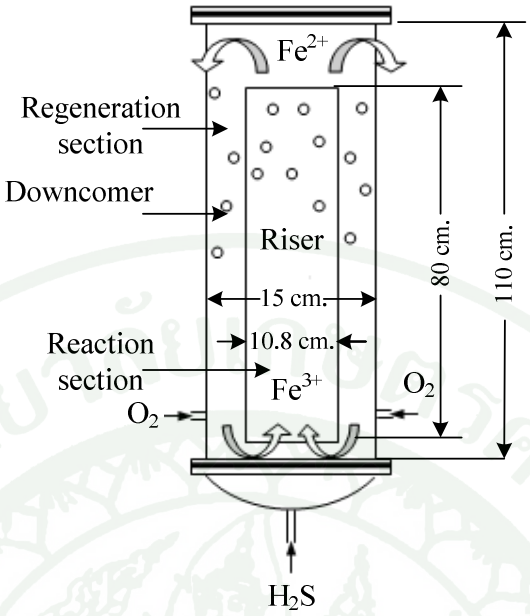

Figure 53 Schematic of gas-lift reactor

The reaction step occurs in the riser of gas-lift. Gas containing H_2S is fed through a gas distributor into the riser filled with Fe^{3+}(EDTA) solution. In the reaction section, H_2S is absorbed and reacted in the riser as follow:

6.1 Reactions

a. Reaction section

H_2S from the gas stream is absorbed into the circulating aqueous Lo-Cat solution in the riser as shown in Eq (119).

Absorption $$H_2S(g) + H_2O(aq) \leftrightarrow H_2S(aq) + H_2O(aq) \quad (119)$$

Once absorbed, H_2S ionizes into hydrogen and hydrosulfide ions as shown in Eq (120).

Ionization $$H_2S(aq) \leftrightarrow HS^-(aq) + H^+(aq) \quad (120)$$

Hydrosulfide ions then react with ferric ions to form elemental solid sulfur and ferrous ions (see Eq (121)).

Oxidation $$HS^{-}(aq) + 2Fe^{3+}(aq) \rightarrow 2H^{+}(aq) + S^{0}(solid) + 2Fe^{2+}(aq) \quad (121)$$

b. Regeneration section

Used simulation mainly containing ferrous ions (Fe^{2+}) from the riser and circulating down into the downcomer. The regenerated solution containing Fe^{3+} can be circulated back into the riser for reusing. The regeneration in the downcomer is accomplished by sparging air through the effluent solution Eq (122). Oxygen is absorbed into the solution, which then oxidizes the ferrous ions back to the ferric state (Eq (123) (Horikawa *et al*., 2004).

Absorption $$O_2(g) + H_2O(aq) \leftrightarrow O_2(aq) + H_2O(aq) \quad (122)$$

Oxidation $$O_2(aq) + H_2O(aq) + Fe^{2+}(aq) \leftrightarrow 2OH^{-}(aq) + H^{+}(aq) + Fe^{3+}(aq) \quad (123)$$

6.2 Reactor

a. Removal Reactor

In reaction section, the riser diameter and height are 0.108 and 0.8 m, respectively. The details of the riser features are given in Table16. The used gas holdup in riser, ε_{gr}, can be obtained from the experimental as shown in Table 17 (Limtrakul *et al.,* 2005). The interfacial area per volume in the riser can be estimated by Eq (125). Table 17 shows the operating conditions for H_2S-Fe^{3+}(EDTA) system. The superficial gas velocity in the riser, U_{gr}^{0}, was varied from 0.03 to 0.11 m/s. The feed gas H_2S concentration is 5.4% (54,000 ppm) according to Rojanamatin's experiments (2000). The liquid circulating from the downcomer is fed into the riser

with the Fe^{3+}(EDTA) of 6 gmol/m^3. Experiments were carried out at ambient temperature and atmosphere pressure condition. The kinetics rate constant, diffusion coefficient solubility parameter used in the reaction of H_2S-Fe^{3+}(EDTA) are shown in Table 18. The rate constant in this reaction, Hennry's law constant, and diffusivity of H_2S-Fe^{3+}(EDTA) were determined from Deberry *et al.*(1993). The hydrodynamics data such as k_L and a (interfacial area) were obtained using correlation of Kaštánek, (1997) (Eq (124)), and Fukuma *et al.* (1987) (Eq (125)), respectively.

b. Regeneration Reactor

In the regeneration section, the diameter and height of the downcomer is 0.15 and 1.1 m, respectively as shown in the Table 19. The interfacial area in the downcomer was also calculated by Eq (125). The gas holdups in the downcomer were carried out from the experimental data as shown in Table 22 (Limtrakul *et al.,* 2005). The operating conditions for regeneration system (O_2-Fe^{2+}(EDTA) system) are given in Table 20. The superficial gas velocity in the downcomer is fixed at 0.01 m/s. The feed concentration of ferrous chelate at the top of the downcomer from the riser is equal to that of the outlet solution circulated from the riser. Furthermore, Table 21 given the kinetics, diffusion, and solubility parameters for O_2-Fe^{2+}(EDTA) system. The reaction rate is appeared to proceed according to $r_1 = k_{O_2} C_{O_2} C^2_{Fe^{2+}}$ with the rate constant, k_{O_2} of 38,000 $m^6/mol^2 \cdot s$ according to Demmink *et al.* (1997). The liquid phase mass transfer coefficient in the downcomer is calculated from the mass transfer coefficient in Equation (124).

As mentioned above, the mass transfer coefficient in liquid phase, $k_l a$, in bubble columns can be obtained from the following correlation *(*Kaštánek*,* 1997*):*

$$k_l a = 0.5736 U_g^{0.65} \varepsilon_g^{0.35} (1-\varepsilon_g)^{0.65} \qquad (124)$$

where U_g^0 is superficial gas velocity and ε_g gas holdup.

Mass transfer in a bubble column reactor depends on interfacial area per volume of reactor related to gas hold up, ε_g and the sauter mean, d_s (Fukuma *et al.,* 1987)

$$a = \frac{6\varepsilon_g}{d_s} \tag{125}$$

In this case study, the interfacial area per volume of reactors depends on the gas hold up in riser and downcomer. The bubble diameter is in the range of 1.55-2 mm (Kaštánek, 1997) and is assumed to be 2 mm here.

Table 16 The features of the riser reactor

Reaction scheme in the riser		
$H_2S + 2Fe^{3+}(EDTA) \xrightarrow{k_1} 2Fe^{2+} + S^0 + 2H^+$	$r_1 = k_{H_2S} C_{H_2S} C_{Fe3+}$	
Features	Value	Reference
Diameter (m)	0.108	
Length of riser (m)	0.8	
Volume of reactor (m^3)	0.018	
Gas hold up (-)	Experiment data	[Table 22]

Table 17 Operating conditions for H_2S-Fe^{3+}(EDTA) system.

Operating conditions	Value	Reference
Superficial gas velocity (m/s)	0.03-0.11	
Superficial liquid velocity (m/s)	Experimental data	Limtrakul *et al*. (2005)
Feed gas concentration of H_2S (ppm)	54,000	
Feed concentration of Fe^{3+}(EDTA) (initial) (mol/m^3)	6	
Pressure (Pa)	1.1035×10^5	
Temperature (K)	298	

Table 18 Kinetics, Diffusion, and Solubility Parameters for H_2S-Fe^{3+} (EDTA) system.

Parameters	Value	Reference
Rate constant (m^3/mol·s)	9	Deberry (1993)
Henry's law constant (Pa·m^3 / mol)	1,950	Deberry (1993)
Gas phase mass transfer coefficient (mol/m^2·s·atm)	0.4	Perry and Green (1997)
Liquid phase mass transfer coefficient (m/s)	Equation (125)	Kastanek (1997)
Diffusion coefficient in liquid of H_2S (m^2/s)	1.44×10^{-9}	Deberry (1993)
Diffusion coefficient of Fe^{3+} (EDTA) (m^2/s)	0.54×10^{-9}	Deberry (1993)

Table 19 The features of gas-lift reaction in the downcomer

Reaction scheme in the downcomer	
$O_2 + 4Fe^{3+}(EDTA)^{3-} + 2H_2O \xrightarrow{k_1} 4Fe^{3+}(EDTA) + 4OH^-$	$r_1 = k_{O_2} C_{O_2} C^2_{Fe^{2+}}$

Features (Annular)	Value	Reference
Inside diameter (m)	0.108	
Outside diameter (m)	0.15	
Length of riser (m)	1.1	
Volume of reactor (m^3)	0.019	
Gas hold up (-)	Experiment data	Limtrakul *et al.* (2005)
Interfacial area (m^{-1})	Equation (125)	Fukuma *et al.* (1987)

Table 20 Operating conditions for regeneration system (O_2-Fe^{2+}(EDTA) system).

Operating conditions	Value	Reference
Superficial gas velocity (m/s)	0.01	
Superficial liquid velocity (m/s)	Experiment data	[Table 22]
Feed gas concentration of O_2 (%)	21	Limtrakul *et al.* (2005)
Inlet concentration of Fe^{2+}(EDTA)	Riser outlet concentration	
Pressure (Pa)	1.1035×10^5	
Temperature (K)	298	

Table 21 Kinetics, Diffusion, and Solubility Parameters for O_2-Fe^{2+}(EDTA) system.

Parameters	Value	Reference
Rate constant ($m^6/mol^2 \cdot s$)	38,000	Demmink (1993)
Henry's law constant ($kPa \cdot m^3/mol$)	121	Demmink (1993)
Gas phase mass transfer coefficient ($mol/m^2 \cdot s \cdot atm$)	0.4	Perry and Green (1997)
Liquid phase mass transfer coefficient (m/s)	Equation (125)	Kastanek (1997)
Diffusion coefficient in liquid of O_2 (m^2/s)	0.78×10^{-9}	Demmink (1993)
Diffusion coefficient of Fe^{2+}(EDTA) (m^2/s)	0.54×10^{-9}	Deberry (1993)

Table 22 Gas holdup, gas superficial velocities in the riser and downcomer, and superficial liquid velocity used for simulation.

Superficial gas velocity		Gas holdup				Superficial liquid velocity (m/s) (calculated)
		Riser		Downcomer		
U_{gr}^{0} (m/s)	U_{gd}^{0} (m/s)	ε_{gr} (-) (Exp.)	u_{lr} (m/s) (calculated)	ε_{gd} (-) (Exp.)	u_{ld} (m/s) (Exp.)	
0.03	0.01	0.0625	0.025	0.056	0.025	0.023
0.06	0.01	0.094	0.056	0.081	0.055	0.049
0.09	0.01	0.108	0.085	0.104	0.085	0.067
0.11	0.01	0.132	0.106	0.125	0.105	0.091

This case study involves studying the performance of the air-lift reactor in co-current (riser) and counter current (downcomer) modes. These studies can be divided into three parts. Firstly, comparison the profile of Fe^{3+}(EDTA) for the experiments and the model in the riser and downcomer. Secondly, the effects of the superficial gas velocity on mixing cell number. Finally, the effect of the superficial gas velocity on the conversion of H_2S, Fe^{3+}(EDTA) and Fe^{2+}(EDTA) in the riser and downcomer. The simulation results shown as follows:

6.3 Comparison of the simulation results with the experimental results

The comparisons of the simulation results with experimental results were obtained in this section. In the mixing cell model, the number mixing cell number is potentially useful to indicate the flow behavior in the reactor. If the number of mixing (N) approaches to one cell, the flow in the reactor is complete mixed (CSTR) which has high degree of mixing. If the number of mixing cell approaches to ∞, the plug flow occurs. The flow behavior in an air-lift reactor is similar to that of bubble column. Additionally, the flow behavior of gas and liquid phases in the riser and the

downcomer of gas-lift, can be indicated by the Peclet number, *Pe* (corresponding to axial dispersion coefficient, D_{ax}). *Pe* can be converted to the number of mixing cell (*N*) as shown in (Equation (126)) (Klein *et al.,* 2004).

$$\frac{1}{N} = \frac{2}{Pe}\left[1 - \frac{1}{Pe}(1 - e^{-Pe})\right] \tag{126}$$

Pe is related to the gas superficial gas velocity as experimentally obtained in the riser and downcomer by Camarasa *et al.* (2001). Although the experimental results of Klein *et al.* (2004) was obtained in a gas-lift reactor with the single sparger in the riser, the Peclet numbers are applied in any work in which two spargers are involved due to lack of available informations. Table 23 shows liquid phase Peclet number (*Pe*) in the dispersion model and corresponding number of mixing cell at different superficial gas velocities in the riser and downcomer. These information are evaluated from the experimental data of Klien et al (2004).

The simulation was carried out with the mixing cell number of 27 and 36 in the riser and downcomer, respectively. The gas feed concentration of H_2S is 54,000 ppm. The feed concentration of Fe^{3+}(EDTA) is 6.00 gmol/m^3. The superficial gas velocity in the riser is 0.03 m/s and the superficial gas velocity in the downcomer is fixed at 0.01 m/s. The experiment data of reactor performances can be obtained from Rojanamatin (2002).

Table 23 The Peclet number (*Pe*) and number of mixing cell (*N*) for difference gas velocities in a gas-lift reactor.

Superficial gas velocity		Peclet number		Number of mixing cell	
u_{gr} (m/s)	u_{gd} (m/s)	Pe_r	Pe_D	Riser	Downcomer
0.03	0.01	53	72	27	36
0.06	0.01	47	64	24	32
0.09	0.01	41	56	21	28
0.11	0.01	38	52	19	26

Figure 54 shows the predicted axial profiles of the Fe^{3+}(EDTA) concentration in the riser at a superficial gas velocity in the riser of 0.03 m/s and that in the downcomer of 0.01 m/s. the number of cells that used in the calculation is 27. The diameter of the bubble was assumed to be 2 mm. The results from the model and experiments are in good agreement. Fe^{3+}(EDTA) concentration decreases along the riser height. The experiment data of reactor performances was also obtained from Rojanamatin (2000) as shown in Figure 1. The measured Fe^{3+}(EDTA) at the top of the riser is slightly higher than the predict value due to the air oxidation occurring at the surface. At the height of 0.3-0.7 m, the experimental concentrations are lower than the model prediction values. This inconsistency may be due to the use of the average value of the hydrodynamic parameter such as the bubble diameter, circulation velocity, and gas hold up for the entire riser.

Figure 55 compares the measured and predicted axial concentration profiles of Fe^{3+}(EDTA) in the downcomer. A number of mixing cells of 32 was used for the downcomer. The flow is less backmixed than that in the riser because of lower gas velocity in the downcomer. The model–predicted conversion of Fe^{3+}(EDTA) agrees well with the experimental value.

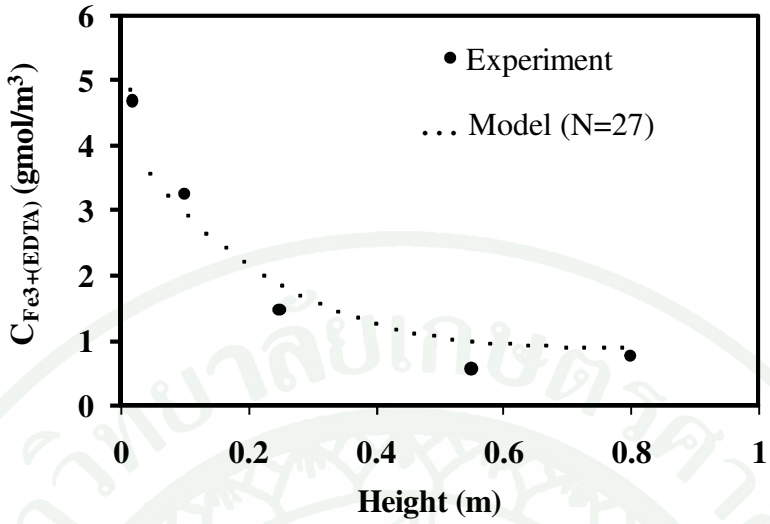

Figure 54 The comparison of concentration profiles of Fe^{3+}(EDTA) obtained by experiment and model in riser at U_{gr}^{0} = 0.03 m/s and U_{gd}^{0} = 0.01 m/s, number of cell =27.

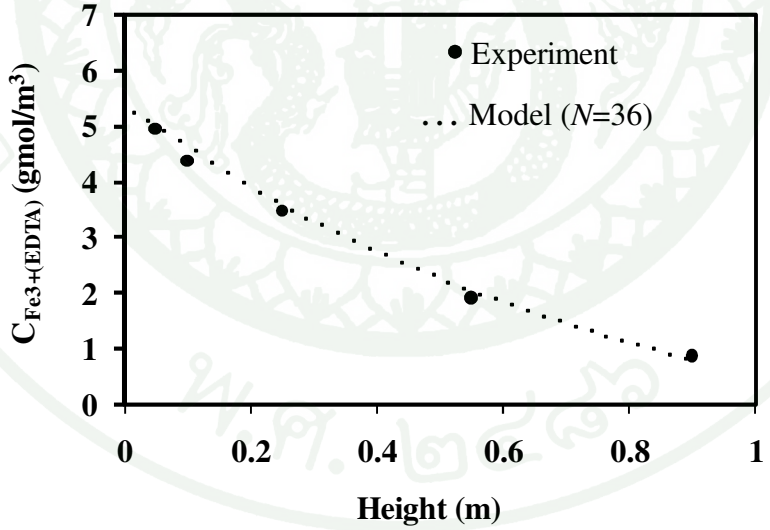

Figure 55 The comparison of concentration profile of Fe^{3+}(EDTA) obtained by experiment and model in downcomer at U_{gr}^{0} = 0.03 m/s and U_{gd}^{0} = 0.01 m/s, number of cell =36.

The effect of gas superficial velocity on conversion in riser and downcomer can be shown. The superficial gas velocity in the riser was varied from 0.03 to 0.11 m/s. The superficial air velocity in the downcomer is fixed of 0.01 m/s.

Figure 56 shows the effect of the gas superficial velocity in the riser on the riser performance. It can be found that, when increasing the gas superficial velocity in the riser the number of mixing cell, *N*, is lower, the flow behavior approaches mixed flow. This means that at higher gas superficial velocity the backmixing increases. The number of cells used in the model predictions was 27, 24, 21, and 19 for the superficial gas velocities of 0.03, 0.06, 0.09, and 0.11 m/s, respectively. At all velocities, the comparisons show good agreements.

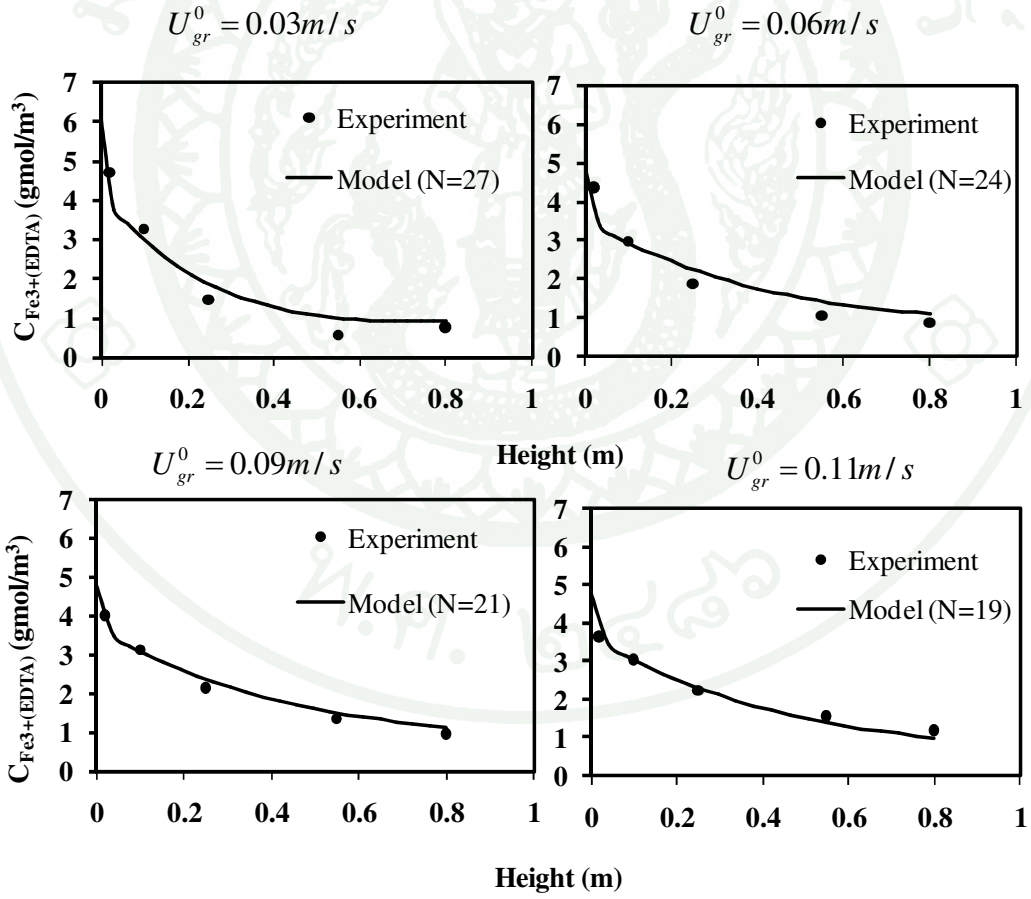

Figure 56 The effect of superficial gas velocity on the riser performance at U_{gr}^{0} = 0.03-0.11 m/s and U_{gd}^{0} = 0.01 m/s.

Figure 57 shows the effect of the gas superficial velocity in the riser on the downcomer performance. The numbers of mixing cells used in the model predictions were 36, 32, 28, and 26 for the superficial gas velocities of 0.03, 0.06, 0.09, and 0.11 m/s, respectively. It can be found that, at lower superficial gas velocity, the number of mixing cell (*N*) is higher than that of a higher superficial gas velocity, this is due to plug flow approaching behavior. Additionally, a number of mixing cells in a downcomer is different from that in the riser because in the downcomer, the superficial gas velocity is slow compared to that of riser, thus the lower degree of mixing occurs. Therefore the behavior of the downcomer is closed to plug flow. Experimental and simulation result are in a good agreement at most of feed velocities. At higher velocity slightly differenceness were found. This may be due to the hydrodynamic data such the interfacial area, overall mass transfer coefficient in liquid phase, and the gas holdup used in the model are the average values. The model should be able to predict better if these parameters can be measured locally and the local values are used in the model.

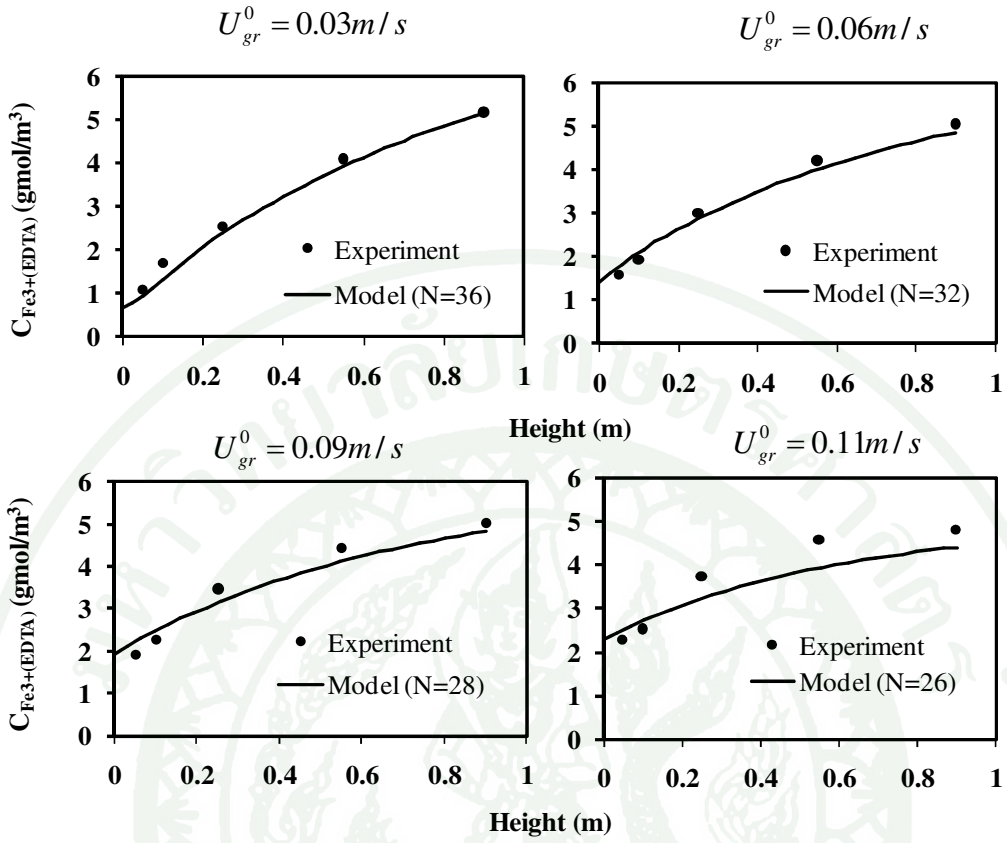

Figure 57 The effect of superficial gas velocity on the downcomer performance at U_{gr}^{0} = 0.03-0.11 m/s and U_{gd}^{0} = 0.01 m/s.

Figure 58 shows the effect of the gas superficial velocity of gas on the conversion of H_2S in the gas phase and Fe^{3+}(EDTA) conversion in the liquid in the riser. It was found that the conversion of H_2S decrease with increase in the superficial gas velocity in the riser due to its low residence time in the riser. H_2S is removed almost completely of 99.51% at the superficial gas velocity of 0.03 m/s and at the superficial gas velocity of 0.11m/s the conversions of H_2S and Fe^{3+}(EDTA) are lowest (73.66 and 63.2%, respectively). At any fixed value of the superficial air velocity in the downcomer, an increase in the superficial velocity in the riser increases the liquid circulation velocity in the reactor. This reduces the residence time of liquid phase in both the riser and downcomer during any one circulation. Consequently, the conversion of Fe^{3+}(EDTA) and Fe^{2+}(EDTA) in the riser and downcomer, respectively, were lower at a higher riser superficial gas velocity. Under the best conditions tested, Fe^{2+}(EDTA) was regenerate to Fe^{3+}(EDTA) in the downcomer with conversion of

84.61%. The comparisons of the simulation and experimental results of H2S removal, conversion in the riser and downcomer are in the same trends.

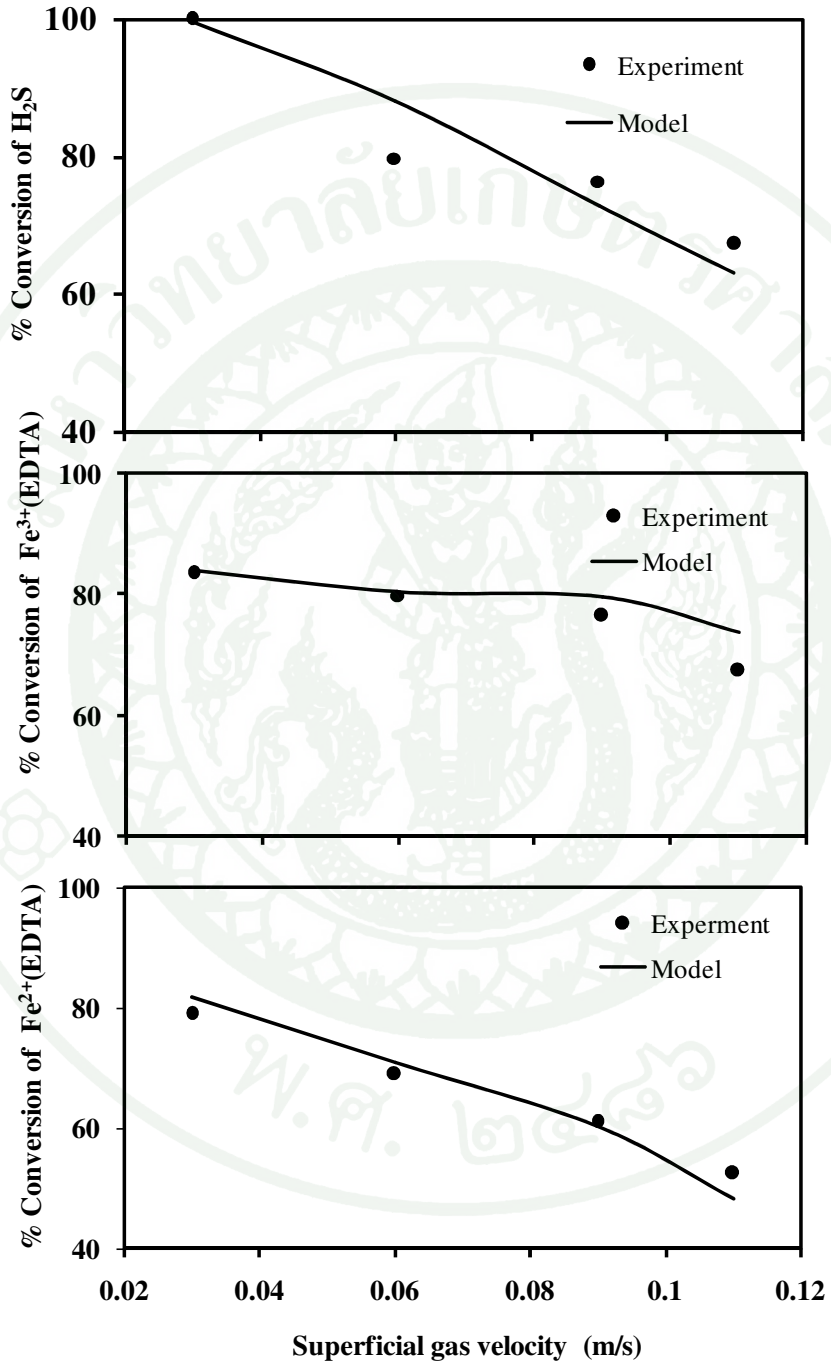

Figure 58 The effect of gas superficial velocity on conversions in riser (a and b) and in downcomer (c) at U_{gr}^{0} = 0.03-0.11 m/s and U_{gd}^{0} = 0.01 m/s.

CONCLUSIONS AND RECOMENDATION

This research is to develop the mathematical models for gas-liquid reactor using mixing cell model coupling with mass transfer and chemical reactions in an isothermal system. The conclusions of the simulation results are follows:

1. The concentration profiles of reactant along the film thickness indicate the reaction regime in a gas-liquid reaction. The chemisorptions of carbon dioxide into aqueous solution of sodium hydroxide is a fast reaction, which takes place only in the liquid film. The mass transfer resistance plays more important roll and controls the rate of reaction. H_2S-Fe^{3+}(EDTA) reaction is an intermediate reaction because the gaseous reactant is not completely used in the liquid film but further reacts in the liquid bulk. Both chemical reaction and mass transfer controls the reaction rate. CO_2-Na_2CO_3 reaction is a slow reaction. The concentration of reactant slightly decreases along the liquid film thickness. The kinetic reaction plays a major roll in the reaction rate.

2. The concentrations of both dissolved gaseous reactant and liquid reactant decrease along the column length for all studied reaction schemes, which are irreversible reactions. On the other hand, the concentration profiles of the product increases with increasing the column length for all reaction schemes.

3. The reactor performance (i.e. the conversion of gas and liquid reactants) was investigated in different flow behavior which is indicated by the number of mixing cells. It can be concluded that the conversions of CO_2-NaOH, H_2S-Fe^{3+}(EDTA) and CO_2-Na_2CO_3 reactions in the system with the mixing cell number of 1 are constant along the column length. The flow is complete mixed. The highest conversions are obtained for the system with the highest number of mixing cells (closed to plug flow). The conversion increases with increasing the number of mixing cells for all reaction schemes.

4. The operating mode of counter current for CO_2-NaOH, H_2S-Fe^{3+}(EDTA) and CO_2-Na_2CO_3 reactions gives higher conversion than that in a co-current mode due to the higher driving force in the counter current mode. This leads to higher mass transfer.

5. In the prediction of Enhancement factor (*Ea*) for various types of reaction regimes in co-current and counter current modes, it was found that if the values of Enhancement factor (*Ea*) of the fast rate reaction and intermediate rate reaction are more than unity, mass transfer rate is enhanced by chemical reaction. Enhancement factor (*Ea*) for a plug flow system (at very high N) is smallest and that for a CSTR is the greatest.

6. In the simulation studies of the gas-lift reactor in the Lo-Cat process, the predictions of the performances of the riser for H_2S removal and the downcomer for Fe^{3+}(EDTA) regeneration in the Lo-Cat air-lift reactor show that the riser reactor can remove H_2S almost completely (>99.5%) and the downcomer regenerator can convert Fe^{2+}(EDTA) to Fe3+(EDTA) with a conversion as high as 84.61% at the superficial gas velocities in the riser and in the downcomer of 0.03 and 0.01m/s, respectively. The comparison of the predictions by the model and the measuremental data shows essentially similar trends.

LITERATURE CITED

Akita, K. and F.Yoshida. 1973. Gas holdup and volumetric mass-transfer coefficient in bubble columns. **Industrial and Engineering Chemistry Process Design and Development.** 12: 76-80.

Akita, K. and F. Yoshida. 1974. Bubble size, interfacial area, and liquid-phase mass transfer coefficient in bubble columns. **Industrial and Engineering Chemistry Process Design and Development.** 13: 84–91.

Barnea, D., O. Shoham, Y. Taitel and A.E. Dukler. 1980. Flow Pattern Transition for Gas - Liquid Flow in Horizontal and Inclined Pipes, Comparison of Experimental Data with Theory. **Int. J. Multiphase Flow.** 6: 217-226.

Brahme P. H., R. V. Chaudhari and P. A. Ramachandran. 1984. Modeling of hydrogenation of glucose in a continuous slurry reactor. **Ind. Eng. Chem. Process Des. Dev.** 23(4): 857–859.

Brauer, H. 1981. Particle/fluid transport processes. **Progress in Chemical Engineering. 19**: 81–111.

Calderbank, P.H. and M.B. Moo-Young. 1961. The continuous phase heat and mass-transfer properties of dispersions**. Chemical Engineering Science.** 16: 39-54.

Camarasa, E., L. A. C. Meleiro, E. Carvalho, A. Domingues, R. Maciel Filho, G. Wild, S. Poncin, N. Midoux and J. Bouillard. 2001. A complete model for oxidation air-lift reactors**. Computers & Chemical Engineering**. 25(4-6): 577-584.

Carlos, G. D. 1998. Three-phase reactor modeling with significant backmixing in the liquid phase using a modified cell model (MCM). **Computers & Chemical Engineering**. 22: S679-S682.

Charpentier, J. C. and G. Wild. 1983 . Absorption avec réaction chimique. **Techniques de l'Ingénieur Paris.** J 2640.

Chaudhari, R.V., R. Jaganathan, D.S. Kolhe, G. Emig and H. Hofmann. 1987. Kinetic modelling of hydrogenation of butynediol using 0.2% Pd/C catalyst in a slurry reactor. **Applied Catalyst.** 29(1): 141-159.

Christine, R. and W. Gabriel. 2002. Mass transfer with chemical reaction: the slow reaction regime revisited. **Chemical Engineer Science.** 57: 3479-3484.

Danckwerts, P.V. and B.E. Kennedy. 1954. Kinetics of liquid-film process in gas absorption. Part I: Models of the absorption process. **Transactions of the Institution of Chemical Engineers and the Chemical Engineer**. 32:S49-S52.

Danckwerts, P.V. 1970. **Gas liquid reactions**. McGraw-Hill Pulb Inc., New York.

Danckwerts, P.V. and M.M. Sharma. 1996. Absorption of carbon dioxide into solutions of alkalis andamines. **The Chemical Engineer.** CE 244–280.

Darmana, D., R.L.B. Henket, N.G. Deen and J.A.M. Kuipers. 2007. Detailed modeling of hydrodynamics, mass transfer and chemical reactions in a bubble column using a discrete bubble model: Chemisorption of CO_2 into NaOH solution, numerical and experimental study. **Chemical Engineering Science.** 62(9): 2556-2575.

Dassori, C. G. 1998. Three-phase reactor modeling with significant backmixing in the liquid phase using a modified cell model (MCM).**Computers & Chemical Engineering.** 22 (1): S679-S682.

Deberry, D. W. 1993, Rates and Mechanism of reaction of Hydrogen Sulfide with iron Chelates, **Topical Report; Gas research Institute Des plaines, IL**.

Deckwer, W.D. 1980. On the mechanism of heat transfer in bubble column reactors, **Chemical Engineering Science.** 35(6):1341–1346.

Dehouche Z. and J. Lieto. 1995. Modelling and experimental study of key parameters of absorption on wetted sphere contactor. **Chemical Engineering Science.** 50(18):2899–2909.

Demmink, J. F., Beenackers, A. A. C. M. 1997, Oxidation of Ferrous Nitrilotriacetric Acid with Oxygen: A Model for Oxygen Mass transfer Parallel to Reaction Kinetics. **J. Ind. Eng. Chem. Res.** 36: 1989: 2005.

Doraiswamy, L.K. and M.M.Sharma. 1984. **Heterogeneous Reactions**. 2nd ed. John Sons, Inc., New York.

Edwards, T.J.,G. Maurer, J. Newman and J.M. Prausnitz. 1978. Vapor–liquid equilibria in multicomponent aqueous solutions of volatile weak electrolytes. **A.I.Ch.E. Journal.** 24: 966–976.

Eigen, M. 1954. Method for investigation of ionic reactions in aqueous solutions with half times as short as 10^{-9}s. **Discussions of the Faraday Society**. 17: 194–205.

Frank, M.J.W., J.A.M. Kuipers, G.F. Versteeg and W.P.M. Van Swaaij. 1995. Modelling of simultaneous mass and heat transfer with chemical reaction using the Maxwell-Stefan theory-I. Model development and isothermal study. **Chemical Engineering Science**. 50: 1645–1659.

Froment, G.F. and K.B. Bischoff. 1990. **Chemical Reactor Analysis and Design**. 2nd ed. John Sons, Inc., New York.

Fukuma, M., Muroyama, K., Yasunishi, A., 1987, Specific gas-liquid interfacial area and liquid-phase mass transfer coefficient is a slurry bubble column, **J. Jpn. Eng. Chem.** 20: 321-324.

Harriott, P. 2003. **Chemical Reactor Design**. 1st ed. Marcel Dekker, Inc., New York.

Hassen, B. and D. Hubert. 2003. Modeling of a gas–liquid reactor in batch conditions. Study of the intermediate regime when part of the reaction occurs within the film and part within the bulk. **Chemical Engineering and Processing**. 42(10): 723-732.

Higbie, R. 1935. The rate of absorption of a pure gas into a still liquid during short periods of exposure. **Trans. Am. Inst. Chem. Eng.** 31: 365–389.

Hikita, H. and H. Kikukawa. 1974. Liquid-phase mixing in bubble columns: effect of liquid properties. **Chemical Engineering Journal**. 8:191-197.

Hikita, H. and S. Asai. 1964. Gas absorption with (m,n) th order irreversible chemical reaction. **International Chemical Engineering**. 4: 332.

Hikita, H. and S Asai. 1976. Gas Absorption with a Two-Step Chemical Reaction, **Chemical Engineering Journal**. 11: 123-129.

Hikita, H., S. Asai, K. Tanigawa, K. Segawa, and M. Kitao. 1980. Gas hold-up in bubble columns. **Chemical Engineering Journal**. 20: 59-6.

Hikita, H., S. Asai and T. Takatsuka. 1976. Absorption of Carbon Dioxide into Aqueous Sodium Hydroxide and Sodium Carbonate-Bicarbonate Solutions. **Chemical Engineering Journal.** 11: 131-141.

Hiraoka, M. and Tanaka, K. 1969. Analysis of Simultaneous Heat and Mass transfer with Chemical Reaction. **Heat and Mass transfer Journal**. 20: 37 – 45.

Horikawa, M.S., F. Rossi, M.L. Gimenes, C.M.M. Costa and M.G.C. da Silva. 2004.Chemical absorption of H_2S for biogas purification. **Braz. J. Chem. Eng.** 20: 415-422.

Howard, F.R. 1977. **Chemical Reactor Design for Process Plants**. 1st ed. John Sons, Inc., New York.

Huang, C.J. and C.H. Kuo. 1965. Mathematical models for mass transfer accompanied by reversible chemical reaction. **AIChE J. 11**:901–910.

Hyndman C. L., F. Larachi and C. Guy. 1996**.** Understanding gas-phase hydrodynamics in bubble columns: a convective model based on kinetic theory. **Chemical Engineering Science**. 52(1): 63-77.

Jaganathan, R., R.V. Chaudhari, D.S. Kolhe, G. Emig and H. Hofmann. 1987. Kinetic modelling of hydrogenation of butynediol using 0.2% Pd/C catalyst in a slurry reactor. **Applied Catalysis**. 29(1):141-159.

Juraj, S., Š. Zuzana and J. Markoš. 2007. Modeling of reactive separations including fast chemical reactions in CSTR. **Chemical Engineer Science.** 139(3): 3479-3484.

Kasab J.J., S.R. Karur and P. A. Ramachandran. 1995. Quasilinear boundary element method for nonlinear Poisson type problems**. Engineering Analysis with Boundary Elements**. 15(3): 277-282.

Kastanek, F. 1997, Volumatric mass transfer coefficient in bubble columns. **Collect. Czech. Chem. Commun**. 42: 2491-2496.

KLEIN, J., A. A. VICENTE and J. A. TEIXEIRA. 2004. Study of Hydrodynamics and Mixing in an Airlift Reactor with an Enlarged Separator using Magnetic Tracer Method. **3rd International Symposium on Two-Phase Flow Modeling and Experimentation**, Pisa._____.

Kongto, A., Limtrakul, S., Ngaosuwan, K., Ramachandran, P.A. 2005. Mathematical modeling and simulation for gas – liquid reactor. **Computers & Chemical Engineering.** 29: 2461 – 2473.

Krishna, R. and J.M. Van Baten. 2003. Mass transfer in bubble columns. **Catalyst Today.** 79–80: 67–75.

Kucka, L., I. Müller, E. Y. Kenig and A. Górak**.** 2003**.** On the modeling and simulation of sour gas absorption by aqueous amine solutions. **Chemical Engineering Science.** 58(16): 3571-3578.

Kumar, A., T.T. Dagaleesan, G.S. Laddha and H.E. Hoelscher. 1976. Bubble swarm characteristics in bubble columns, The **Canadian Journal of Chemical Engineering**. 54: 503-507.

Lesage, F., M.A. Latifi and N. Midoux. 2000. Boundary Element in Modeling of Momentum Transport and Liquid -to- Wall Mass Transfer in a Packed – Bed reactor. **Chemical Engineering Science.** 55: 455 – 460.

Levenspiel, O. 1999. **Chemical Reaction Engineering**. 3rd ed. John Sons, Inc., Singapore.

Lewis, W.K. and W.G.Whitman. 1924. **Principles of gas absorption. Industrial and Engineering Chemistry.** (16):1215–1230**.**

Limtrakul Sunun, Sudtida Rojanamatin, Terdthai Vatanatham, Palghat A. Ramachandran. 2005. Gas-Lift Reactor for Hydrogen Sulfide Removal. **J. Ind. Eng. Chem. Res.** 44: 6115-6122.

Lopez, J.P. 1991. **Les Rideaux de Fluides Appliqués au Contrôle des Rejets Accidentals de Gaz Dangereux: Modélisation et Dimensionnement.** In: *Thèse de Doctorat*, Université Claude Bernard-Lyon.

Luo, D.J., R. Lee Lau, G.Q. Yang and L.S. Fan. 1999. Maximum stable bubble size and gas hold up in high-pressure slurry bubble column. **A.I.Ch.E. Journal.** 45: 665–680.

Marko, J., M. Pisu and M. Morbidelli. 1998. Modeling of gas-liquid reactors. Isothermal semibatch and continuous stirred tank reactors. **Computers & Chemical Engineering**. 22(4-5): 627-640.

Maćkowiak, J.F., A. Górak and E.Y. Kenig. 2008. Modelling of combined direct-contact condensation and reactive absorption in packed columns. **Chemical Engineering Journal**, In Press, Corrected Proof.

Missen, R.W., C.A. Mims and B. A. Saville. 1998**. Introduction to Chemical Reaction Engineering and Kinetic**s. 1st ed. John Sons, Inc., Singapore.

Munz, C. and P. V. Roberts. 1989. Gas and liquid-phase mass transfer resistances of organic compounds during mechanical surface aeration. **Water Res**. 23 (3): 589-601.

Niesen, P.H. and J. Villadsen. 1983. Absorption with exothermic reaction in a falling film column. **Chemical Engineering Science.** 38: 1439-1454.

Ngoasuwan, k. 2001. **Mathematical modeling for gas – lift reactors.** M.S. Thesis, Kasetsart University.

Nysing, R.A.T.O. and H. Kramers. 1958. Absorption of CO_2 in carbonate-bicarbonate buffer solutions in a wetted-wall column. **Chem. Eng. Sci.** 8: 81–89.

Olander, D.R. 1960. Simultaneous mass transfer and equilibrium chemical reaction, **A.I.Ch.E. Journal**. 6(2):233–239.

Pohorecki, R. and W. Moniuk. 1988. Kinetics of reaction between carbon dioxide and hydroxyl ions in aqueous electrolyte solutions. **Chemical Engineering Science**. 43(7): 1677–1684.

Pohorecki, R., E. Molga and W. Moniuk. 2007. Heat and Mass Transfer During Gas Absorption with Simultaneous Second-Order Chemical Reaction**. Heat transfer research.** 38(4): 339-349.

Ramachandran, P. A. 1991. Boundary Element Method for Diffusion-Reaction with Boundary Condition. **Chemical Engineering science.** 47: 69-85.

Ramachandran, P. A. 1991. Boundary integral element method for linear diffusion-reaction problems with discontinuous boundary conditions. **The Chemical Engineering Journal.** 47(3): 169-185.

Ramachandran, P. A. 1994. **Boundary element methods in transport phenomena.** Elsevier Science Pulb. Ltd., London.

Ramachandran, P.A. 2005. Boundary integral method for multispecies 1-D convection-diffusion-reaction problems. **Computers & Mathematics with Applications.** 49(9-10): 1575-1583.

Ratcliff, G.A. and J.G. Holdcroft. 1963. Diffusivities of gases in aqueous electrolyte solutions. **Transactions of the Institution of Chemical Engineers and the Chemical Engineer.** 41: 315–319.

Robert H. P. and D.W.Green. 1997. **Perry's chemical engineers' Handbook.** 7th ed. McGraw – Hill Ltd., New York.

Roberts, P.V., C. Munz and P. Dandliker. 1984. Modeling volatile organic solute removal by surface and bubble aeration. **Water Pollut. Control Fed Journal**. 56(4):157-163.

Roizard, C. and G. Wild. 2002. Mass transfer with chemical reaction: the slow reaction regime revisited. **Chemical Engineering Science.** 57(16): 3479-3484.

Rojanamatin, S. 2002. **Auto-Circulation Reactor for hydrogen Sulfide Removal.** M. S. Thesis, Kasetsart University.

Romanainen, J. J and T. Salmi. 1991. Numerical strategies in solving gas-liquid reactor models-1. Stagnant films and a steady state CSTR **Computers & Chemical Engineering.** 15(11): 769-781.

Romanainen, J. J and T. Salmi. 1991. Numerical strategies in solving gas-liquid reactor models-2. Transient films and dynamic tank reactors **Computers & Chemical Engineering.** 15(11): 783-795.

Romanainen, J. J and T. Salmi. 1995. Numerical strategies in solving gas-liquid reactor models-3. Steady state bubble columns. **Computers & Chemical Engineering.** 19(2): 139-154.

Savage, D.W. 1982. **Recent developments in Separation Science. 7**:73.

Smith, R. 1992. Waste Minimization in the Process Industries, Part 3: Separation and Recycle Systems. **The chemical engineer.** 513: 24.

Schulzke, T., S. Schlüter, P.M. Weinspach. 1998. Experimental studies and simulation of the dynamic behaviour of bubble column reactors. **Computers & Chemical Engineering.** 22(1): S667-S670.

Schumpe, A. and G. Grund. 1986. The Gas Disengagement Technique for Studying Gas Holdup Structure in Bubble Columns. **The Canadian. Journal of Chemical Engineering.** 64: 891-896.

Shah, Y. T., B.G Kelkar, S.P. Godbole and W.D. Deckwer. (1982). Design parameters estimations for bubble column reactors. **AIChE Journal**. 28(3); 353-379.

Taghizadeh, M., C. Jallut, M. Tayakout-Fayolle and J. Lieto. *2001*. Non-isothermal gas–liquid absorption with chemical reaction studies: Temperature measurements of a spherical laminar film surface and comparison with a model for the CO_2/NaOH system.**Chemical Engineering Journal**. 82 (1-3): 143-148.

Taitel, Y., D. Barnea and Dukler, A. E. 1980. Modelling flow pattern transitions for steady upward gas-liquid flow in vertical tubes. **A.I.Ch.E Journal.** 26: 345-354.

Tsonopolous, C., D.M. Coulson and L.W. Inman. 1976. Ionization constants of water pollutants, **Journal of Chemical and Engineering Data.** 21(2): 190–193.

Van Krevelen, D.W. and P.J. Hoftijzer. 1948. Kinetics of gas–liquid reactions. Part 1: general theory. **Recueil des Travaux Chimiques des Pays-Bas Journal of the Royal Netherlands Chemical Society**. 67: 563–568.

Versteeg, G.F. and W.P.M. van Swaaij.1988. Solubility and diffusivity of acid gases (CO_2 and N_2O) in aqueous alkaloamine solutions. **Journal of Chemical and Engineering Data.** 33: 29–34.

Wei Gao, X and J. Wang. 2008. Interface integral BEM for solving multi-medium heat conduction problems. **Engineering Analysis with Boundary Elements.** In Press, Corrected Proof.

Weisenberger, S. and A. Schumpe. 1996. Estimation of gas solubility in salt solutions at temperatures from 273 to 363 K. **A.I.Ch.E. Journal**. 42: 298–300.

Westerterp, K.R., W.P.M. van Swaaij and A.A.C.M. Beenackers. 1984. **Chemical Reactor Design and Operation**.1st ed. Wiley, Inc., New York.

Whitman, G. 1923. Preliminary experimental confirmation of the two-film theory of gas absorption. **Chemical and Metallurgical Engineering.** 29: 146–148.

Wubs, J. H., Beenacker, A. A. C. M. 1994, Kinetic of H2S Absorption into Aqueous Ferric solution of HEDTA. **J. AIChE**. 40(3): 433-444.

Zadravec, M., M. Hriberšek and L. Škerget. 2008. Natural convection of micropolar fluid in an enclosure with boundary element method. **Engineering Analysis with Boundary Elements**, Corrected Proof.

APPENDICIES

Appendix A

Mass Balances in Gas and Liquid Phases

1. Mass balance for component i in gas bulk of the mixing cell, jj,

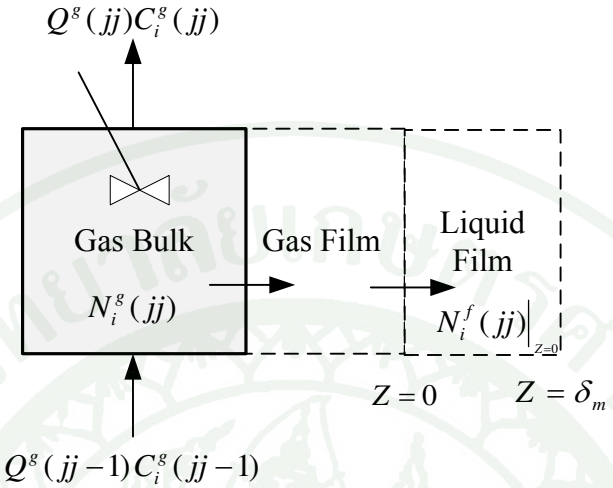

Appendix Figure A1 Diagram of mass balance in gas phase. Control volume for gas bulk is shown in shaded area.

Mass in - mass out + generation - consumption = accumulation

$$n^g(jj-1)-(n_i^g(jj)+aV_{cell}N_i^f\big|_{Z=0}(jj)=0 \tag{127}$$

$$aV_{cell}N_i^f\big|_{Z=0}(jj)=n_{i,}^g(jj-1)-n_i^g(jj) \tag{128}$$

$$(n_i^g)_{in}=Q^gC_i^g \text{ and } N_i^g=N_{i,z=0}^f=-D_i\frac{dC_i^f}{dZ} \tag{129}$$

Substituted Equation (129) into Equation (130)

$$-aV_{cell}D_i\frac{dC_i^f(jj)}{dZ}\bigg|_{Z=0}=Q^g(jj-1)C_i^g(jj-1)-Q^g(jj)C_i^g(jj) \tag{130}$$

$$-a\frac{V_R}{N_G}D_i\left.\frac{d(c_i^f C_{i,ref}^g / H_{i,ref})}{d(\xi\delta_m)}\right|_{Z=0} = f^g(jj-1)Q_{ref}^g c_i^g(jj-1)C_{i,ref}^g - f^g(jj)Q_{ref}^g c_i^g(jj)C_{i,ref}^g \quad (131)$$

$$-a\frac{V_R}{N_G}D_i\frac{C_{i,ref}^g}{H_{i,ref}\delta_m}\left.\frac{dc_i^f}{d\xi}\right|_{Z=0} = f^g(jj-1)Q_{ref}^g c_i^g(jj-1)C_{i,ref}^g - f^g(jj)Q_{ref}^g c_i^g(jj)C_{i,ref}^g \quad (132)$$

divided Equation (132) by $Q_{ref}^g C_{i,ref}^g$

$$-a\frac{V_R}{N_G}D_i\frac{C_{i,ref}^g}{H_{i,ref}\delta_m Q_{ref}^g C_{i,ref}^g}\left.\frac{dc_i^f(jj)}{d\xi}\right|_{Z=0} = f^g(jj-1)c_i^g(jj-1) - f^g(jj)c_i^g(jj) \quad (133)$$

$$-\frac{a}{N_G}\frac{A_r LD_i}{H_{i,ref}\delta_m A_r u_{ref}^g}\left.\frac{dc_i^f(jj)}{d\xi}\right|_{Z=0} = f^g(jj-1)c_i^g(jj-1) - f^g(jj)c_i^g(jj) \quad (134)$$

$$-\frac{a}{N_G}\frac{LD_i}{H_{i,ref}\delta_m u_{ref}^g}\left.\frac{dc_i^f(jj)}{d\xi}\right|_{Z=0} = f^g(jj-1)c_i^g(jj-1) - f^g(jj)c_i^g(jj) \quad (135)$$

define from film theory

$$k_L = \frac{D_{ref}}{\delta_m} \quad (136)$$

and multiply $\frac{u_{ref}^{L}}{u_{ref}^{L}}$ in Equation (136)

$$-\frac{a}{N_G}\frac{LD_i k_L}{H_{i,ref} D_{ref} u_{ref}^{g}}\frac{u_{ref}^{L}}{u_{ref}^{L}}\left.\frac{dc_i^f(jj)}{d\xi}\right|_{\zeta=0} = f^g(jj-1)c_i^g(jj-1) - f^g(jj)c_i^g(jj) \quad (137)$$

$$f^g(jj-1)c_i^g(jj-1) - f^g(jj)c_i^g(jj) + \left[\frac{\alpha_{gL}}{N_G}\right]\gamma_{Fi}s_i\left.\frac{dc_i^f(jj)}{d\xi}\right|_{\xi=0} = 0 \quad (138)$$

$$\alpha_{gL} = \frac{aV_{cell}k_L}{u_{ref}^{L}A_r} \quad (139)$$

$$\gamma_{Fi} = \frac{u_{ref}^{L}}{u_{re}^{g}H_{i,ref}} \quad (140)$$

$$s_i = \frac{D_i}{D_{ref}} \quad (141)$$

2. Mass balance for component i in liquid bulk of the mixing cell, kk,

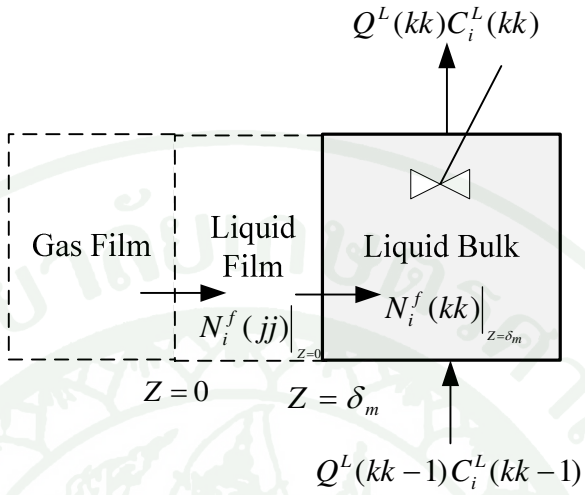

Appendix Figure A2 Diagram of mass balance in liquid phase. Control volume for liquid bulk is shown in shaded area.

Mass in - mass out + generation - consumption = accumulation

$$V_R a N_i^f\big|_{Z=\delta_m}(kk-1)+n_i^L(kk-1)-n_i^L(kk) - \sum_{j=1}^{NR} V(\varepsilon_L - a\delta_m)\upsilon_j R_j^b(kk)=0 \quad (142)$$

Substituted the molar flow rates, (n_L), into Equation (139)

$$V_R a N_i^f\big|_{Z=\delta_m}(kk-1)+Q^L C_i^L(kk-1)-Q^L C_i^L(kk) - \sum_{j=1}^{NR} V(\varepsilon_L - a\delta_m)\upsilon_j R_j^b(kk)=0 \quad (143)$$

The rate function for reaction *m* in liquid bulk, R_j^b, is written as

$$R_j^b = k_{ref,j}\, exp\left[\frac{E_a}{R}\left[\frac{1}{T^L}-\frac{1}{T_{ref}}\right]\right] C_A^L C_B^L \tag{144}$$

Substituted R_j^b into Equation (144)

$$-a\frac{V_R}{N_L}D_i\left.\frac{d(C_{i,ref}c_i^f)}{d(\xi\delta_m)}\right|_{Z=\delta_m} = f^L Q_{ref}^L c_i^L(kk-1)C_{i,ref} - f^L Q_{ref}^L c_i^L(kk)C_{i,ref} - \sum_{j=1}^{NR}\frac{V_R}{N_L}(\varepsilon_L - a\delta_m)v_{ij}k_{ref,j}\, exp\left[-\frac{E_a}{R}\left[\frac{1}{T^L}-\frac{1}{T_{ref}}\right]\right] C_A^L C_B^L \tag{145}$$

liquid phase mass balance, Equation (145) can be written in dimensionless form as

$$-a\frac{V_R C_{i,ref}}{N_L\delta_m}D_i\left.\frac{dc_i^f(kk)}{d\xi}\right|_{Z=\delta_m} = f^L Q_{ref}^L c_i^L(kk-1)C_{i,ref} - f^L Q_{ref}^L c_i^L(kk)C_{i,ref} - \sum_{j=1}^{NR}\frac{V_R}{N_L}(\varepsilon_L - a\delta_m)v_{ij}k_{ref,j}\, exp\left[-\frac{E_a}{RT_{ref}}\left[\frac{1}{\frac{T^L}{T_{ref}}}-\frac{1}{\frac{T_{ref}}{T_{ref}}}\right]\right] c_A^L C_{ref,A} c_B^L C_{ref,B} \tag{146}$$

$$-\frac{aV_R}{N_L\delta_m Q_{ref}^L}D_i\left.\frac{dc_i^f(kk)}{d\xi}\right|_{Z=\delta_m} = f^L c_i^L(kk-1) - f^L c_i^L(kk) - \sum_{j=1}^{NR}\frac{V_R}{N_L}(\varepsilon_L - a\delta_m)v_{ij}k_{ref,j}\, exp\left[-\frac{E_a}{RT_{ref}}\left[\frac{1}{\frac{T^L}{T_{ref}}}-\frac{1}{\frac{T_{ref}}{T_{ref}}}\right]\right] c_A^L C_{ref,A} c_B^L C_{ref,B} R_{ref}^b \tag{147}$$

$$-\frac{aA_rL}{N_L\delta_m A_r u_{ref}^L} D_i \frac{dc_i^f(kk)}{d\xi}\bigg|_{Z=\delta_m} = f^L c_i^L(kk-1) - f^L c_i^L(kk)$$

$$-\sum_{j=1}^{NR} \frac{A_r L}{N_L Q_{ref}^L C_{i,ref}} (\varepsilon_L - a\delta_m) v_{ij} k_{ref,j} \exp\left[-\frac{E_a}{RT_{ref}}\left[\frac{1}{\frac{T^L}{T_{ref}}} - \frac{1}{\frac{T_{ref}}{T_{ref}}}\right]\right] c_A^L C_{ref,A} c_B^L C_{ref,B} \quad (148)$$

$$-\frac{aLk_L}{N_L u_{ref}^L}\frac{D_i}{D_{ref}}\frac{dc_i^f(kk)}{d\xi}\bigg|_{Z=0} = f^L c_i^L(kk-1) - f^L c_i^L(kk)$$

$$-\sum_{j=1}^{NR} \frac{L}{N_L u_{ref}^L C_{i,ref}} (\varepsilon_L - a\delta_m) v_{ij} r^b(kk) R_{ref}^b \quad (149)$$

$$r_j^b = c_A^b c_B^b \exp\left[\gamma_j\left(1-\frac{1}{\theta^L}\right)\right] \quad (150)$$

$$R_{ref}^b = k_{ref,j} C_{ref,A} C_{ref,B} \quad (151)$$

$$-\frac{\alpha_{gL}}{N_L} s_i \frac{dc_i^f(kk)}{d\xi}\bigg|_{\xi=0} = f^L c_i^L(kk-1) - f^L c_i^L(kk)$$

$$-\frac{1}{C_{i,ref}}\frac{C_{ref}}{C_{ref}}\sum_{j=1}^{NR} \frac{L(\varepsilon_L - a\delta_m) R_{ref}^b}{N_L u_{ref}^L} v_{ij} r_j^b(kk) \quad (152)$$

$$-\frac{\alpha_{gL}}{N_L} s_i \frac{dc_i^f(kk)}{d\xi}\bigg|_{\xi=0} = f^L c_i^L(kk-1) - f^L c_i^L(kk)$$

$$-\frac{1}{\omega_i}\sum_{i=1}^{NR} \frac{L(\varepsilon_L - a\delta_m) R_{ref}^b}{N_L u_{ref}^L C_{ref}} v_{ij} r^b(kk) \quad (153)$$

$$-\frac{\alpha_{gL}}{N_L} s_i \frac{dc_i^f(kk)}{d\xi}\bigg|_{\xi=0} = f^L c_i^L(kk-1) - f^L c_i^L(kk) - \frac{1}{\omega_i}\sum_{j=1}^{NR}\frac{M}{N_L} v_{ij} r^b(kk) \tag{154}$$

$$M = \frac{L(\varepsilon_L - a\delta_m)R_{ref}^b}{u_{ref}^L (C_{i,ref}^g / H_{i,ref})} \tag{155}$$

3. Mass Balance in liquid Film

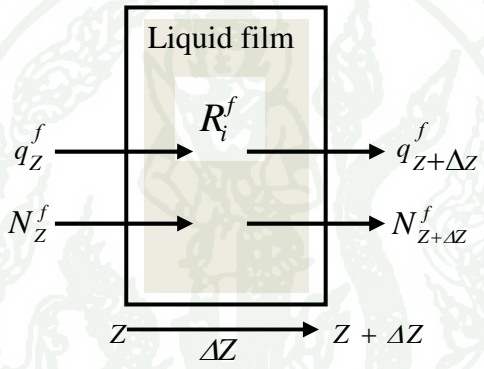

Appendix Figure A3 Diagram of mass balance in liquid film. Control volume for liquid film is shown in shaded area.

Mass in - mass out + generation - consumption = accumulation

$$aVN\big|_z^f - aVN\big|_{z+\Delta z}^f - \sum_{j=1}^{NR} aV\Delta z \upsilon_j R_j^f = 0 \tag{156}$$

$$N^f = -D\frac{dC^f}{dZ} \tag{157}$$

Substituted N^f into Equation (157)

$$-aVD_i\left(\frac{dC_i}{dZ}\right)\Big|_Z^f - \quad -aVD_i\left(\frac{dC_i}{dZ}\right)\Big|_{Z+\Delta Z}^f = \sum_{j=1}^{NR} aV\Delta Z\upsilon_j R_j^f \tag{158}$$

divided $aV\Delta Z$ and take $lim\,\Delta Z \longrightarrow 0$

$$-\frac{d}{dZ}\left(-D_i\frac{dC_i^f}{dZ}\right) = \sum_{j=1}^{NR} R_i^f \tag{159}$$

$$D_i\frac{d^2C_i^f}{dZ^2} = \sum_{j=1}^{NR} R_j^f \tag{160}$$

liquid film mass balance , Equation (160) can be written in dimensionless form as

$$D_i\frac{d^2(c_i^f C_{i,ref})}{d(\delta_m\xi)^2} = \sum_{j=1}^{NR} r_j R_j(C_{ref,}) \tag{161}$$

$$\frac{s_i D_{ref} C_{i,ref}}{\delta_m^2}\frac{d^2c_i^f}{d\xi^2} = \sum_{j=1}^{NR} r_j R_j(C_{ref,}) \tag{162}$$

$$\frac{d^2c_i^f}{d\xi^2} = \sum_{j=1}^{NR}\frac{\delta_m^2}{s_i D_{ref} C_{ref,i}} r_j R_j(C_{ref,}) \tag{163}$$

$$\frac{d^2c_i^f}{d\xi^2} = \sum_{j=1}^{NR}\frac{\delta_m^2}{s_i D_{ref} C_{ref,i}}\frac{C_{ref}}{C_{ref}} r_j R_j(C_{ref,}) \tag{164}$$

$$\frac{d^2c_i^f}{d\xi^2} = \sum_{j=1}^{NR}\frac{\delta_m^2}{s_i D_{ref}}\frac{1}{\omega_i}\frac{R_j(C_{ref,})}{C_{ref}} r_j \tag{165}$$

$$\frac{d^2c_i^f}{d\xi^2} = \frac{1}{s_i\omega_i}\sum_{j=1}^{NR} Ha^2 r_j \tag{166}$$

$$Ha^2 = \frac{\delta_m^2}{D_{ref}}\frac{R_j(C_{ref,})}{C_{ref}} \tag{167}$$

Appendix B

Linearization

The linearization for second order chemical reaction in isothermal is can be written as

$$r^b = c_A c_B \tag{168}$$

The equation for the linearization of a function r^b is:

$$r^b = c_A^* c_B^* + \frac{\partial r^b}{\partial c_A}(c_A - c_A^*) + \frac{\partial r^b}{\partial c_A}(c_B - c_B^*) \tag{169}$$

$$\frac{\partial r^b}{\partial c_A} = c_B^* \tag{170}$$

$$\frac{\partial r^b}{\partial c_B} = c_A^* \tag{171}$$

Substituted Equation (170) and (171) into (169)

$$r^b = c_A^* c_B^* + c_B^*(c_A - c_A^*) + c_A^*(c_B - c_B^*) \tag{172}$$

$$r^b = c_A^* c_B^* + c_A c_B^* - c_B^* c_A^* + c_A^* c_B - c_A^* c_B^* \tag{173}$$

$$r^b = c_A c_B^* + c_A^* c_B - c_A^* c_B^* \tag{174}$$

$$r^b = c_A k_1 + c_B k_2 - k_3 \tag{175}$$

where $k_1 = c_B^*$, $k_2 = c_A^*$, and $k_3 = c_A^* c_B^*$ respectively

Appendix C

Reactor model

1. Calculation the dimensionless of flow rates of gas

The mass balance for component in the gas bulk of each cell is written as

$$aV_{cell}N_i^f(\,jj\,)\Big|_{Z=0} = n_i^g(\,jj-1\,) - n_i^g(\,jj\,) \tag{176}$$

Equation (176) can be rearranged as follow:

$$n_i^g(\,jj\,) = n_i^g(\,jj-1\,) - aV_{cell}N_i^f(\,jj\,)\Big|_{Z=0} = 0 \tag{177}$$

The total molar flow rate of component *i* in gas bulk as

$$n_{i,}^{total}(\,jj\,) = n_i^{total}(\,jj-1\,) - \sum_{i=1}^{m} N_m(\,jj\,)\Big|_{z=0}\,) \tag{178}$$

From ideal gas law

$$PQ^* = n^*RT \tag{179}$$

$$Q^g(\,jj\,) = \frac{n^{total}(\,jj\,)RT^g(\,jj\,)}{P(\,jj\,)} \tag{180}$$

Substituted Equation (178) into Equation (180.). The volumetric flow rate of gas for *jj* cell as shown Equation (181).

$$Q^g(\,jj\,) = \frac{(\,n_{i,}^{total}(\,jj\,) - \sum_{i=1}^{m} N_m(\,jj\,)\Big|_{z=0}\,)RT^g(\,jj\,)}{P(\,jj\,)} \tag{181}$$

$$Q^g(\,jj-1\,) = \frac{n^{total}(\,jj-1\,)RT^g(\,jj-1\,)}{P\,(\,jj-1\,)} \tag{182}$$

The dimensionless flow rate is defined as:

$$f^{g}(jj)=\frac{Q^{g}(jj)}{Q^{g}(jj-1)}=\frac{T^{g}(jj)P(jj-1)}{T^{g}(jj-1)P(jj)}\left(1-\frac{\sum_{i=1}^{m}N_{m}(jj)\big|_{z=0}}{n^{total}(jj-1)}\right) \tag{183}$$

$$N_{m,}^{f}=-D\frac{dc_{i,}^{f}}{dz} \text{ and } n^{total}=Q^{total}C^{total}=A_{r}U^{total}C^{total} \tag{184}$$

$$f^{g}(jj)=\frac{T^{g}(jj)P(jj-1)}{T^{g}(jj-1)P(jj)}\left(1+\frac{D_{i}\sum_{i=1}^{m}\frac{dC_{i}^{f}(jj)}{dZ}\Big|_{z=0}}{A_{r}U^{total}(jj-1)C^{total}(jj-1)}\right) \tag{185}$$

The gas phase mass balance given by Equation (185) can be formulate into dimensionless form as follows:

$$f^{g}(jj)=\theta^{g}p^{*}\left(1+\alpha_{gL}\gamma_{Fi}y_{ref}(jj)\sum_{i=1}^{m}s_{i}\frac{dc_{i}^{f}(jj)}{d\xi}\Big|_{\xi=0}\right) \tag{186}$$

2. Calculation of dimensionless concentration of gas out from cell, jj^{th}.

The mass balance equation for gas phase and liquid film (Appendix A)

$$f^{g}(jj-1)c_{i}^{g}(jj-1)-f^{g}(jj)c_{i}^{g}(jj)+\left[\frac{\alpha_{gL}}{N_{G}}\right]\gamma_{Fi}s_{i}\frac{dc_{i}^{f}(jj)}{d\xi}\Big|_{\xi=0}=0 \tag{187}$$

$$Bi_{mi}(c_{i,}^{g}(jj)-h_{i}(\theta_{\zeta=0}^{f})c_{i,\xi=0}^{f}(jj)=-\left(\frac{dc_{i}^{f}(jj)}{d\xi}\right)_{\xi=0} \tag{188}$$

$$\left(\frac{dc_{i}^{f}(jj)}{d\xi}\right)_{\xi=0}=-Bi_{mi}c_{i}^{g}(jj)+h_{i}(\theta_{\zeta=0}^{f})Bi_{mi}c_{i,\xi=0}^{f}(jj) \tag{189}$$

substituted Equation (189) into Equation (186)

$$f^{g}(jj-1)c_i^{g}(jj-1)-f^{g}(jj)c_i^{g}(jj)+\left[\frac{\alpha_{gL}}{N_G}\right]\gamma_{Fi}s_i(-Bi_{mi}c_{i,}^{g}(jj)+h_i(\theta_{\zeta=0}^{f})Bi_{mi}c_{i,\xi=0}^{f}(jj))=0 \quad (190)$$

rearranging Equation (190)

$$c_i^{g}(jj)=\frac{c_i^{g}(jj-1)f^{g}(jj-1)+\alpha_{gL}\gamma_{Fi}Bi_{m,i}h(\theta_{\xi=0}^{f})c_{i,\xi=0}^{f}(jj)}{(f^{g}(jj)+\alpha_{gL}\gamma_{Fi}s_iBi_{m,i})} \quad (191)$$

3. Boundary condition at $\xi=0$

Substituted Equation (191) into Equation (189)

$$\left(\frac{dc_i^{f}(jj)}{d\xi}\right)_{\xi=0}=-Bi_{mi}\left[\frac{c_i^{g}(jj-1)f^{g}(jj-1)+\alpha_{gL}\gamma_{Fi}Bi_{m,i}h(\theta_{\xi=0}^{f})c_{i,\xi=0}^{f}(jj)}{(f^{g}(jj)+\alpha_{gL}\gamma_{Fi}s_iBi_{m,i})}\right]+h_i(\theta_{\zeta=0}^{f})Bi_{mi}c_{i,\xi=0}^{f}(jj) \quad (192)$$

$$\left(\frac{dc_i^{f}(jj)}{d\xi}\right)_{\xi=0}=-Bi_{mi}\left[\frac{c_i^{g}(jj-1)f^{g}(jj-1)-f^{g}(jj)h(\theta_{\xi=0}^{f})c_{i,\xi=0}^{f}(jj)}{(f^{g}(jj)+\alpha_{gL}\gamma_{Fi}s_iBi_{m,i})}\right] \quad (193)$$

$$\left(\frac{dc_i^{f}(jj)}{d\xi}\right)_{\xi=0}=-Bi^{*}{}_{mi}(c_i^{g}(jj-1)f^{g}(jj-1)-f^{g}(jj)h(\theta_{\xi=0}^{f})c_{i,\xi=0}^{f}(jj)) \quad (194)$$

$$Bi^{*}{}_{mi}=\frac{Bi_{m,i}}{(f^{g}(jj)+\alpha_{gL}\gamma_{Fi}s_iBi_{m,i})} \quad (195)$$

4. Boundary condition at $\xi = 1$

The mass balance in liquid film in Equation (154) (from Appendix A) is written as

$$-\frac{\alpha_{gL}}{N_L} s_i \left.\frac{dc_i^f(kk)}{d\xi}\right|_{\xi=\delta_m} = f^L c_i^L(kk-1) - f^L c_i^L(kk) - \frac{1}{\omega_i}\sum_{j=1}^{NR}\frac{M}{N_L} v_{ij} r^b(kk) \tag{196}$$

The linearization of the dimensionless reaction rate of the component in Equation (196) (See Appendix B) is written as

$$r^b = c_A k_1 + c_B k_2 - k_3 \tag{197}$$

Substituted Equation (197) into Equation (196)

$$-\frac{\alpha_{gL}}{N_L} s_i \left.\frac{dc_i^f(kk)}{d\xi}\right|_{\xi=\delta_m} = f^L c_i^L(kk-1) - f^L c_i^L(kk) - \frac{1}{\omega_i}\sum_{j=1}^{NR}\frac{M}{N_L}(c_A^L(jj)k_1 + c_B^L(jj)k_2 - k_3) \tag{198}$$

$$-\frac{\alpha_{gL}}{N_L} s_i \left.\frac{dc_i^f(kk)}{d\xi}\right|_{\xi=\delta_m} = f^L c_i^L(kk-1) - f^L c_i^L(kk) - \frac{1}{\omega_i}\frac{M}{N_L} c_A^L(jj)k_1 - \frac{1}{\omega_i}\frac{M}{N_L} c_B^L(jj)k_2 + k_3\frac{1}{\omega_i}\frac{M}{N_L} \tag{199}$$

The boundary condition at $\xi = 1$

$$c_{i,\xi=1}^f = c_i^L \tag{200}$$

Substituted Equation (200) into Equation (199)

$$-\frac{\alpha_{gL}}{N_L}s_i\frac{dc_i^f(kk)}{d\xi}\bigg|_{\xi=\delta_m} = f^L c_i^L(kk-1) - f^L c_i^f(kk)\big|_{\xi=\delta_m} - \frac{1}{\omega_i}\frac{M}{N_L}c_A^f(kk)\big|_{\xi=\delta_m}k_1 - \frac{1}{\omega_i}\frac{M}{N_L}c_B^f(kk)\big|_{\xi=\delta_m}k_2 + k_3\frac{1}{\omega_i}\frac{M}{N_L} \tag{201}$$

The Equation (201)) can be formulated into the Robin condition.

$$-\frac{\alpha_{gL}}{N_L}s_i\frac{dc_i^f(kk)}{d\xi}\bigg|_{\xi=\delta_m} + \frac{1}{\omega_i}\frac{M}{N_L}c_A^f(kk)\big|_{\xi=\delta_m}k_1 + \frac{1}{\omega_i}\frac{M}{N_L}c_B^f(kk)\big|_{\xi=\delta_m}k_2 + c_i^f(kk)\big|_{\delta_m} = c_i^L(kk-1) + k_3\frac{1}{\omega_i}\frac{M}{N_L} \tag{202}$$

liquid phase mass balance, for component *A* in liquid phase is written as

$$-\frac{\alpha_{gL}}{N_L}s_A\frac{dc_A^f(kk)}{d\xi}\bigg|_{\xi=\delta_m} + (1+\frac{1}{\omega_A}\frac{M}{N_L}k_1)c_A^f(kk)\big|_{\xi=\delta_m} + \frac{1}{\omega_A}\frac{M}{N_L}c_B^f(kk)\big|_{\xi=\delta_m}k_2 = c_A^L(kk-1) + k_3\frac{1}{\omega_A}\frac{M}{N_L} \tag{204}$$

The mass balance of component *B* in liquid phase is written as

$$-\frac{\alpha_{gL}}{N_L}s_B\frac{dc_B^f(kk)}{d\xi}\bigg|_{\xi=\delta_m} + (1+\frac{1}{\omega_B}\frac{M}{N_L}k_2)c_B^f(kk)\big|_{\xi=\delta_m} + \frac{1}{\omega_B}\frac{M}{N_L}c_A^f(kk)\big|_{\xi=\delta_m}k_1 = c_A^L(kk-1) + k_3\frac{1}{\omega_B}\frac{M}{N_L} \tag{205}$$

Appendix D

Cubic Osculation

The idea behind cubic osculation is given the values of a function and its derivatives at the end points, one can form a cubic equation to describe the variation of function in the given interval. The procedure is known as osculation since the slopes are involved. The principle shows in Appendix Figure 4 and which show how one may proceed to construct the osculating polynomial.

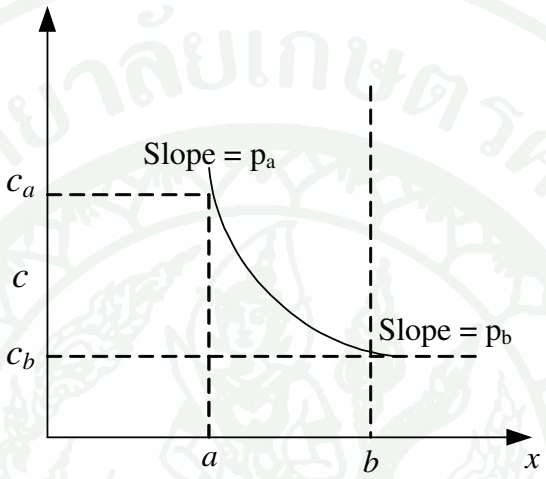

Appendix Figure D1 Diagram of Cubic Osculation

Source: Ramacharndran (1999)

The general equation of cubic in terms of the dimensionless variable η can be expressed as:

$$c = A + B\eta + C\eta^2 + D\eta^3 \tag{206}$$

Here A, B, C and D are four coefficients to be determined. Two required conditions are as follows: $c(\eta = 0) = c_a$ and $c(\eta = 1) = c_b$. Hence

$$c_a = A \tag{207}$$

and

$$c_b = A + B + C + D \tag{208}$$

Further more

$$\frac{dc}{d\eta} = B\eta + 2C\eta + 3D\eta^2 \tag{209}$$

also

$$\frac{dc}{d\eta} = \frac{dc}{dx}\frac{dx}{d\eta} = (b-a)\frac{dc}{dx} \tag{210}$$

Using the above relationships at the end points we obtain two additional conditions:

$$(b-a)p_a = B \tag{211}$$

$$(b-a)p_b = B + 2C + 3D \tag{212}$$

The four Equations (207), (208), (211), and (212) can be solved for A, B, C and D. Substituted the Equation (207) into (208) and (211) into (212)

$$c_b = c_a + (b-a)p_a + C + D \tag{213}$$

$$(b-a)p_b = (b-a)p_a + 2C + 3D \tag{214}$$

x2 Equation (213)

$$2c_b = 2c_a + 2(b-a)p_a + 2C + 2D \tag{215}$$

Equation (214)-(215)

$$D = (b-a)p_a + (b-a)p_b + 2c_a - 2c_b \tag{216}$$

Substituted Equation (216) into Equation (213)

$$C = 3c_b - 3c_a - (b-a)p_b - 2(b-a)p_a \tag{217}$$

Substituted Equation (207), (211), (216), and (217) into Equation (206)

$$\begin{aligned} c = c_a + [(b-a)p_a]\eta + [3c_b - 3c_a - (b-a)p_b - 2(b-a)p_a]\eta^2 \\ + [(b-a)p_a + (b-a)p_b + 2c_a - 2c_b]\eta^3 \end{aligned} \tag{218}$$

The coefficients in Equation (219) can be regrouped and the resulting equation can be rearranged as:

$$c = \varphi_1(b-a)p_a + \varphi_2 c_a + \varphi_3(b-a)p_b + \varphi_4(b-a)c_b \tag{219}$$

where the osculating polynomials coefficient, φ_i, are defined as follows:

$$\varphi_1 = \eta - 2\eta^2 + \eta^3 \tag{220}$$

$$\varphi_2 = 1 - 3\eta^2 + 2\eta^3 \tag{221}$$

$$\varphi_3 = -\eta^2 + \eta^3 \tag{222}$$

$$\varphi_4 = 3\eta^2 - 2\eta^3 \tag{223}$$

CURRICULUM VITAE

NAME : Mr. Teeranun Nakyai

BIRTH DATE : January 11, 1984

BIRTH PLACE : Si Sa Ket, Thailand

EDUCATION :

YEAR	**INSTITUTE**	**DEGREE/DIPLOMA**
2007	Burapha Univ.	B.En. (Chemical-Engineering)

SCHOLARSHIP : Kasetsart University Research and Development Institute (KURDI), National Research Council of Thailand (NRCT), and Research Development Program in